THE UNIVERSITY OF MANITOBA

MECHANICAL PROPERTIES OF UNIDIRECTIONALLY SOLIDIFIED ALLOY CASTINGS

BY

LEONARD STUPAK

A THESIS

SUBMITTED TO THE FACULTY OF GRADUATE STUDIES

IN PARTIAL FULFILMENT OF THE REQUIREMENTS FOR THE DEGREE

OF MASTER OF SCIENCE IN ENGINEERING (MECHANICAL)

DEPARTMENT OF MECHANICAL ENGINEERING

WINNIPEG, MANITOBA

OCTOBER, 1971

ACKNOWLEDGEMENTS

The author wishes to express his gratitude to Dr. J. R. Cahoon, Associate Professor at the University of Manitoba, for his guidance and constant encouragement during the course of the investigation. National Research Council of Canada operating grant A5403 is gratefully acknowledged. Financial support in the form of a National Research Council scholarship and University of Manitoba fellowship is also appreciated.

ABSTRACT

Al-Ni, Al-Cu and Al-Si eutectic and off-eutectic alloys were unidirectionally solidified by an uncontrolled water quench at a solidification rate of about 80 cm/hr. The microstructures of the eutectics exhibit some alignment but are badly faulted. The ultimate tensile strengths of the three eutectics are 28,000 psi, 29,000 psi and 24,700 psi respectively which, except for Al-Ni, are superior to strengths reported by other investigators for better aligned structures obtained via slow unidirectional solidification (2-10 cm/hr). In all cases the unidirectionally solidified specimens exhibited much improved properties over as cast (random) structures. Although the microstructures are unstable at elevated temperatures thus adversely affecting room temperature properties after high temperature exposure, reinforcement is evident at elevated temperatures with Al-Cu and Al-Si eutectic strengths being significantly higher than those of well aligned but coarser structures. Cold rolling of the Al-Ni eutectic results in broken fibers but a strength increase is obtained by cold rolling at the optimum value of 22% reduction in thickness.

TABLE OF CONTENTS

INTRODUCTION

It has been shown by a number of researchers that the mechanical properties of a metal or alloy can be improved by reinforcing the material with fibers of a high strength, high modulus material. The properties of the resulting fiber composite may be controlled by manipulating various parameters such as volume fraction of fibers, length of fibers and fiber strength and elastic modulus. One way to produce a fiber composite material is by the unidirectional solidification of eutectic or off-eutectic alloys in which a hard, strong phase solidifies in the form of fibers surrounded by a ductile matrix. Some alloys solidify with a lamellar structure and can be analyzed by the same principles which describe fiber composite behaviour. Most of the investigative work on unidirectionally solidified alloys has involved careful control of solidification parameters thus necessitating rather elaborate apparatus. Because of this and the very slow solidification rates used (usually less than 10 cm/hr.), the production techniques are not suited to industrial application and especially not to mass production applications where production time should be minimized. The slow, controlled solidification process can be used for only the most simple shapes (e.g. rods, bars, small plates) and cannot be easily utilized in the solidification of complex parts.

The present investigation concerning the solidification of Al-Ni, Al-Cu and Al-Si alloys with emphasis on the eutectic alloys, evaluates the efficacy of producing aligned structures using the technique of relatively uncontrolled unidirectional solidification.

Solidification was effected by impinging a water jet on a steel base plate which supported a cylindrical mold containing the molten alloy. The water quench produced very high solidification rates (in the order of 80 cm/hr.) which, when considered together with the simple apparatus used, is much more suitable to industrial application than other laboratory techniques. Uncontrolled unidirectional solidification is amenable to application in solidifying complex shapes since, by the appropriate placement of chills in the mold, aligned structures can be formed in highly stressed regions of the casting.

HISTORICAL REVIEW

(A) General

"The progress of science can be compared to a tide advancing up a beach. As the water comes in, it makes a series of major conquests, and following each conquest there comes a rapid filling in of all the tiny creeks and hollows ... Progress in science is not such an orderly process, since the minor advances sometimes precede the major, but nevertheless, the analogy is not too inexact."[1]

The analogy does apply to the development of fiber composite technology. The "major conquests" began with the development of glass fiber reinforced plastics in the 1930's and their utilization in the 1940's. Herring and Galt in 1952 discovered that tiny filaments possessed strengths approaching the theoretical.[2] This suggested that material strengths could be increased by incorporating the very strong filaments in a weaker material. In 1958 Webb and Forgeng[2] found that microcrystals precipitated in various alloys can possess a high degree of crystal perfection and strengths approaching the theoretical. This observation led to speculation that fibrous reinforcement in whisker from might be possible by controlling the solidification of selected alloys. The practicality of growing whiskers "in situ" has been proven in a number of alloy systems and the process of unidirectional solidification offers the possibility of producing strong alloys at relatively low cost with mass production applicability.

Solid materials are divided into two general classes:

a) monolithic or microscopically homogeneous materials such as aluminum (or any of the pure metals) and glass;

b) multiphase materials such as concrete and multiphase alloys.

It is to the second classification that composite materials belong. A composite material is a solid which is fabricated by combining two or more differing materials to produce a multiphase material with properties differing from those of the constituents. Composite materials have been in use for many years and may take a variety of forms. The Israelites as early as 800 B.C. added straw to earthen bricks to form a crude composite material. Mortar and concrete were used in Roman times. Modern day reinforced concrete is an example of a fiber composite with very large "fibers".

The theoretical strength of materials has been studied by Polanyi who found that for cleavage of a perfectly brittle crystal (cleavage between two atomic planes) the ideal strength is:[3]

$$\sigma_{th} = \left(\frac{4\gamma E}{a}\right)^{\frac{1}{2}}$$

where γ = surface energy of the fracture surface

E = elastic modulus

a = interplanar atomic spacing.

For Al_2O_3 crystals using $E = 3.8 \times 10^{12}$ dynes/cm^2, $\gamma = 1200$ ergs/cm^2 and $a = 4.32\text{Å}$, $\sigma_{th} = 0.17E$.

Since plastic flow is much easier if planes of atoms slide over each other, Frenkel proposed that the theoretical strength is described by the relationship:[3,4]

$$\tau_{th} = \frac{b}{a}\,\frac{G}{2\pi}$$

where b = sliding distance of plane of atoms from one equilibrium position to another

a' = distance between slip planes

If $b \simeq a$ and $\frac{\tau}{G} \simeq \frac{\sigma}{E}$:

$$\sigma_{th} = \frac{E}{2\pi} \simeq 0.16E$$

However, in a perfect crystal plastic deformation may occur more easily by slippage of an isolated region enclosed by a dislocation loop requiring $\sigma \simeq 0.06E$.[3] Other estimates place the theoretical strength closer to 0.03E. The strengths of commonly used structural materials do not even approach these values. If steel had a $\sigma_{ult} = 0.03E$, it would have a strength of 900,000 psi. The reason for the relatively low strengths of materials used in industry is their intrinsic imperfection. Crystalline solids such as metals have an abundance of dislocations which cause premature plastic flow by their motion at low stress. Grain boundaries themselves may be regarded as imperfections since they are regions of disorder and high energy when compared to the crystal lattice. Impurities, voids and surface imperfections (e.g. scratches) all serve as stress raisers and are prime causes of the discrepancy between theoretical and observed strengths.

The distribution of defects in a solid obeys the laws of statistics. Thus, the smaller a specimen is, the fewer defects it will contain and with no defects the strength should equal the theoretical.

There are two main reasons why materials in fibrous form have higher strengths than in bulk form. In bulk form:

1. Brittle materials contain stress concentrators.
2. Ductile materials contain glissile dislocations.

Fibers and whiskers seek to improve upon bulk strengths by minimizing the number of stress concentrators and glissile dislocations. Stress con-

centrators are usually in the form of surface scratches. The Griffith formula for the bulk strength of a brittle solid is:[5]

$$\sigma_G = \left(\frac{E\gamma}{C}\right)^{\frac{1}{2}}$$

where σ_G = bulk strength

E = elastic modulus

γ = surface energy/unit area

C = depth of sharp crack (not a machined notch)

For cleavage, the surface energy of the fracture surfaces is equal to the work of fracture[5] so that:

$$2\gamma = \int_o^\infty \sigma_t du$$

where σ_t is the stress at the tip of an advancing crack and du is the incremental strain of atoms on either side of the cleavage plane. Beyond a characteristic displacement, u_f, the force necessary to separate the two cleaved portions is zero so that:

$\int_o^\infty du = u_f \simeq b$, the atomic spacing. σ_t is the theoretical strength of the material assumed to be $\frac{E}{10}$. Then:

$$2\gamma = \frac{E}{10}u_f = \frac{E}{10}b$$

and $$\gamma = \frac{Eb}{20}$$

The Griffith formula then becomes:

$$\sigma_G = \left(\frac{E^2 b}{20C}\right)^{\frac{1}{2}}$$

For a small scratch of 500b:

$$\sigma_G = \left(\frac{E^2 b}{20 \cdot 500b}\right)^{\frac{1}{2}} = \frac{E}{100}$$

which is a decrease in strength by a factor of 10 compared to σ_t. This is why brittle fibers (such as glass) present such a delicate handling problem.

The problem of glissile dislocations as a cause of decreasing material strength may be solved by the use of ceramic or intermetallic fibers since at room temperature dislocations in these materials are immobile. Only above the inflection temperature which is approximately 0.5 T_{MP} (absolute) do dislocations become mobile enough to allow significant plastic flow to occur. Since for ceramics and intermetallics T_{MP} is very high, these fibers in metallic matrices provide considerable strengthening even at temperatures at which the matrix is softened.

The failure of brittle whiskers at room temperature is affected very little by the dislocation density as exemplified by the work of Pearson et al.[2] on silicon whiskers. By introducing dislocations into silicon whiskers by deformation at elevated temperature and subsequent testing at room temperatures it was found that whisker strength was essentially the same as dislocation-free whiskers. Conversely, ductile whiskers such as copper, nickel and iron are quite sensitive to dislocation density. Their strengths may be decreased several orders of magnitude by the introduction of dislocations. The interpretation of these observations is that in brittle materials, the stress necessary to initiate and propagate a cleavage crack is less than the stress necessary to form and/or move a dislocation. In ductile materials the opposite is the case.

Whiskers with very few defects have been grown with strengths equal to the theoretical. (ASTM definition of whisker: a single crystal in the form of a fiber. Fiber: any material in elongated form so that the minimum length to maximum average transverse dimension ratio is at least 10:1 with a maximum cross-sectional area of 7.9×10^{-5} in^2 (corresponding to a diameter of 0.01") and a maximum transverse dimension of 0.01".[6]) Some whisker strengths are ($\times 10^{-6}$ psi):[2,6]

Al_2O_3	3.0
BeO	2.8
B_4C	2.0
SiC	3.0
C	3.5
Cr	1.29
Cu	0.427
Fe	1.9

The high strengths are a result of the small number of defects which in turn is a result of the small size of whiskers. Thus, in order to utilize the potential strength of materials, they must be used in whisker form. The result of this conclusion is the fiber composite material in which whiskers or fibers are surrounded by a suitable matrix which protects the reinforcing phase and transfers the applied load to it. Although the strengths of fibers are not as high as those of whiskers, they are much greater than those of bulk materials. The cost of fibers is not prohibitively high as is the case with most whiskers and most industrial applications of fiber composites utilize fibers. Some fiber strengths and costs are given below:[6]

Fiber	Strength($\times 10^{-3}$ psi)	Cost ($/lb, 1966)
Carbon	200	>500
SiO_2	850	30
Tungsten	580	710
Steel	600	50
Beryllium	185	10,000

For clarification, a fiber composite is defined as:[6] "a material consisting of two or more discrete physical phases in which a fibrous phase

is dispersed within a continuous matrix phase." In order to utilize the high strength of the reinforcing phase to the fullest, the fibers are aligned with their axes parallel to the direction of the applied load. However, fibers may be in the form of a mat as is the case with "fiberglass" to provide reinforcement in two directions.

Some advantages of fiber composites over conventional materials are:[6]

1. High strength and strength/density ratio
2. Good high temperature strength
3. High stiffness/density ratio
4. Good fatigue and creep strengths.

Fiber composite materials may have continuous or discontinuous fibers which may be aligned parallel to the stress axis or have a random orientation. The fibers may comprise a large proportion of the composite volume or only a small part of it. They may be either brittle or ductile in a brittle or ductile matrix. Composite strength, stiffness and other properties are functions of these variables, a fact which is partly responsible for the enthusiastic interest in composite materials and which indicates the potential of fiber composites; by manipulating these variables, a fiber composite can be tailor-made for a particular application with properties such as yield strength, U.T.S., E, Poisson's ratio, thermal conductivity and expansion and electrical conductivity controlled by varying composite parameters.

There are two ways to produce a unidirectional fiber composite (fibers aligned parallel to stress axis). The more popular method, the one used to produce essentially all industrial fiber composites in use today, is to grow whiskers or produce fibers separately and, after

arranging them in the desired configuration, to introduce the matrix material. A fairly recent and very promising technique is the unidirectional solidification of certain alloys. In this method, as solidification proceeds, a hard, strong second phase solidifies from the melt in the form of whiskers or platelets surrounded by a ductile matrix which in most cases is a solid solution.

(B) Theoretical Considerations

i) The Composite

The properties, both physical and chemical, of a fiber composite are determined by the properties and interactions of its constituents. These are the fiber, the matrix and the interface between the two. Any study of fiber composites must, of necessity, examine these three areas.

Notwithstanding the complexity of fiber composite behaviour and the variability of constituents, the strength and thermoelastic properties (E, u, thermal expansion and conductivity) of many fiber composites may be described by a few relatively simple relationships.

Several models are used to simulate and interpret fiber composite behaviour. The most straightforward of these is the rule of mixtures model which is a micromechanical approach wherein the primary components are equivalent to springs in a mechanical system,[7] and which applies only for continuous fibers. The longitudinal property of the composite is equal to the weighted sum of the properties of the constituents acting in parallel so that:

$$P_c = V_f P_f + V_m P_m \qquad 1$$

where P_c = composite property, P_f and P_m are the properties of the constituents,

and V = volume fraction of the constituent

Subscripts f and m signify fiber and matrix respectively. For transverse properties the constituents act in series so that:

$$\frac{1}{P_c} = \frac{V_f}{P_f} + \frac{V_m}{P_m} \qquad 2$$

Both longitudinal and transverse properties depend on the degree of perfection of the composite. The presence of voids or impurities can cause discrepancies between theoretical and experimental composite properties. The mechanical properties are especially sensitive to voids, fiber flaws and the degree of interfacial bonding. Nevertheless, agreement between practical and theoretical longitudinal properties is excellent in most fiber composite systems studied. McDanels, Jech and Weeton[8] were the first to show that the tensile strength of fiber reinforced metals could be predicted by the rule of mixtures. They showed that for copper reinforced with continuous tungsten wire:

$$\sigma_c = A_f\sigma_f + A_m\sigma_m' \qquad 3$$

where A = area fraction in a cross-section of fiber composite

σ_m' = stress in matrix at failure strain of fiber

σ_f = tensile strength of fiber

Transverse properties are only approximated by the rule of mixtures. Fig. 1 illustrates the comparison between experimental values and the rule of mixtures.[7] The transverse properties as predicted by other models vary greatly depending on geometrical variables and assumptions made.

It should be noted that in equations 1 and 2 there is no mention of geometrical variables such as fiber shape or interfiber spacing nor is there consideration of the degree of interfacial bonding. The mechanical properties are known to depend implicitly upon these variables

but properties such as thermal and electrical conductivities may be assumed to be independent of these parameters.

For a composite containing continuous brittle fibers the strain in the matrix and fiber is the same neglecting end conditions and if the volume fraction of fibers, V_f, exceeds a minimum value, V_{min}, (Fig. 2) composite strength is given by:[9] (cf. equ'n.[3])

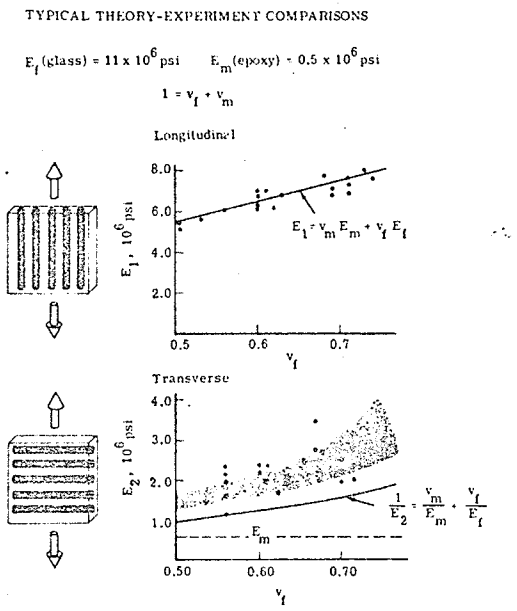

Fig. 1[7] Comparison of experimental and theoretical moduli of elasticity for glass fiber reinforced epoxy.

$$\sigma_c = V_f\sigma_f + (1 - V_f)\,\sigma_m' \qquad 4$$

where $(1 - V_f) = V_m$, $(V_f + V_m = 1)$

A typical variation of composite strength with V_f is shown in Fig. 3 for tungsten wire reinforced copper.

It is important to note that σ_f in equation 4 is the strength of the fiber in the matrix which may be different from the strength of an isolated fiber because of adverse chemical reactions between fiber and

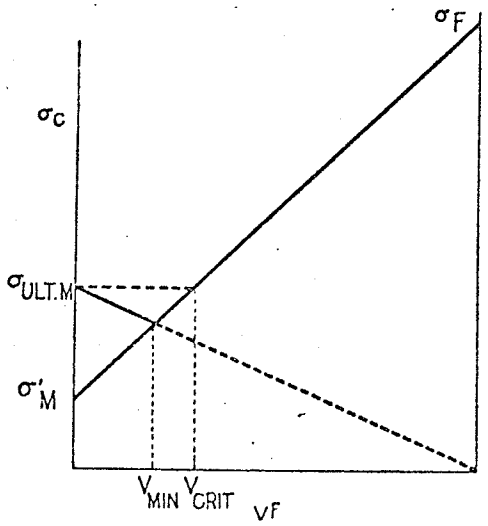

Fig. 2[10] Illustration of V_{min} and V_{crit} Nomenclature

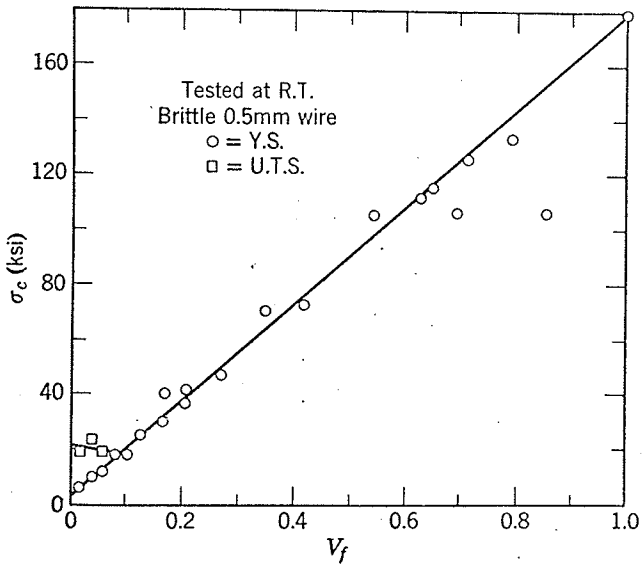

Fig. 3 Variation of composite strength with fiber volume fraction.[11]

matrix or because of annealing of the fiber during incorporation into the matrix.

Although the model used to develop the theoretical background assumes that the fibers are brittle and the matrix is ductile, the treatment also holds true for ductile fibers.[12] Fracture phenomena will differ depending on which type of fiber is present.

In a ductile matrix if the volume fraction of brittle fibers is small (less than V_{min}), the composite will not fail when the fibers fail but rather the matrix will work harden and assume the load of the broken fibers. In this case, the strength of the composite is governed by the strength of the matrix, and is given as:

$$\sigma_c = \sigma_{um} (1 - V_f) \qquad 5$$

where σ_{um} = UTS of the matrix.

If composite strength is to be described by equation 4, V_f must be greater than V_{min} in which case the composite will fail when the fibers fail. V_{min} may be found by equating σ_c in equations 4 and 5.

$$V_f\sigma_f + (1 - V_f)\sigma'_m = \sigma_{um} (1 - V_f)$$

Here $V_f = V_{min}$ so that:

$$V_{min} (\sigma_f - \sigma'_m + \sigma_{um}) = \sigma_{um} - \sigma'_m$$

and

$$V_{min} = \frac{\sigma_{um} - \sigma'_m}{\sigma_f + (\sigma_{um} - \sigma'_m)} = \frac{\sigma_{WH}}{\sigma_f + \sigma_{WH}}$$

where σ_{WH} = increase in tensile stress in the matrix due to work hardening.

It is seen from Figures 2 and 3 that if the fiber composite is to be stronger than the pure matrix material, the volume fraction of fibers must exceed V_{crit}. V_{crit} may be found by equating σ_c from equation 4 to the ultimate matrix strength so that:

$$\sigma_c = \sigma_{um} = V_{crit}\,\sigma_f + (1 - V_{crit})\sigma'_m$$

and solving for V_{crit}:

$$V_{crit} = \frac{\sigma_{WH}'}{\sigma_f - \sigma_m} \qquad 6$$

The effect of a decrease in σ_f is to increase V_{min} and V_{crit} and to lower the strength of the composite as shown in Fig. 4.

The preceding discussion applies to composites with continuous fibers but not all composites possess continuous fibers. Some fibers may be broken in handling or may break under a small stress due to imperfections or the fibers may be inherently discontinuous such as whiskers are. Composites containing discontinuous fibers behave slightly differently from those with continuous fibers. The matrix transfers the applied load to discontinuous fibers by means of shear stresses. Because the elastic modulus of the matrix material is less than that of the fibers, the matrix strain will be greater than the fiber strain under load.

The transfer of stress from the matrix to the fibers may be in one of two ways. First, if the interfacial bond is "hard", there will be no relative motion between the fiber and the layer of matrix atoms next to it, and load transfer is by matrix shear stresses. Secondly, the bond may be of a friction type in which the fiber is loaded by friction between itself and the matrix as is the case for glass fiber reinforced resins. In either case the fiber is loaded by a shear stress but the difference between the two types of load transfer is that in the first case the matrix shear strength is the limiting factor while in the second case it is the interfacial shear strength which limits the degree of stress transfer to the fibers.

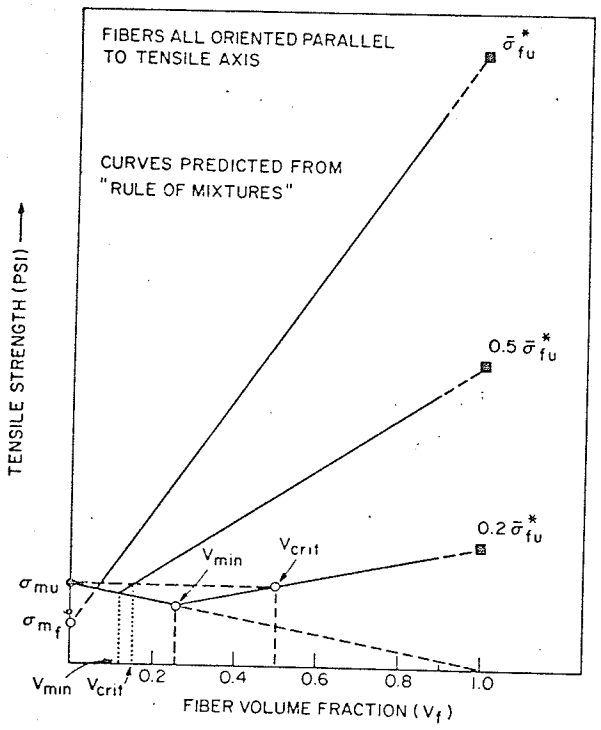

Fig. 4 Effect on V_{min}, V_{crit} and rule of mixtures composite strength of decreasing the UTS of the fibers to 50% and 20% of ultimate fiber strength, σ^*_{fu}. [6]

On loading a composite with discontinuous fibers the shear stress, τ, in the matrix is greatest at the ends of fibers as shown in curve 1 of Fig. 5(A).

As loading is continued the shear stress in the matrix will reach the yield stress and plastic flow will occur. If it is assumed that no work hardening occurs, the stress distribution in the matrix adjacent to the fiber at a later stage of loading will be as shown in curve 2 of Fig. 5(A). As loading is continued, provided that the fiber strength is high enough or the yield stress in the matrix is low enough, plastic deformation will occur in the matrix along the whole length of the fiber,

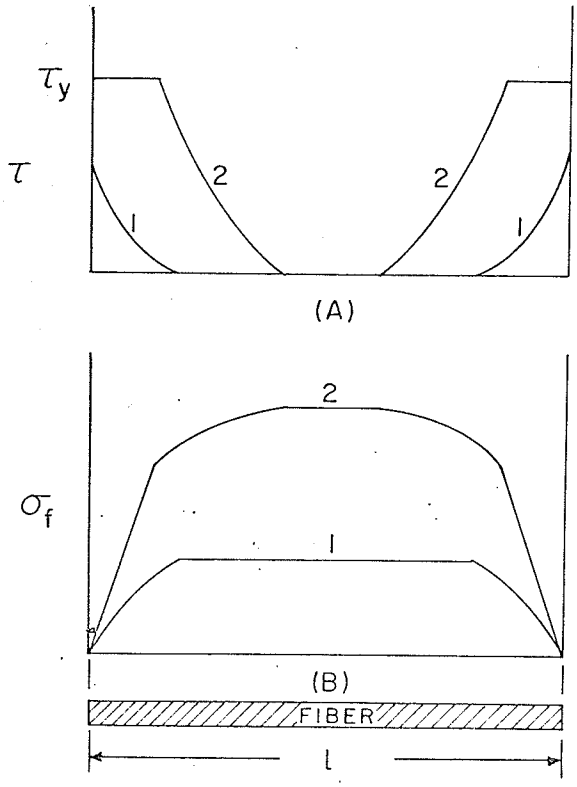

Fig. 5 Variation of matrix shear stress (A) and fiber tensile stress (B) with distance along the fiber. l = fiber length.

since in most fiber composite systems the fracture strain of the fibers is greater than the yield strain of the matrix. The stress distribution in the fiber as the applied load is increased is shown in Fig. 5(B). After plastic flow has occurred along the length of fiber, the fiber stress distribution is as shown in Fig. 6 which indicates a linear build-up of stress from the fiber ends to the UTS of the fiber.

There is a minimum length of fiber necessary to develop the UTS of the fiber and cause fracture. If the length of fiber is less than 2a in Fig. 6, the fiber will not fail because the length available for the matrix shear stress to act upon in inadequate. This minimum length

of 2a is the critical length, l_c.

Following the analysis of Kelly and Tyson[11] the response of a fiber composite may be described by reference to Fig. 7.

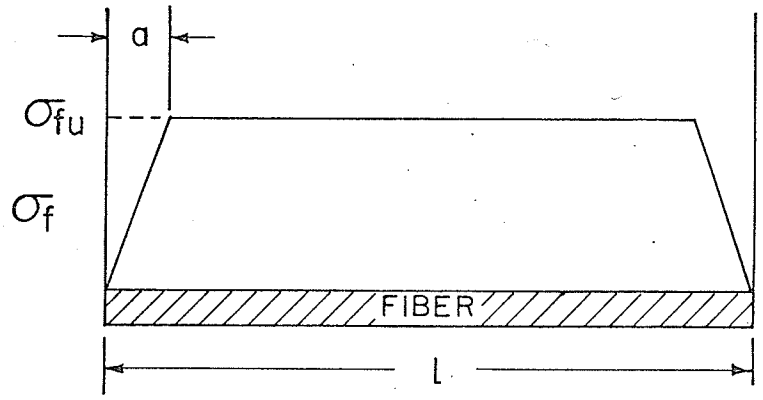

Fig. 6 Stress distribution in fiber.

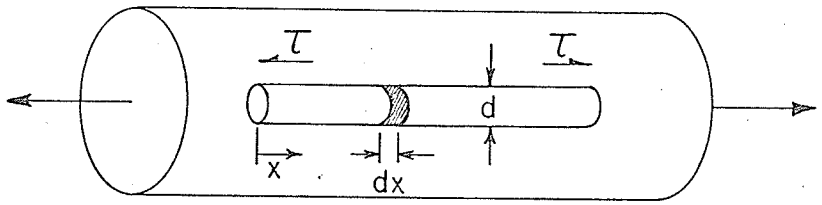

Fig. 7 Fiber embedded in a ductile matrix.

Assuming that the matrix does not work harden, $\tau = \tau_y$, the yield stress in shear of the matrix. Considering an element of fiber dx long:

$$dP = \pi d\tau dx \qquad (7)$$

Integrating from x = o to x = x:

$$P = \pi d\tau x$$

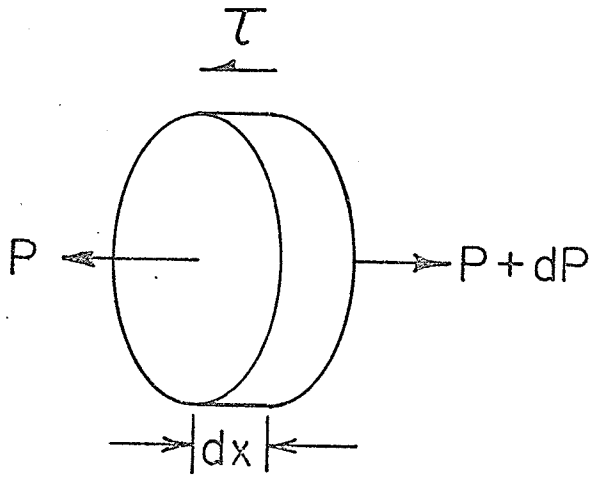

If σ_f' is the stress in the fiber, then:

$$P = \frac{\pi d^2}{4}\sigma_f'$$

and $$\frac{\pi d^2}{4}\sigma_f' = \pi d\tau x$$

For x<a in Fig. 6:

$$\sigma_f' = \frac{4\tau}{d}x \qquad 8$$

And solving for x:

$$x = \frac{\sigma_f' d}{4\tau} \qquad 9$$

In order to transfer enough load to the fiber so that its UTS may be attained x must be at least equal to a in Fig. 6 and $a = \frac{l_c}{2}$ Thus in equation 9:

$$\frac{l_c}{2} = \frac{\sigma_f d}{4\tau}$$

or $$\frac{l_c}{d} = \frac{\sigma_f}{2\tau} \qquad 10$$

where $\frac{l_c}{d}$ is called the aspect ratio which is defined as the ratio of the length to thecharacteristic transverse dimension of an elongated body. If the interface is weaker than the matrix in shear, τ as shown in Fig. 7 is the shear stress developed by the interface.

The rule of mixtures as given in equation 4 can be modified to describe the strength of composites containing discontinuous fibers. If the fiber stress distribution is as shown in Fig. 6 and the fiber length, $l > l_c$, σ_f in equation 4 is replaced by $\overline{\sigma}_f$, the average stress in a discontinuous fiber. Thus:

$$\overline{\sigma}_f = \sigma_f\left(\frac{l - l_c}{l}\right) + \sigma_f\left(\frac{l_c}{2l}\right) = \sigma_f\left[1 - \frac{l_c}{2l}\right]$$

Substituting this value into equation 4, for discontinuous fibers:

$$\sigma_c = \sigma_f V_f\left(1 - \frac{l_c}{2l}\right) + \sigma'_m \ (1 - V_f) \qquad 11$$

In most fiber composites the combined behaviour of fiber and matrix yields a stress distribution in the fibers as shown in Fig. 6. However, in cases where the U.T.S. of the fibers is attained before plastic flow of the matrix occurs all along the fibers or when the matrix work hardens to produce a non-linear stress build-up at the fiber ends the final state of fiber stress may be as shown in curve 1 of Fig. 5(B). In this case $\overline{\sigma}_f$ will be different from the value for a linear stress build-up. Kelly[12] solves for $\overline{\sigma}_f$ using a constant, β, which is dependent on the type of stress build-up. Following Kelly:

$$\overline{\sigma}_f = \sigma_f\left(\frac{l - l_c}{l}\right) + \sigma_f \beta \frac{l_c}{l} = \sigma_f \left[1 - (1 - \beta)\frac{l_c}{l}\right]$$

Substituting into equation 4:

$$\sigma_c = \sigma_f V_f \left[1 - (1 - \beta)\frac{l_c}{l}\right] + \sigma'_m (1 - V_f) \qquad 12$$

If the stress build-up is linear, $\beta = 0.5$ and equation 12 is the same as equation 11.

An alternate approach to determine the stress distribution in the fiber and matrix is to consider a fiber embedded in a matrix which is given a strain ε.[9,10] Both fiber and matrix are strained elastically and the fiber is stressed by shear stresses in the matrix due to differing elastic moduli between matrix and fiber. From Fig. 7:

$$\frac{dP}{dx} = \pi d\tau = H(u - v) \qquad 13$$

where H = a constant

u = fiber displacement

v = matrix displacement

Differentiating equ'n 13:

$$\frac{d^2P}{dx^2} = H\left(\frac{du}{dx} - \frac{dv}{dx}\right) \qquad 14$$

But $\frac{du}{dx} = \varepsilon_f = \frac{\sigma_f}{E_f} = \frac{P}{E_f A_f}$

and $\frac{dv}{dx} = \varepsilon$

Therefore $\frac{d^2P}{dx^2} = H\left(\frac{P}{E_f A_f} - \varepsilon\right)$

Solving for $\frac{P}{A_f}$ $(= \sigma_f)$:

$$\sigma_f = \varepsilon E_f \left[1 - \frac{\cosh \beta\left(\frac{l}{2} - x\right)}{\cosh \beta\left(\frac{l}{2}\right)}\right] \qquad 15$$

where $\beta = \left[\frac{H}{E_f A_f}\right]^{\frac{1}{2}}$

and H depends on the geometry of the composite.

For a composite with fibers of length l and radius r_o and a distance 2R apart (centre to centre) neglecting the effect of fiber ends:

$$H = \frac{2\pi G_m}{\ln(R/r_o)}$$

where G_m = shear modulus of matrix

and $$\beta = \left[\frac{G_m}{E_f}\ \frac{2\pi}{A_f \ln(R/r_o)}\right]^{\frac{1}{2}} \qquad 16$$

From equations 13 and 15:

$$\tau = \varepsilon E_f \left[\frac{G_m}{2E_f \ln(R/r_o)}\right]^{\frac{1}{2}}\ \frac{\sinh\beta(\frac{l}{2} - x)}{\cosh\beta(\frac{l}{2})} \qquad 17$$

The variation of σ and τ as given in equations 15 and 17 is shown in Fig. 8.

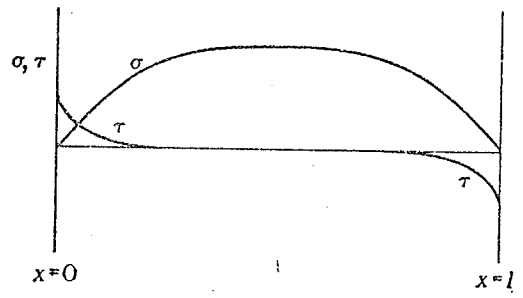

Fig. 8[9] Variation of σ and τ along a fiber as given in equations 15 and 17.

σ_f will increase more rapidly from zero at the fiber ends with increasing values of $\frac{G_m}{E_f}$ in equ'n. 16 i.e. for a given reinforcement, composite strength will increase with increasing values of G_m.

An insight into composite behaviour can be obtained by dividing the maximum shear stress, $\varepsilon E_f \left[\frac{G_m}{2E_f \ln(R/r_o)}\right]^{\frac{1}{2}}$ (equ'n. 17)

by the maximum fiber stress, εE_f (equ'n. 15). The result is:

$$\frac{\tau_{max}}{\sigma_{fmax}} = \left[\frac{G_m}{2E_f \ln(R/r_o)}\right]^{\frac{1}{2}}$$

$\ln(R/r_o) \simeq 0.5$ describes a reasonable composite geometry for moderate V_f so that:

$$\frac{\tau_{max}}{\sigma_{fmax}} \simeq \left[\frac{G_m}{E_f}\right]^{\frac{1}{2}}$$

from which it can be concluded that for a reasonable value of G_m/E_f of 0.1, $\tau_{max} \simeq 0.3\ \sigma_{max}$ which would place τ_{max} well above its yield stress in shear. This treatment exemplifies the desirability of a ductile matrix to relieve the matrix shear stress along the fibers. In a brittle matrix fracture would likely occur at the fiber ends if the high matrix stress could not be relieved.

It is obvious from equations 4 and 11 that, all things equal, a composite utilizing discontinuous fibers will be weaker than one using continuous fibers since $\bar{\sigma}_f < \sigma_f$. But the decrease in strength is not serious in most cases. If $l/l_c = 10$, then equ'n. 11 indicates that 95% of the continuous fiber composite strength will be realized. Fig. 9 illustrates the variation of σ_c with l/l_c.

Gordon[13] has succeeded in growing silicon nitride whiskers up to 3 cm long (2μ diameter) with strengths of approximately 10^6 psi. For these whiskers in an aluminum matrix:

$$\tau \simeq \frac{\sigma_{ym}}{2} = 2000 \text{ psi}$$

Substituting into equation 10:

$$l_c = \frac{10^6 (2 \times 10^{-4})}{2(2000)} = 0.05 \text{ cm.}$$

$$\text{and } \frac{l}{l_c} = \frac{3}{0.05} = 60$$

These whiskers would strengthen the fiber composite to essentially the same degree as continuous whiskers. But the minimum length of Gordon's

whiskers was 1 mm. For these whiskers:

$$\frac{l}{l_c} = \frac{0.1}{0.05} = 2$$

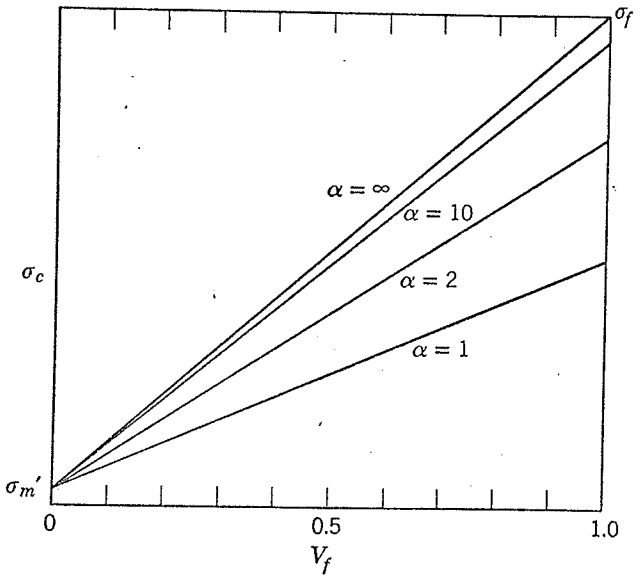

Fig. 9[11] Theoretical variation of σ_c with V_f for discontinuous fibers ($\alpha = l/l_c$)

From Fig. 9 it is seen that the strength of a fiber composite with l/lc = 2 is significantly less than for continuous fibers. In equation 11 the term $(1 - \frac{l_c}{2l})$ becomes 0.75 so that only 75% of the continuous fiber strength is utilized for $\frac{l}{l_c} = 2$. The main disadvantage of whiskers is their short lengths but their high strengths tend to mitigate the effect of a small l/l_c ratio.

Equations 11 and 12 apply to composites containing fibers of only one length. It is quite likely that there will be a distribution of fiber lengths in a given composite so that some fibers will be shorter than l_c and some will be longer. The rule of mixtures may be modified to apply to this situation also. The average stress in fibers of length $\bar{l}$ which

is less than l_c is from equation 8:

$$\bar{\sigma}_{fl^-} = \tfrac{1}{2}\left[\frac{4\tau}{d}\left(\frac{l^-}{2}\right)\right] = \frac{\tau l^-}{d}$$

If V_{fl^-} is the volume fraction of fibers of length l^- and l^+ is the length of fibers whose lengths are greater than l_c, then adding a term for each of these types of fibers to equation 11 yields:

$$\sigma_c = \sigma_f(V_f - V_{fl^-})\left(1 - \frac{l_c}{2l^+}\right) + V_{fl^-}\frac{\tau l^-}{d} + (1 - V_f)\sigma'_m \qquad 18$$

Composite strength is also a function of fiber orientation. Ideally, the angle, ϕ, between the fiber axes and the stress direction should be zero. This is not a problem with continuous fibers but when whiskers or the method of unidirectional solidification is used to achieve a strong material, the degree of alignment may be a crucial factor in determining composite behaviour. Kelly and Davies[14] have delineated three regions of orientation each having its own characteristic failure mode. For a small misalignment, ϕ, of the fibers tensile failure of the fibers is the controlling factor and composite strength, σ, is described by:[14]

$$\sigma = \frac{\sigma_o}{\cos^2\phi} \qquad 19$$

where σ_o = composite strength at $\phi = 0$.

It is interesting to note that this relationship indicates a higher composite strength for ϕ small than for $\phi = 0^o$. This occurs because, when the fibers are slightly misaligned, the applied stress resolved onto the fibers is less than for perfect alignment.

The second region is for intermediate values of ϕ where failure is due to shear of the matrix or the interface. Here composite strength is given by:

$$\sigma = \frac{\tau}{\sin\phi\cos\phi} \qquad 20$$

where τ = shear strength of matrix or interface, whichever is weaker.

For large misorientations (ϕ approaching 90^{o}) it is proposed that the controlling factor is tensile failure of the matrix and:

$$\sigma = \frac{\sigma_{MP}}{\sin^{2}\phi} \qquad 21$$

where σ_{MP} = tensile strength of the matrix in plane strain.

It should be noted that τ and σ_{MP} in equations 20 and 21 respectively are not bulk properties of the matrix material since restraint by the fibers will slightly strengthen the matrix.

The strength-orientation behaviour is as shown below:

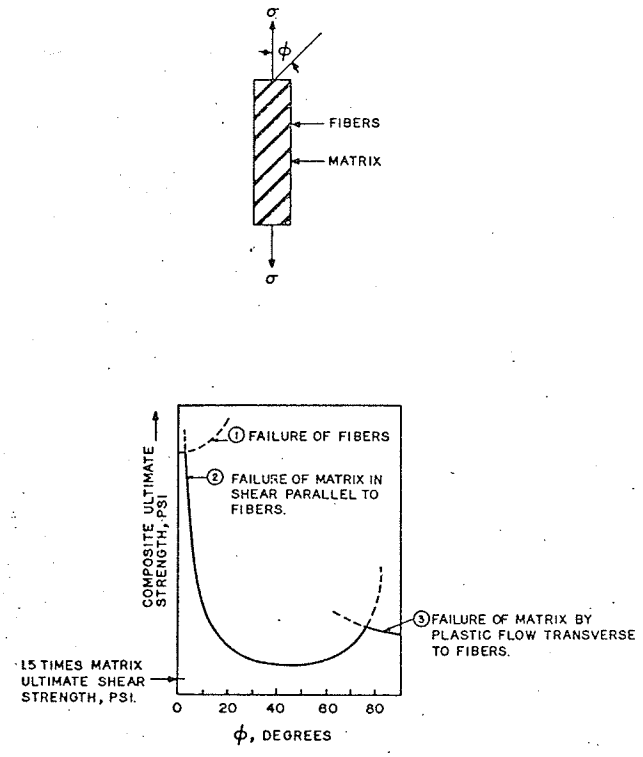

Fig. 10[15] Variation of composite strength with fiber orientation.

Maximum composite strength will be obtained when ϕ is at a maximum value limited by the transition point of the failure mode from fiber failure to matrix shear.[15] In order to find this value the stresses given in equations 19 and 20 are equated.[15]

$$\frac{\sigma_o}{\cos^2\phi} = \frac{\tau}{\sin\phi\cos\phi}$$

$$\text{and } \phi = \tan^{-1}\frac{\tau}{\sigma_o} \qquad 22$$

which is the value of ϕ at which composite strength is highest.

Jackson and Cratchley[15] in work on aluminum reinforced with stainless steel wires and Al-SiO_2 found good agreement of their results with equations 19 - 21. In the intermediate region of misalignment where composite failure is controlled by matrix shear they found that composite strengths were higher than values predicted by equation 20 because of the rotation of misaligned fibers toward the tension axis. The Al-Steel and to a lesser extent the Al-Silica composites exhibited a significant drop in strength only at large misalignments. At $\phi = 20^o$ for Al-Steel, composite strength was approximately the same as for $\phi = 0$ as is shown below.

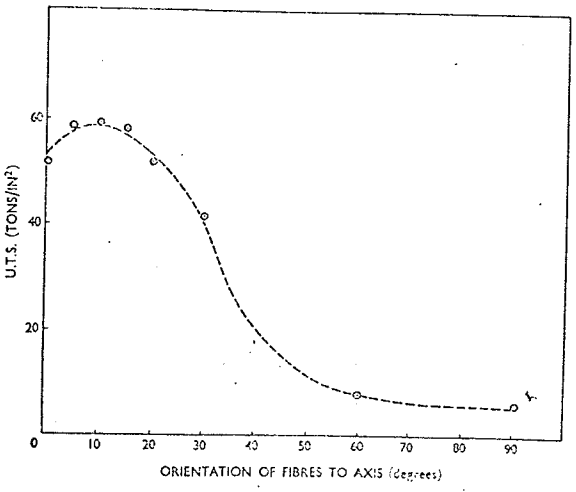

Fig. 11[15] U.T.S. of Al-Steel fiber composite

Whereas Kelly and Davies arrived at the above strength-orientation relationships via a micromechanical approach, Azzi and Tsai[16] using a macromechanical approach have advanced the following equation to describe the variation of composite strength with respect to orientation:

$$\frac{1}{\sigma^2} = \frac{\sin^4\phi}{\sigma_{90}^2} + \frac{\cos^4\phi}{\sigma_o^2} + \left(\frac{1}{s_1^2} - \frac{1}{\sigma^2}\right)\sin^2\phi\cos^2\phi$$

where: σ_{90} = transverse tensile strength of composite

σ_o = tensile strength of composite at $\phi = 0^o$

s = shear strength of composite.

They found results of tests on glass fiber reinforced resins to be in good agreement with this relationship.

ii) The Fiber

The previous analysis assumes that all fibers have the same

ultimate strength, σ_f. In many cases there will exist a random distribution of defects in the fibers which seriously impair their strengths. As the composite is loaded and fiber stresses increase, some fibers will fracture at their weak points at relatively low stresses. The load at cross-sections where fiber failures occur must then be carried by either the matrix (by work hardening) or by the other fibers. If the composite stress is high enough, failure of one fiber may increase the stress on the other fibers beyond their capacity and fracture will result. Thus, σ_f as used in equation 4 should actually be the mean UTS of a bundle of fibers and composite strength will depend on the distribution of fiber strengths which is dependent on the distribution of fiber defects. A statistical model is described by Rosen in Ref. 17.

Since it is statistically predicted that large diameter fibers contain more defects than smaller fibers, it would be expected that fiber strength would decrease as fiber size increases. The strength of fibers and whiskers has indeed been found to exhibit a dependence on size.[3,5] Although the scatter of strengths is usually quite large due to the method used to measure stress (bend tests usually give a higher strength than tensile tests) and the degree of perfection of the filament or whisker (dependent upon the method of fabrication) it may be stated that in general the strength of a fiber is inversely proportional to its characteristic transverse dimension. This behaviour is illustrated below.

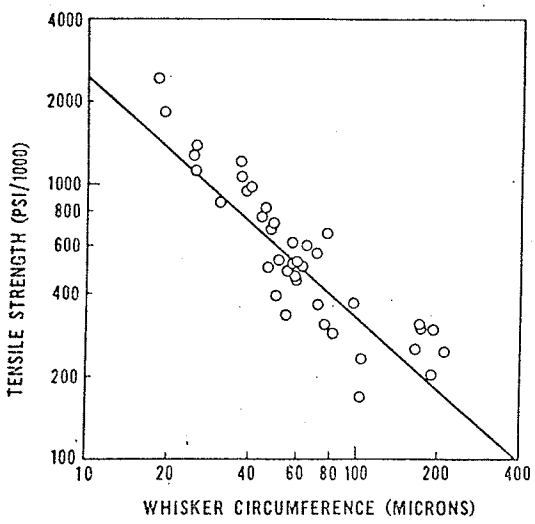

Fig. 12 Variation of the strength of Al_2O_3 whiskers with size.[3]

Davies,[5] in studying directionally solidified Sn - 5 wt.% Cu found that Cu_6Sn_5 intermetallic fibers exhibit this size dependence of strength. His findings are shown in Fig. 13.

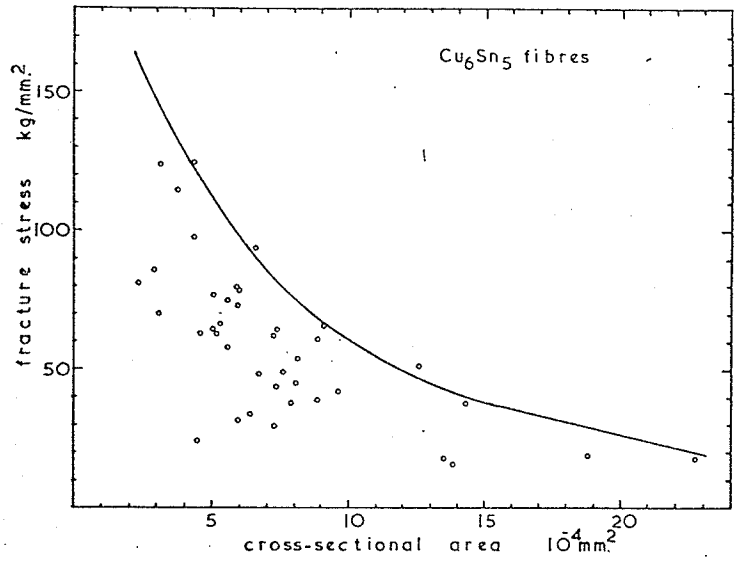

Fig. 13 Size dependence of Cu_6Sn_5 whiskers.[5]

The Cu_6Sn_5 whiskers were removed from the matrix and during testing failed on the (0001) plane (whisker axes were [0001]) by cleavage with cleavage planes located at surface steps formed during growth. Thus the size dependence of strength was attributed to the surface steps and observed scatter in strengths was attributed to variations in step geometry.

In work on Al_3Ni fibers[5], it was concluded that Al_3Ni fibers are tougher than Cu_6Sn_5 fibers because of a different growth step geometry.

The results of McDanels, Jech and Weeton[8] on cold drawn tungsten fibers in a copper matrix exemplifies the size-strength dependence of fibers of a large diameter.

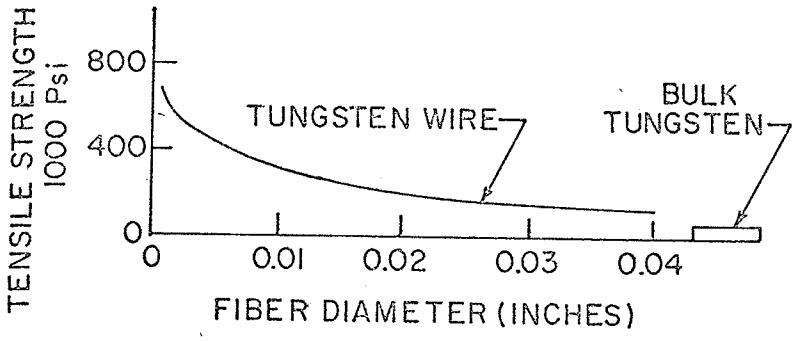

Fig. 14 Variation of UTS of W fibers with size.[8]

iii) The Matrix

The fact that most of the attention surrounding fiber composites is directed toward the reinforcing phase should not eclipse the importance of the matrix. In most composites the matrix is the only continuous phase and as such affects all composite properties as well as performing various special functions. Firstly, the matrix acts as a protective shield for the delicate fibers and whiskers. Exposed fibers

are easily damaged; the drastic reduction of fiber strength due to minute surface scratches was described in the previous section. A small shock would shatter the fibers because of their extreme brittleness in most cases if they were not protected by a cushioning matrix. The most important function of the matrix is to bond the fibers together so they may act as a unit and to distribute the applied load to them.

As was indicated, a very important property of the matrix material is its shear strength. It is important not only in relieving large localized stresses but in determining the transverse strength of the composite. It is seen in equation 20 that matrix shear strength is the controlling factor in composite failure at intermediate fiber misorientations. The shear strength in equation 22 is instrumental in determining the maximum tolerable fiber misalignment without loss of strength.

The strain hardening characteristics of the matrix are inherently involved in determining matrix strength and hence composite behaviour. Work by Mitra and Dorn[18] on the strain hardening behaviour of aluminum suggests that polycrystalline matrices have higher stress levels at given strains and have a higher UTS than single crystal matrices. The initial dislocation density in Al-Mg alloys (up to 3% Mg) tested was greater than in pure Al specimens and the density increased more rapidly with strain. It was concluded that large numbers of dislocations and the interactions and back stresses were responsible for the faster rates of strain hardening and higher strengths of polycrystalline and alloy aluminum compared to pure single crystal aluminum. Thus a matrix may be strengthened by alloying or by grain size refinement just as bulk materials are.

The tensile behaviour of the matrix influences the mode of fracture of the composite. Hertzberg and Kraft[19] working with unidirectionally solidified Cu-Cr eutectic found that fracture of the composite occurred by the linking up of voids due to fiber fracture and voids formed in the matrix with most of the matrix voids occurring at inclusions, grain boundaries and proeutectic Cr. Relatively few voids were formed at Cr whiskers. This behaviour illustrates the importance of matrix behaviour in affecting composite properties. If void formation in the matrix can be suppressed, composite strength may be increased. Hertzberg and Kraft[19] noticed a dependence of void formation on matrix grain size. With large grain size the number of voids was few and most of the deformation was confined to two slip bands at 45^{o} to the tension axis with eventual failure occurring by the coalescence of a sheet of voids at a boundary between a deformation band and a relatively undeformed region. (At the boundary the strain gradient is highest.) The larger number of voids with a small grain size is explained by the restraint on individual grains. With small grain size restraint is large and triaxial stresses are relieved by void nucleation. Inclusions offer prime sites for void formation so that void nucleation may be suppressed by the use of inclusion-free (high purity) materials.

Rogers[20] describes in detail the mechanisms of double-cup and cup-cone fracture in ductile materials. Chin et al.[21] in an explanation of ductile fracture consistent with that of Rogers state that inclusion free aluminum was found to neck to 100% reduction in area thus negating vacancy condensation or dislocation pile-ups as a cause of void formation. In relatively pure materials with few inclusions void formation is suppressed and failure is of the double-cup form. In more impure

materials where void formation is easier failure is of the cup-cone type. The conclusion drawn from these results is that void formation is dependent on impurity content and the mode of ductile failure is affected by the ease with which voids are nucleated. These same types of failure would be expected in fiber composite materials especially in failure of ductile lamellae in a unidirectionally solidified eutectic.

It is possible for the strength of a fiber composite to exceed the strength predicted by the rule of mixtures. Ductile fibers may be restrained from necking by the matrix thereby strengthening the composite[22] or dispersion strengthening may present a secondary strengthening mechanism. Kelly[9] suggests that for dispersion strengthening interparticle spacing should be less than 1000Å (0.1μ). In most fiber composites the interfiber spacing is greater than this but may approach 0.1μ for large V_f. The resistance to dislocation motion through a particle in a ductile matrix is due to:[12]

1. Disordering of the particle either internally or at the particle-matrix interface caused by passage of the dislocation.

2. Differences in elastic moduli between particle and matrix.

With incoherent ductile particles dispersed in a ductile matrix the resistance to passage of a dislocation may not be great. The stress necessary for a dislocation to be forced between particles is the Orowan stress which is approximately:

$$\tau = \frac{Gb}{l}$$

where G = Shear modulus of the matrix

b = Burgers vector

l = interparticle spacing.

This is the maximum stress possible to cause plastic flow (i.e. maximum

yield stress) but plastic flow may occur at a lower stress if dislocations pass through dispersed particles. Webb and Forgeng[2] offer arguments supporting the inefficacy of ductile particles in strengthening. Thus it would be expected that under conditions of dispersion strengthening brittle fibers would contribute more than ductile fibers to composite strength. The parameter used by Webb and Forgeng to measure the degree of strengthening by a dispersed phase is the specific strengthening effect, Σ_β which is given as:[2]

$$\Sigma_\beta = \frac{S - S_\alpha y_\alpha}{y_\beta}$$

where S = strength of alloy

y = volume fraction

α and β signify matrix and dispersed phases respectively.

In tests on Cu - 1% Cr, Σ_β^y (specific strengthening effect calculated from yield strengths) was the same as the yield strength of Cu-Cr saturated solid solution i.e. Cr precipitate was ineffective in increasing the yield strength. Cr crystals tested separately exhibited ductile behaviour. Other systems reinforced by Fe_3C and Si particles showed a Σ_β^y much higher than the yield strengths of the corresponding solid solutions. The large specific strengthening effect for brittle particles means that the Orowan stress is less than the flow stress of the dispersed particles and passage of a dislocation results in formation of dislocation loops around the particles thereby increasing the dislocation density of the matrix and causing a rapid rate of work hardening.

That fibers offer resistance to dislocation motion in the matrix has been verified by Koppenaal and Parikh[2 3] who have found that for silver containing mild steel, molybdenum and tungsten wires the Petch equation holds:

$$\sigma_y = \sigma_o + kd^{-\frac{1}{2}}$$

where σ_y = 0.2% offset yield strength

σ_o = friction stress

k = a constant

d = interfiber spacing.

In microstrain tests Koppenaal and Parikh established that the stress necessary to initiate plastic flow in the composite was independent of fiber volume fraction which indicates that plastic flow occurs first in the matrix. The 0.2% offset yield strength was dependent on fiber volume fraction and at larger strains the rate of work hardening increased with increasing fiber density because of resistance to dislocation motion by pile-ups at the fibers. Hence the analogy to grain boundary strengthening and the integrity of the Petch relationship.

iv) The Interface

The fiber-matrix interface may also be a source of toughness. It has been shown[24] that at the tip of an elliptical crack (an approximation to an actual crack) there is a tensile stress parallel to the plane of the crack as well as perpendicular to it. This stress tends to initiate a void or crack in a plane perpendicular to the plane of the crack. Crack arrest may occur by delamination at the fiber-matrix interface and composite toughness may thus be increased. Fiber composites strengthened by delamination are[25] Al-SiO_2, glass fiber reinforced resins, Cu-W and Cu-SiO_2.

Another mechanism of strengthening by interfaces was described by Cline and Stein.[26] In observing the tensile behaviour of directionally solidified Ag-Cu eutectic over a range of temperatures they noticed that

the flow stress of the lamellar composite (alternating platelets of Cu rich and Ag rich solid solutions) exceeded that of either pure silver or pure copper. Since solid solution strengthening was ruled out, the increased strength of the eutectic was explained by an image force concept wherein resistance to dislocation motion toward and across a platelet interface was explained by the assumed presence of a "mirror image" dislocation on the opposite side of the interface. The silver and copper platelets have the same F.C.C. crystal structure and because of the similarity of the lattice parameters, the interface is partially coherent. The resistance to dislocation motion across the interface is due to the change in strain energy of the dislocation because of a change in shear modulus as a dislocation crosses an interface and because of disordering the interface itself (formation of a step by the passage of a dislocation). The reader is referred to the original paper for a mathematical treatment. It should be noted, however, that interfacial strengthening is not present in all composites. In the Ag-Cu eutectic both phases are ductile possessing glissile dislocations and the partially coherent interface permits dislocations to pass from one phase to another. The possibility of significant coherency strains which would affect dislocation motion also exists. Interlamellar spacings ranged from a "normal" 3.8μ down to an extraordinarily fine 0.1μ. In most fiber composites (or lamellar eutectics) one phase is a brittle ceramic or intermetallic with an incoherent interface. Thus the behaviour of the reinforcement is completely different from the behaviour of the matrix (brittle vs ductile behaviour) in contrast to the two similar phases studied by Cline and Stein. The brittle reinforcement would not contain glissile dislocations at room temperature and any dislocations

in the matrix would not be able to cross the interface. Thus the model proposed by Cline and Stein would apply only to a composite comprising two ductile phases. An apparent shortcoming of Cline and Stein's analysis is their omission of any reference to a size effect of the platelets on composite strength. With interlamellar spacings comparable to whisker diameters one would expect platelet strengths to be significantly higher than the bulk strengths to which composite strength was compared. Consideration of the size effect would be expected to narrow and possibly even eliminate the gap between the flow stress of the Ag-Cu eutectic and that of pure Ag and Cu.

v) Transverse Strength

The transverse strength of a fiber composite may be described by the rule of mixtures, equation 2, as an approximation, but it is largely dependent on interfacial strength. If the interface is stronger than the matrix, composite failure will occur through the matrix avoiding the fibers. If the interface is very weak, failure will occur through the interfaces passing through as little matrix material as possible. A rigorous treatment considering the transverse tensile strength of a fiber composite material when interfacial strength is less than the matrix strength but still of significant magnitude has not been attempted. For a very weak interface an approximate description of composite strength is possible.[24]

The mean distance between fiber axes is estimated as $L = \frac{1}{\sqrt{N}}$ where N = number of fibers/unit transverse area. If the fiber radius is "a", the mean interfiber spacing is $d = \frac{1}{\sqrt{N}} - 2a$. Considering a composite of unit cross-section:

Area of fibers = V_f

Area/fiber $= \pi a^2$

so that N $= V_f/\pi a^2$

and $d = \left[\frac{\pi a^2}{V_f}\right]^{\frac{1}{2}} - 2a = a[(\pi/V_f)^{\frac{1}{2}} - 2]$

Since transverse strength decreases as the ratio $\frac{d}{L}$ increases, for weak interfaces the transverse tensile strength is:

$$\sigma_t = \sigma_m \left(1 - \frac{d}{L}\right) = \sigma_m \left[1 - 2(V_f/\pi)^{\frac{1}{2}}\right] \qquad 23$$

If the interfaces are stronger than the matrix phase, Kelly and Davies[14] suggest that:

$$\sigma_t \simeq 1.15\sigma_m$$

where σ_m = U.T.S. of the matrix material

which considers that the matrix is restrained by the fibers and is in a condition of plane strain. When the strength of the fiber-matrix interface is greater than zero but less than the matrix strength, Cooper and Kelly[24] suggest the application of the rule of mixtures which yields:

$$\sigma_t = \sigma_m \left[1 - (4V_f/\pi)^{\frac{1}{2}}\right] + \sigma_i' \, (4V_f/\pi)^{\frac{1}{2}} \qquad 24$$

where σ_i' is the stress required to separate the fiber from the matrix.

vi) Compression Behaviour

The behaviour of fiber composites in compression was studied by Rosen[17] who concluded that composite failure occurs by short wavelength buckling of the fibers. The buckling may be (A) in phase (Fig. 15(A)) in which case the matrix is deformed mainly by shear or (B) out of phase (Fig. 15 (B)) in which case the matrix is alternately in tension and compression.

Utilizing the strain energy approach Rosen states that for in phase

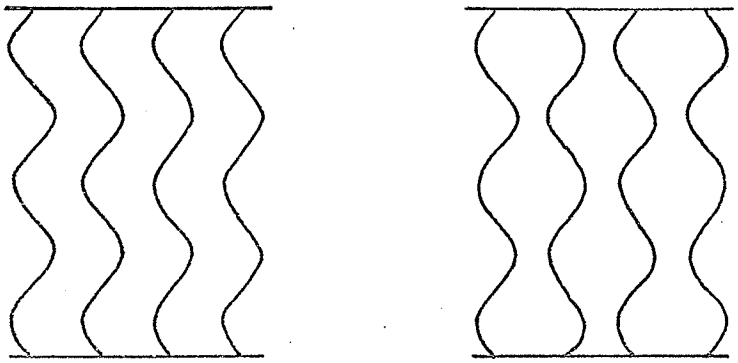

Fig. 15 Compression failure modes.

buckling the compressive strength of the composite, σ_{comp}, is given by:

$$\sigma_{comp} = \frac{Gm}{(1 - V_f)} \qquad 25$$

and for out of phase buckling:

$$\sigma_{comp} = 2V_f \left[\frac{V_f E_f E_m}{3 (1 - V_f)}\right]^{\frac{1}{2}} \qquad 26$$

The type of buckling (in phase or out of phase) must be determined experimentally but for large volume fractions of fiber the in phase mode is expected to occur. In tests on glass fiber reinforced resin Rosen found that at fiber volume fractions greater than 25% failure was by in phase buckling. The wavelength of buckling was found to decrease with decreasing fiber diameter. Because of approximations in the strain energy method and considering experimental results[17] equations 25 and 26 appear to describe an upper limit of compressive strengths.

vii) Stress-Strain Behaviour

Various researchers have studied the deformation behaviour of fiber composites in tension resulting in an understanding of the composite stress-strain curve. McDanels, Jech and Weeton[27] using the copper-tungsten model system have delineated four regions of the fiber composite stress-strain curve.

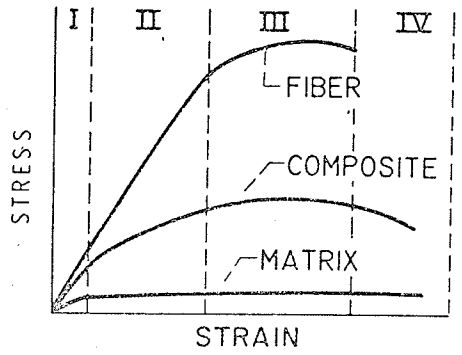

Fig. 16 Four regions of a fiber composite stress strain curve.

Figure 16 illustrates the four stages of deformation which are:[27]

1. Fiber and matrix both deform elastically. Stage 1 is then a linear relationship between stress and strain and represents only a small portion of the composite stress-strain curve since plastic flow of the matrix (which is usually ductile) occurs at very small strains (in the range of 0.03% for copper). The rule of mixtures gives the composite stress, σ', at any strain as:

$$\sigma'_c = \sigma'_f V_f + \sigma'_m (1 - V_f) \qquad 27$$

Assuming that in Stage 1 the fiber and matrix are strained equally (strictly true only for continuous fibers), $\varepsilon = \varepsilon_f = \varepsilon_m$.

Dividing equation 27 by ε:

$$\frac{\sigma_c'}{\varepsilon} = \frac{\sigma_f'}{\varepsilon_f} V_f + \frac{\sigma_m'}{\varepsilon_m} (1 - V_f)$$

and $E_1 = E_f V_f + E_m(1 - V_f)$ 28

which is the primary elastic modulus of the composite.

The type of interfacial bond affects the modulus of elasticity of the fiber composite. In a composite with well bonded fibers the composite modulus is given by the rule of mixtures (equation 28) but if some fibers have a partial bond or no bond at all, the modulus is decreased. For some fibers not bonded Greszczuk[28] states that the composite modulus obeys the relationship:

$$\frac{E_L^*}{E_L} = 1 - \left(\frac{E_f}{E_L}\right) k^*$$

where E_L^* = elastic modulus of composite with bonded and unbonded fibers

E_L = elastic modulus of composite with bonded fibers only

E_f - elastic modulus of fibers

k^* = volume fraction of unbonded fibers.

II. Fibers deform elastically while the matrix deforms plastically. Stage 2 exists when the onset of plastic flow in the matrix and fibers occurs at different strains and usually begins at a strain slightly higher than the yield strain of the matrix.[9] If the stress-strain curve of the matrix is linear at small plastic strains, the composite curve will have a linear secondary "elastic" region. The secondary modulus of elasticity which is usually much more prominent than the primary modulus is given as:

$$E_{11} = E_f V_f + \left(\frac{d\sigma_m}{d\varepsilon_m}\right) (1 - V_f)$$ 29

where $\frac{d\sigma_m}{d\varepsilon_m}$ is the slope of the matrix stress-strain curve in Stage 2.

If the slope of the matrix stress-strain curve in Stage 2 is not constant, then $\frac{d\sigma_m}{d\varepsilon_m}$ is the instantaneous slope at any particular strain and E_{11} will vary with $\frac{d\sigma_m}{d\varepsilon_m}$. If the composite is loaded to a stress in Stage 2 and then unloaded, a permanent set will remain since the matrix was strained plastically. As the applied load is decreased to zero, the fibers and matrix will contract but, because of the plastic deformation of the matrix, the residual condition of the composite will have the fibers in tension and the matrix in compression. If work hardening of the matrix is very slight, $\frac{d\sigma_m}{d\varepsilon_m}$ will be small and to a close approximation equation 29 becomes:

$$E_{11} = E_f V_f$$

III. Fibers and matrix deform plastically. This region occurs only for composites containing ductile fibers. The U.T.S. of the composite occurs at the same strain as the U.T.S. of the fibers.

IV. Fiber failures occur. For composites containing ductile fibers Stage 4 has a negative slope and is characterized by the random failure of fibers at their weak points. The fractured fibers continue to reinforce but their effect is decreased as the number of fractures increases. Eventually a single cross-section is sufficiently weakened to cause composite fracture. A characteristics stress-strain curve of a composite containing a large volume fraction of brittle fibers is shown in Fig. 17. In this case some random fiber failures may occur in Stage 2 but effective fiber loading is permitted to ε_{fu} at which point failure of one fiber initiates composite fracture at the cross-section of the fiber breakage.

A composite containing a fiber volume fraction less than V_{min} would be expected to exhibit a stress-strain curve as shown in Fig. 18.

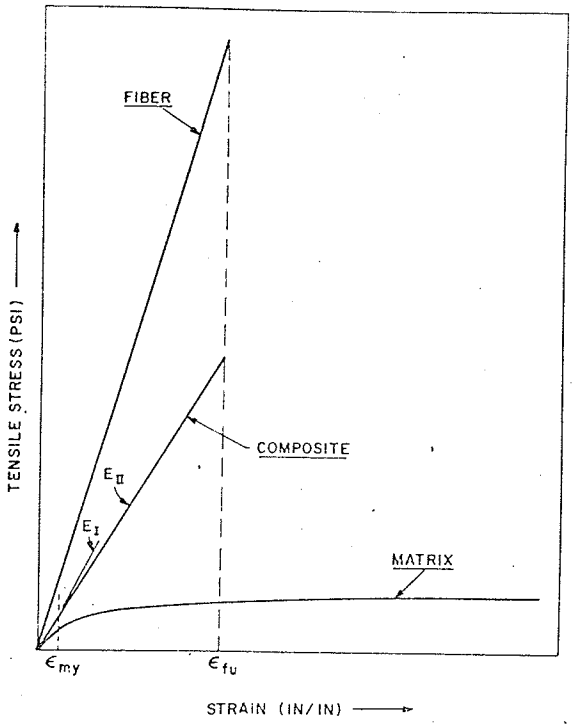

Fig. 17 Tensile stress-strain relationship of a brittle fiber, composite and matrix.[29]

As the composite is loaded, failure occurs at the highly stressed fiber midsections (or at random weak points) thus relieving the load which is soon built up again causing further failures. This process repeats causing strain hardening of the matrix and composite fracture eventually occurs at a stress given by equation 5.

Composites containing discontinuous fibers exhibit the same four stage behaviour as continuous fiber composites and, providing the ratio l/l_c is greater than about 5, their elastic properties are virtually identical to those of continuous fiber composites. McDanels, Jech and Weeton[27] found excellent agreement between equation 29 and experimental results for both continuous and discontinuous tungsten wire reinforced copper. Equation 28 predicted values of E, lower than experimental

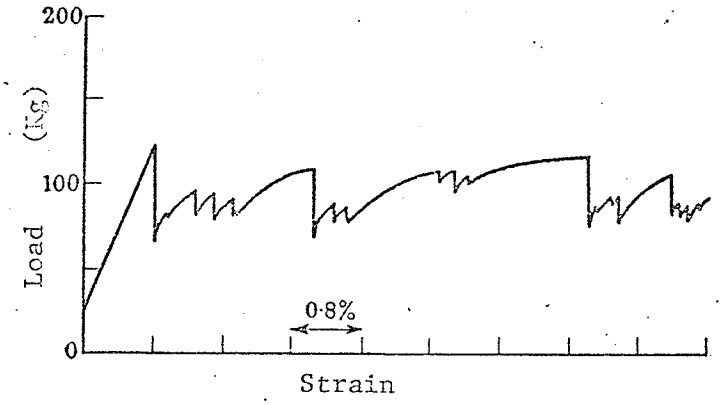

Fig. 18 Stress-strain curve of a fiber composite with $V_f < V_{min.}$[12]

values at fiber volume fractions above 30%. Hill[30] has, in fact, shown that equation 28 is a lower bound for composite elastic moduli. Hill also derived the "best possible" bounds for longitudinal fiber composite moduli independent of geometry but for statistical homogeneity and transverse isotropy. They are:

$$E \geqslant E_f V_f + E_m(1 - V_f) + \frac{4V_f\,(1 - V_f)(\nu_f - \nu_m)^2}{\frac{V_f}{k_m} + \frac{(1 - V_f)}{k_f} + \frac{1}{m_m}} \qquad 30$$

$$\text{and} \quad E \leqslant E_f V_f + E_m(1 - V_f) + \frac{4V_f\,(1 - V_f)\,(\nu_f - \nu_m)^2}{\frac{V_f}{k_m} + \frac{(1 - V_f)}{k_f} + \frac{1}{m_f}} \qquad 31$$

where: ν = Poisson's ratio

k = plane strain bulk modulus for lateral dilatation

m = modulus of rigidity for shear in a transverse direction.

$m_f > m_m$

The reason for deviation of composite elastic behaviour from the rule of mixtures is the difference in Poisson's ratio between the fiber and matrix. During the longitudinal extension the two components tend to contract transversely by differing amounts thereby restricting the freedom of the component with the larger Poisson's ratio. From equations 30 and 31 it is seen that as the two values of Poisson's ratio approach each other the bounds converge and for $\nu_f = \nu_m$ the rule of mixtures is exact.

Hill also derives the bounds for the composite Poisson's ratio:[30]

$$\nu_c > \nu_f V_f + \nu_m(1 - V_f) \quad \text{for } (\nu_f - \nu_m)(k_f - k_m) > 0$$

and $$\nu_c < \nu_f V_f + \nu_m(1 - V_f) \quad \text{for } (\nu_f - \nu_m)(k_f - k_m) < 0$$

As k_f approaches k_m the bounds converge and the rule of mixture applies for $k_f = k_m$.

The verification of the competence of equation 29 does not prove its universal applicability. The fibers used by McDanels, Jech and Weeton[27] were larger than 100μ in diameter and as such did not influence the independent behaviour of the matrix to a great extent. For a given fiber volume fraction interfiber spacing decreases with decreasing fiber size (diameter) and the constraint on the matrix increases. Kelly and Lilholt[31] working also with tungsten fiber reinforced copper but with fiber diameters of 10μ and 20μ calculated the matrix stresses in Stage 2 of the stress-strain curve from equation 4. The type of matrix behaviour they found is shown in Figure 19.

Kelly and Lilholt discount a dispersion strengthening effect because: A) It is thought that dislocation pile-ups would weaken the fibers and hence the composite. Composite strengths obeyed the rule of

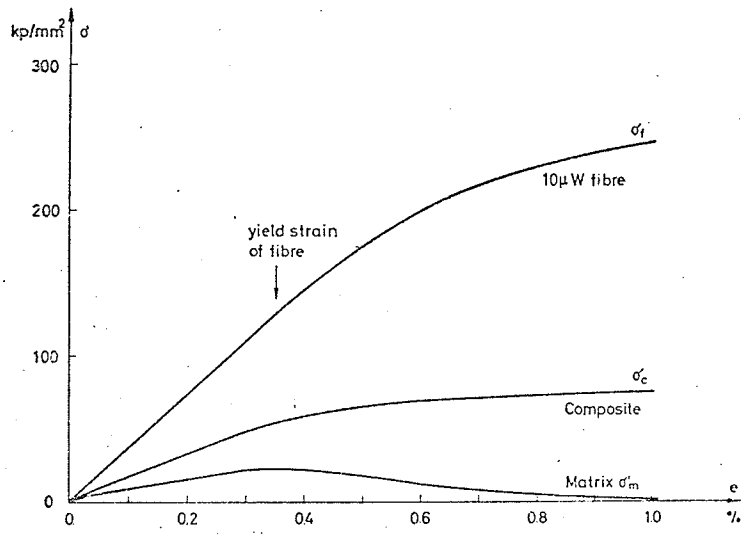

Fig. 19 Experimental stress-strain curves of 10µ tungsten fiber and of a composite with 30% fibers and the derived matrix stress-strain curve.[31]

mixtures. B) The large matrix stresses decreased as soon as the yield point of the fibers was reached as shown in Figure 19. C) A quantitative analysis indicates that the dispersion strengthening effect is not of sufficient magnitude to account for the large matrix stresses. On the basis of these considerations it was concluded that the large matrix stresses are due to constraint of the matrix caused by differing Poisson's ratios between fiber and matrix. In Stage 2 the effective matrix Poisson's ratio is 0.5 while the fiber Poisson's ratio is 0.28. The drop in matrix stress after fiber yielding is attributed to the relieving of matrix constraint when ν_f approaches ν_m. In Stage 3 where $\nu_f \simeq \nu_m$ the rule of mixtures behaviour is followed. Hill[32] states that equations 30 and 31 apply also in Stage 2 if instantaneous values of the matrix parameters are used. Further, he suggests that the secondary modulus will be close to the value given by equation

30. However, Kelly and Lilholt have used equation 31 with $E_m = 0$ and $\nu_m = 0.5$ in order to obtain the upper limit of E_{11}. Solving for σ'_m from equations 4 and 31 and differentiating to get $\frac{d\sigma'_m}{d\varepsilon_m}$ enabled them to compare experimental and theoretical values of the slope of the stress-strain curve of the matrix in Stage 2. The theoretical values of $\frac{d\sigma'_m}{d\varepsilon_m}$ (which are really the upper limits of this slope) were much lower than the experimental values. It is assumed that the discrepancy is due to a gradual transition to plasticity of the matrix rather than instantaneous yielding as equation 31 requires. Since some of the matrix remains elastic after initial yielding, its contribution to the composite modulus is greater than that indicated in equation 31 and as a result $\frac{d\sigma'_m}{d\varepsilon_m}$ is greater. By the assumption of different values of the ratio of volumes of yielded and unyielded matrix in Stage 2, experimental and theoretical values of $\frac{d\sigma'_m}{d\varepsilon_m}$ can be made to coincide.

The transverse elastic modulus does not lend itself to a simple description but the following bounds apply:[33]

$$\frac{1}{E_t} > \frac{V_f}{E_f} + \frac{(1 - V_f)}{E_m}$$

$$\frac{3}{E_t} < \frac{1}{G} + \frac{1}{3K}$$

where G = rule of mixtures modulus of rigidity

K = rule of mixtures bulk modulus.

viii) Fracture

In Stage 4 of the composite stress-strain curve after the first fiber fracture or after initiation of a matrix crack com-

posite fracture may be gradual or rapid depending on the nature of the constituents and fiber volume fraction. With a strong interface and continuous fibers composite fracture is expected to be planar and normal to the tension axis if matrix and fiber properties are uniform.[24] However, random fiber flaws detract from uniformity. Bonded in a ductile matrix, fibers fail randomly in Stage 4 and composite failure occurs by plastic flow of the matrix linking up adjacent fiber failures. The failure in this case is rapid at large fiber volume fractions with the work of fracture attributed to plastic flow of the matrix. This type of failure is shown in Figure 20.

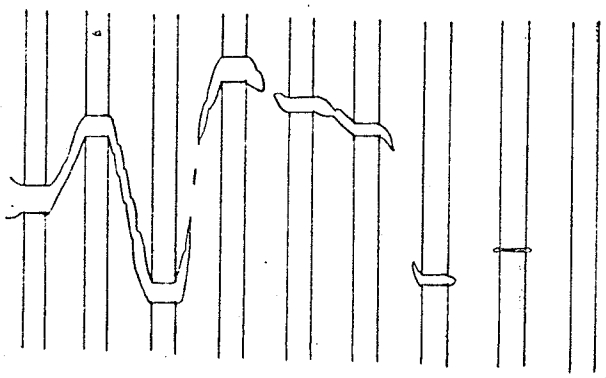

Fig. 20 (A)[24]
Failure of composite with ductile matrix

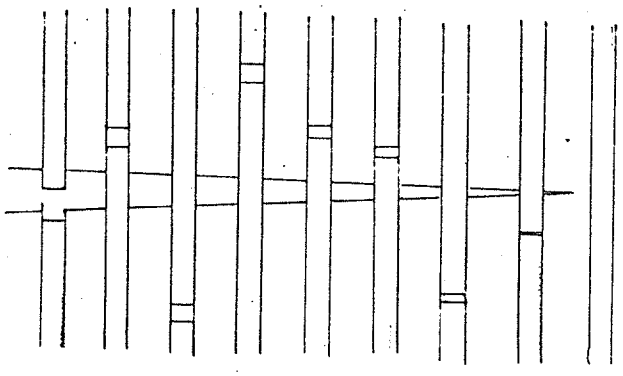

Fig. 20 (B)[24]
Failure of composite with brittle matrix

A composite with a brittle matrix (e.g. armoured glass, reinforced concrete or metal wire reinforced ceramics) will fail by initial crack propagation through the matrix and fiber failure adjacent to the matrix crack. Fiber pull-out is then responsible for the work of fracture.[24] This failure mode is also shown in Fig. 20.

Fracture toughness by fiber pull-out in either a brittle or ductile matrix is amenable to mathematical analysis. Although the ratio l/l_c should be large to maximize composite strength, for maximum toughness a value of $l = l_c$ is required. If $l < l_c$, failure of one fiber will not cause a rapid composite failure but rather the fibers will be pulled out of the matrix because the ultimate fiber strength cannot be attained. The greatest toughness occurs when l_c is large. In equation 10 it is seen that l_c is inversely proportional to τ so that a large fracture toughness can be obtained by the use of a ductile matrix or a weak interface. When $l = l_c$, the work of fracture is given as[34]:

$$W = \frac{1}{12} A_f \sigma_f l_c$$

where A_f = area fraction of fibers at the failure cross-section. Cooper and Kelly offer a more detailed mathematical analysis of fracture toughness for fiber composites with brittle matrices and for those with uniform fibers in Ref. 24.

ix) Elevated Temperature Application

Since the ceramics and intermetallics so often used as fibers retain much of their strength at elevated temperatures, fiber composites appear to be well suited to high temperature uses. Although the strengths of some refractory materials decrease steadily with increasing temperature, some refractories exhibit an inflection temper-

ature (the temperature above which rapid softening occurs). However, the inflection temperatures of refractories are high and even above the inflection temperatures refractories are relatively strong so they still continue to reinforce the matrix. For composites exhibiting an inflection temperature, it marks the transition from brittle to ductile fracture. From equation 10 $\frac{l_c}{d}$ is dependent on the matrix shear strength. At elevated temperatures the shear strength of ductile matrices is very small thus necessitating a long transfer length of fiber in order to load the fibers to failure (i.e. $\frac{l}{d}$ must be large). If the fibers are not long enough to develop a breaking stress, they will pull out of the matrix. Figure 21 gives an indication of the dependence of failure mode on aspect ratio.

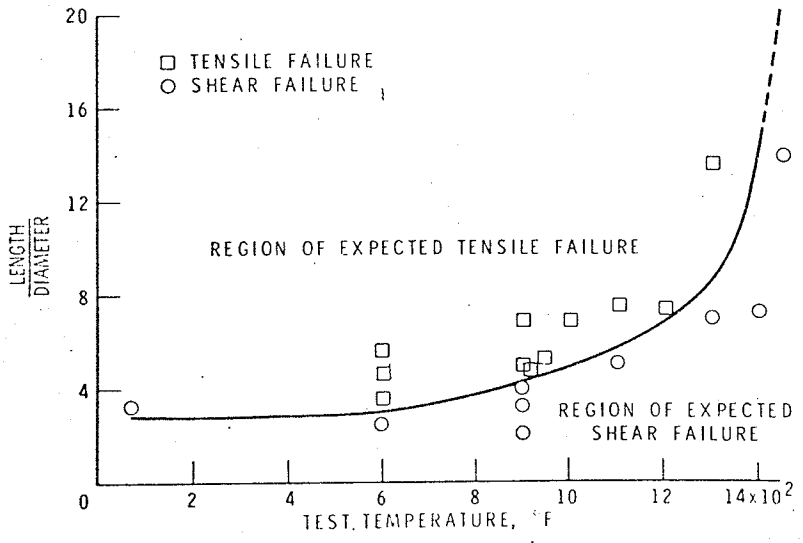

Fig. 21 Experimentally determined length/diameter ratios as a function of temp. for W wires in Cu.[22]

In the region of shear failure, $\frac{l}{l_c}$ is too small for fiber fracture to occur and the fibers pull out of the matrix.

The rule of mixtures describes composite strength at elevated

temperatures[22] but the fiber and matrix strengths used must be values at the temperature of interest.

The superiority of fiber composites over SAP and dispersion strengthened silver at elevated temperatures is indicated in Figures 22 and 23.

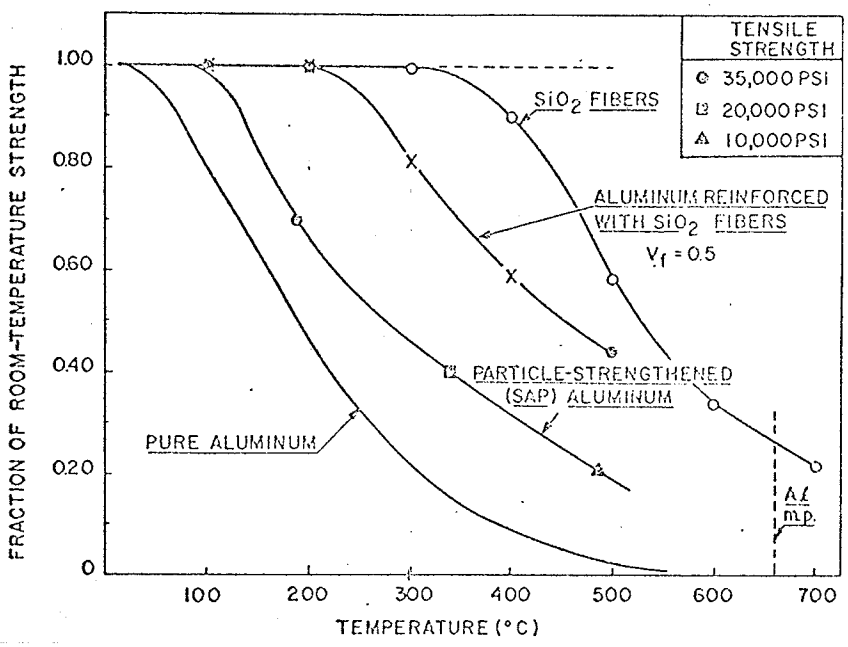

Fig. 22 Indication of superior high temperature strength of Al-SiO_2 fiber composite.[29]

(C) Unidirectional Solidification

Most metal matrix fiber composites are manufactured by infiltrating the fibers with the molten matrix. The methods of manufacture are expensive and are not amenable to mass production. The problem of fiber breakage during handling, especially when the fibers are in whisker form, increases production costs and adversely affects composite properties.

In order to achieve the full potential of fiber composites, fibers in whisker form must be used but the high cost of whiskers detracts

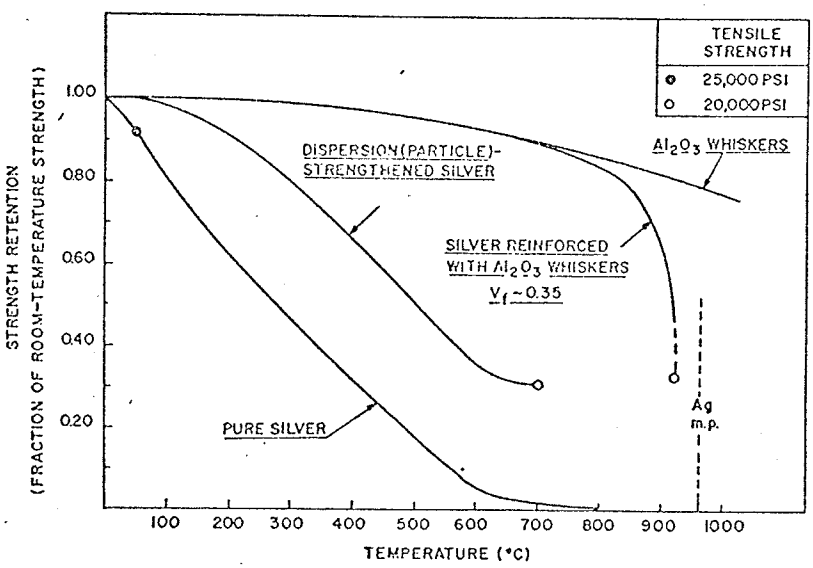

Fig. 23 Indication of superiority of fiber strengthening over dispersion strengthening in silver.[29]

from their appeal to manufacturers who are content with using fine wires as reinforcement because they are less expensive. Thus, economics necessitates a trade-off of composite properties for a less attractive but cheaper reinforcement.

Attempts have been made to produce an aligned microstructure by solid state transformations. The production of needle-like precipitates in Al-Mg-Si and Al-Mg-Cu alloys has not yielded the desired morphology because of small volume fractions of precipitate and lack of alignment.[14] Kraft[35] has attempted to produce an aligned structure at the eutectoid transformation in the iron-carbon system. His and other attempts have proved futile supposedly because the diffusion coefficient in the solid phase is orders of magnitude less than in the liquid thus requiring an impractically slow growth rate to produce alignment. Some success has been achieved in obtaining alignment when the solid state transformation

of a magnetic material was allowed to proceed in a magnetic field[9] but this method is applicable only to magnetic materials.

Thus a controlled microstructure must be produced during unidirectional solidification of a molten alloy. There are two possible methods of accomplishing this. One is by solidification of a eutectic and the other is by dendritic solidification (i.e. an off-eutectic composition). Flemings[36] defines unidirectional solidification as solidification such that the flow of heat is through only one mold-metal interface. Since the reinforcement is grown simultaneously with the matrix, the interfacial bond is excellent and no compatibility problems (e.g. dissolution of the reinforcement) between fibers and matrix exist (if solid solubility changes little with temperature).

Eutectic alloy solidification has been investigated by several researchers[35,37,38,39,40,41] and as a result the solidification process and variables are qualitatively quite well understood. "Eutectic" will be used to mean binary eutectic although it has been reported[35] that ternary eutectics can be unidirectionally solidified with a lamellar morphology to yield lamellae in the order ABCBABCBA ... A description of attempts to produce a composite structure in a ternary alloy system is given in Ref. 42.

Solidification of a binary eutectic is an invariant reaction fixed by free energy considerations in the liquid and solid phases. A description of the determination of the eutectic point is given by Chadwick[38] and Cottrell.[43] When the molten alloy at the eutectic composition is cooled slightly below the eutectic temperature two phases solidify in a proportion fixed by the eutectic point and the solid solubility limits of the two phases. A simple eutectic system is shown in Fig. 24.

A eutectic will form a strong fiber composite only if one of the two phases possesses a high strength. A binary system which forms an intermetallic compound upon eutectic solidification is a good example of a prime candidate for a fiber composite because of the high strength and strength retention at elevated temperatures of intermetallics. The eutectics considered to be of interest can be divided into two categories: continuous and discontinuous. Continuous eutectics are characterized by the continuity of both phases in the growth direction i.e. once nucleation of a phase occurs, the crystal grows unbroken into the melt. Discontinuous eutectics are those in which growth of one of the phases is arrested at intervals during solidification resulting in a dispersion of the discontinuous phase in a matrix of the continuous phase. Continuous eutectics are further divided into two groups. One group has a lamellar microstructure with transverse sequence ABABA ... and the other group has a rod-like structure in which the phase with the smaller volume fraction is in the form of rods embedded in the matrix phase.

Continuous Eutectics:

A description of the nucleation and initial stages of growth of a eutectic alloy has been advanced by Chadwick[38] wherein it is assumed that heterogeneous nucleation sites are provided by impurity particles since it is believed that the liquid temperature is unlikely to drop to the homogeneous nucleation temperature of the melt. Once one of the phases, say α, is nucleated on an impurity particle, it grows to a small sphere which then acts as a heterogeneous nucleation site for the second phase, β, which has a definite crystallographic relationship with the α nucleus although this may not be the equilibrium relationship.

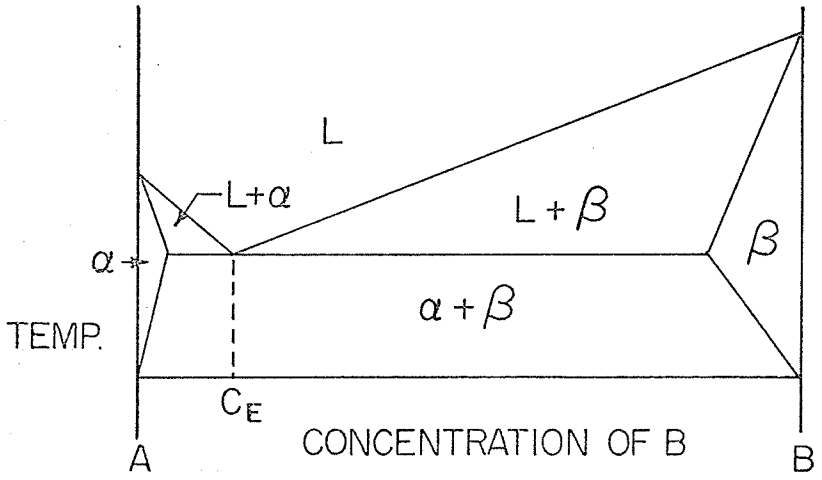

Fig. 24 Simple eutectic system
L represents liquid alloy
C_E is the eutectic composition
α,β are solid solutions.

β then grows circumferentially around the α nucleus bounded by regions enriched in A (A and B are the two component metals of the eutectic. See Fig. 24). These enriched regions promote the growth of α lamellae circumferentially adjacent to the β lamella. As growth proceeds radially outward, the β lamella overlaps the α lamellae and initiates the growth of other β lamellae. This process continues until the α nucleus is surrounded by radiating α and β lamellae. If α is not a heterogeneous nucleation site for β, the α first nucleated grows dendritically while enriching an adjacent layer of liquid in B until β is nucleated. Once nucleated, β will envelop the α dendrite because of its surrounding B-rich layer and α will be heterogeneously nucleated on this β layer. The process of eutectic growth then continues as described above for heterogeneous nucleation of β by α. As growth continues, the interfacial

crystallographic relationship gradually approaches the equilibrium orientation.

During growth of the eutectic a colony or cellular structure may result due to constitutional supercooling. Fig. 25 shows a typical colony structure. In single phase alloys constitutional supercooling is caused by a solute concentration gradient in the liquid preceding an advancing solid-liquid interface. In eutectics the concentration gradient is due to impurity content. It has been shown that a normally cellular solid-liquid interface can be made planar by the use of very pure metals.[38]

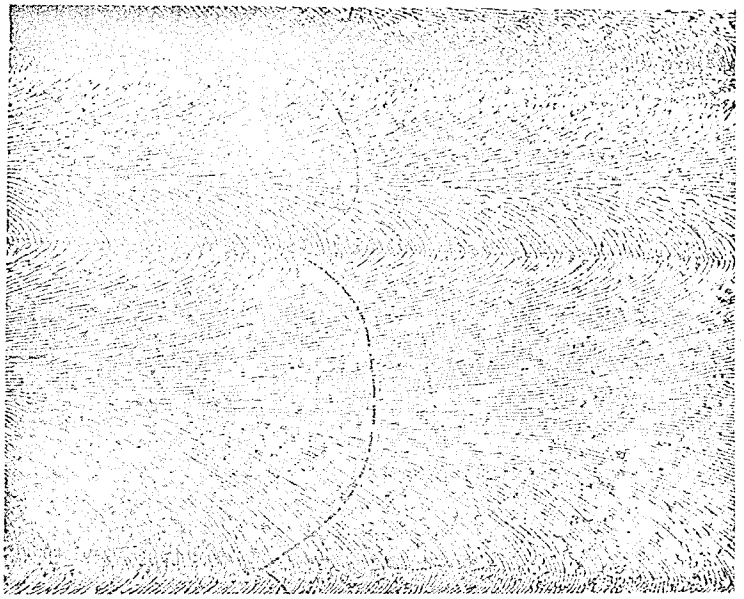

Fig. 25[38] Colony type lamellar eutectic structure. Broken lines indicate shape of the solid-liquid interface during growth.

In describing eutectic colony formation it is helpful to enlist the use of a ternary phase diagram wherein the three constituents are the metals A and B and some impurity, X. The X depleted region is shown in Fig. 26 where it is assumed for convenience that the dis-

tribution coefficients are as follows: $k_X^\alpha = k_X^\beta = k < 1$ where k_X^α is the distribution coefficient of impurity X in α. Similarly for k_X^β.

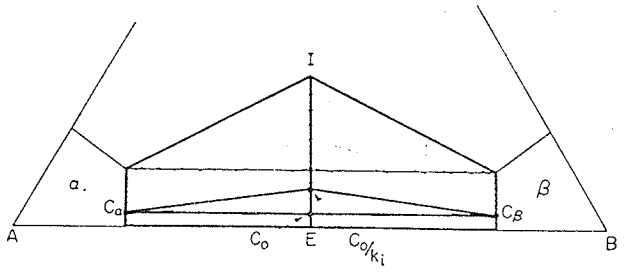

Fig. 26[38] X depleted portion of A-B-X ternary system.
I = ternary eutectic point
E = binary eutectic point
k_i = k, the overall distribution coefficient

Upon solidification, X will be rejected in equal amounts by α and β and the liquid composition will be Co/k. The concentration of X will vary in the liquid ahead of the interface in the same manner as solute concentration varies in the melt of a single phase alloy. For solute (impurity) motion by diffusion only:[39]

$$C_L = C_o \left[1 + \frac{1 - k}{k} \exp\left(-\frac{Rx}{D}\right)\right] \qquad 32$$

where C_L = concentration of X in the liquid

R = growth rate, cm/sec

D = liquid diffusion coefficient

x = distance from the interface at which the concentration is C_L.

The liquid concentration and temperature variation are given in Fig. 27.

The liquidus temperature corresponding to the concentration given in equation 32 is:[39]

$$T_L = T_o - mC_o \left[1 + \frac{1-k}{k} \exp\left(-\frac{Rx}{D}\right)\right] \qquad 33$$

where T_o = eutectic temperature of pure A-B

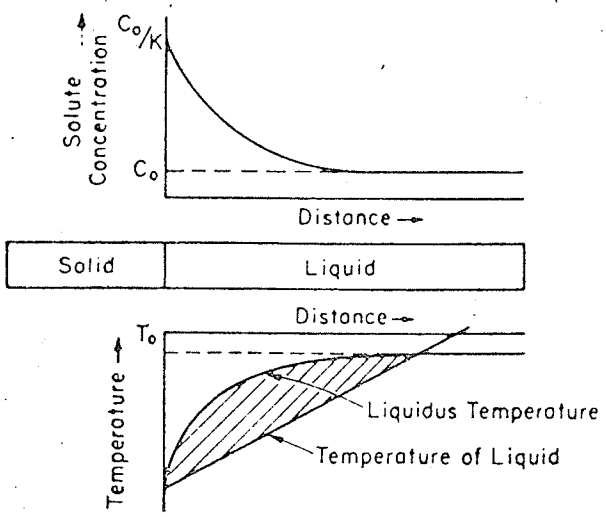

Fig. 27[38] Concentration and temperature gradients ahead of advancing solid liquid interface.

m = slope of line EI in Fig. 26

T_L is shown in Fig. 27

The actual temperature of the liquid is:[39]

$$T_A = T_o - m\frac{C_o}{k} + Gx \qquad 34$$

where G is the temperature gradient in the liquid, $^oC/cm$.

The formation of a cellular structure occurs when a portion of a planar interface protrudes into the constitutionally supercooled region which is shaded in Fig. 27. The protrusion will continue to grow until the degree of supercooling is just enough to sustain steady state growth. The protuberance is convex with curvature increasing as the cell edge is approached. Due to variation of curvature impurity concentration varies across the cell cap being greatest at the cell boundaries. Since the equilibrium (liquidus) temperature decreases with increasing impurity concentration, the convex cellular surface is stable and may possess deep grooves between the cells. Cellular segregation

is described in detail in Ref. 44.

The value of G/R necessary to maintain a planar solid liquid interface can be found knowing that elimination of the constitutionally supercooled region will prevent formation of a cellular interface. For the constitutionally supercooled region to be nonexistent, the slope of the actual temperature gradient in the liquid must be equal to or greater than the slope of the liquidus temperature curve at x = 0 in Fig. 27. Differentiating equation 33 with respect to x:

$$\frac{dT_L}{dx} = \frac{mC_o R(1-k)}{kD} \exp(-\frac{Rx}{D})$$

Setting this equal to G and x = 0:

$$\left.\frac{G}{R}\right|_{crit} = \frac{mC_o(1-k)}{kD} \qquad 35$$

At values of $G/R > (G/R)_{crit}$ plane front solidification occurs.

Thus cellular solidification can be prevented by varying G/R such that there is no constitutionally supercooled zone ahead of the solid-liquid interface. This may be done by increasing G or by decreasing R. A planar interface becomes increasingly more stable with decreasing impurity content.

Lamellar Solidification:

Since there is reason to believe that most pure eutectics solidify with a lamellar morphology,[38] lamellar growth will be described as being typical of unidirectional eutectic growth. Factors affecting lamellar growth will be shown to be responsible for a transition to rod-like morphology.

For simplicity it is assumed initially that the solid-liquid interface is approximately planar and that the α and β lamellae are of the same thickness.[45] During lamellar solidification atoms of B will be

rejected by solidifying α and atoms of A will be rejected by solidifying β so that a concentration gradient with transverse periodicity λ (interlamellar spacing--the sum of the thickness of α and β lamellae) will cause lateral diffusion of A and B. Since the rejected A is balanced by rejected B, there is no long-range concentration change in the liquid and the concentration is assumed to be affected ahead of the advancing lamellae to a distance not greater than λ. It is not unreasonable to assume that the solid-liquid interface is an isothermal surface with a constant undercooling ΔT. The undercooling required for steady state growth is the sum of three separate undercoolings: ΔT_c, constitutional undercooling because of solute enrichment of the interfacial liquid, ΔT_r, an undercooling due to curvature of the interface and ΔT_k, an undercooling necessary to provide the kinetic driving force for solidification. Since ΔT_k is relatively small, it will be neglected so that:

$$\Delta T = \Delta T_c + \Delta T_r \qquad 36$$

The concentration gradient and undercooling are shown in Fig. 28. Since the concentration varies across the lamellae, ΔT_c will also vary as shown in Fig. 28 (B). Because the total undercooling is constant, $\Delta T_r (= \Delta T - \Delta T_c)$ must also vary. Since ΔT_r increases with curvature of the interface, it is concluded that curvature of the lamellae increases toward the α-β interfaces and must be of the form shown in Fig. 28 (C). The exact shape of the solid-liquid interface also depends on a balance of forces at the α-β-liquid juncture due to the energies of the α-β, α-liquid and β-liquid interfaces.[38] (See Fig. 29)

Because the flux of solute between adjacent lamellae occurs by liquid diffusion, it would be expected that the thickness of lamellae

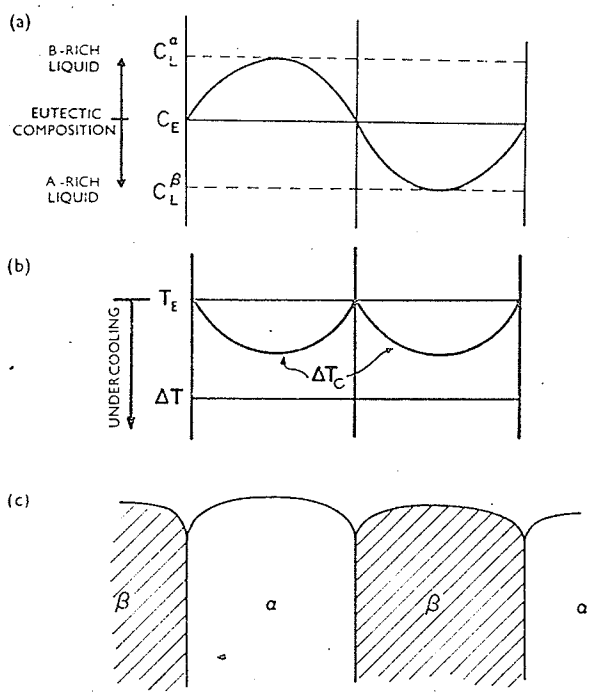

C_L^α = concentration ahead of α lamella

C_L^β = concentration ahead of β lamella

Fig. 28[45] A) Concentration distribution ahead of eutectic interface
B) Constitutional undercooling and total undercooling
C) Shape of interface

would be inversely proportional to solidification rate but a tendency to minimize interfacial area requires that lamellar thickness be as large as possible.[39] Several analyses of the effect of growth rate on interlamellar spacing have been carried out with that by Jackson and Chalmers[38] being most straightforward. Their treatment deals with conditions of undercooling at the solid-liquid interface at a position of termination of a lamella. The undercooling at the termination is equated to the undercooling at a position of normal lamellar growth. The assumptions made are that the solid-liquid interface is isothermal, that equation 36 applies, that the widths of adjacent lamellae are equal and that curvatures of the lamellae are equal and constant. The

solid-liquid interface with surface energy components is given in Fig. 29.

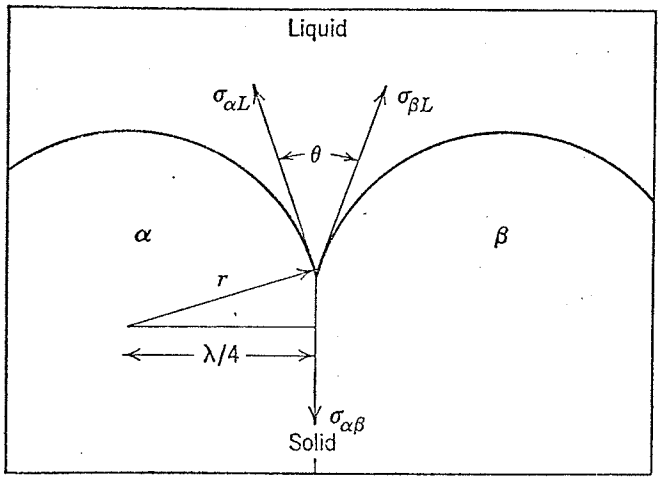

Fig. 29 Region of interface at junction of two lamellae[39]

Since the curvature of adjacent lamellae must be equal when they meet, the surface energies, $\sigma_{\alpha L}$ and $\sigma_{\beta L}$ must also be equal. Equilibrium requires a balance of surface energies in the vertical direction yielding:

$$2\sigma_{\alpha L} \cos\frac{\theta}{2} = \sigma_{\alpha\beta}$$

and since $\frac{\lambda}{4} = r \cos\frac{\theta}{2}$,

$$\frac{\sigma_{\alpha L}}{r} = \frac{2\sigma_{\alpha\beta}}{\lambda}$$

The undercooling at the centre of a lamella due to curvature is:[38]

$$\Delta T_r = \frac{\sigma_{\alpha L} T_E}{Lr}$$

Substituting for $\sigma_{\alpha L}$:

$$\Delta T_r = \frac{2\sigma_{\alpha\beta} T_E}{L\lambda} \qquad 37$$

where: L = latent heat of fusion

T_E = equilibrium temperature

Assuming a linear relationship, the transverse solute distribution in front of an α lamella is given by:[38]

$$C_\alpha^L - C_E = \frac{(1 - k_\alpha)\, C_E R\lambda}{8D}$$

where C_α^L = concentration of solute in the liquid in front of an α lamella and midway between α-β interfaces

C_E = eutectic composition

k_α = distribution coefficient for α and liquid

and assuming that the liquidus is a straight line, the associated constitutional supercooling is:

$$\Delta T_c = \frac{(1 - k_\alpha)\, C_E R\lambda m_\alpha}{8D} \qquad 38$$

where m_α = slope of liquidus

The above undercoolings (equations 37 and 38) are for a regular lamellar interface. Considering the interface at a position of lamellar termination, T, in Fig. 30:

$$\Delta T_r = \frac{4\sigma_{\alpha\beta} T_E}{L\lambda} \qquad 39$$

since curvature at point T is in two perpendicular directions.

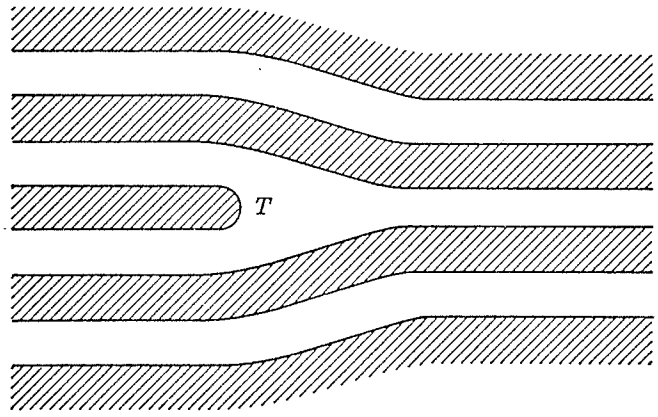

Fig. 30 Lamellar termination[39]

The transverse concentration gradient at the interface at the termination is given by:[38]

$$C_{\alpha}^{L} - C_E = \frac{(1 - k_{\alpha})\, C_E R\lambda}{16D}$$

And the constitutional supercooling is:

$$\Delta T_c = \frac{(1 - k_{\alpha})\, C_E R\lambda m_{\alpha}}{16D} \qquad 40$$

Since it was assumed that the solid-liquid interface is isothermal, the supercooling as given by equation 36 is the same at the position of lamellar termination as it is at a position of normal lamellar growth. Equating the sum of equations 37 and 38 to the sum of equations 39 and 40 yields:

$$\lambda^2 R = \frac{32\sigma_{\alpha\beta} T_E D}{m_{\alpha}(1-k_{\alpha})C_E L} = \text{constant}$$

$$\text{i.e. } \lambda \alpha R^{-\frac{1}{2}} \qquad 41$$

The relationship in equation 41 has been proven experimentally to apply to eutectic alloys.[38] Chadwick,[46] varying the growth rate from 1-60 cm/hr in solidifying the Al-Cu eutectic, found that λ obeyed equation 41 and varied only 4% in any one eutectic grain. The variation is attributed to slight misorientations of the lamellae thus projecting varying apparent interlamellar spacings on any given cross-section plane. Variation of the temperature gradient by an order of magnitude had no effect on λ.

The underlying cause for certain alloys to produce an aligned (lamellar or rod-like) structure is the minimization of interfacial energy between phases. The minimization of interfacial energy is also thought to be responsible for the characteristic crystallographic relationships between adjacent lamellae. The observed matching of low

index planes across the interface in most eutectic systems examined seems to support this contention. A method of attainment of a low energy structure is exemplified in the Al-Cu eutectic. It has been observed[38] that soon after nucleation (211) planes are established as boundaries for the $CuAl_2$ lamellae. As growth continues the Al lamellae gradually align (111) planes parallel to the interphase boundaries and this relationship is preserved during further growth. However, it has also been shown that a definite interfacial relationship between adjacent lamellae is not a mandatory condition in establishing a lamellar (or rod-like) structure. An Al-Cu eutectic ingot melted back such that the solid-liquid interface was at an angle with the unmelted lamellae and resolidified exhibited two growth directions, the section melted back growing normal to the meltback interface at an angle of about 15^{o} to the original lamellae. Since it is assumed that the crystal structure is continuous across the meltback interface, the interfacial relationships in the two regions must be different.

Most eutectics which exhibit a lamellar morphology at "normal" growth rates depart from lamellar growth at very slow growth rates ($R<0.5$ cm/hr) and equation 41 no longer applies. An example of a degenerate Al-Cu eutectic structure is shown in Fig. 31. Although degeneracy is not dependent on the presence of impurities since it occurs in zone refined specimens, the precise cause is not known. Chadwick[38] suggests that it occurs to minimize the total interphase boundary energy since the commonly observed interphase crystallographic relationships may not possess the lowest possible energy. This assumption would appear to contradict the description of steady state eutectic growth described above. Cooksey et al.[40] postulate that degeneracy is permitted

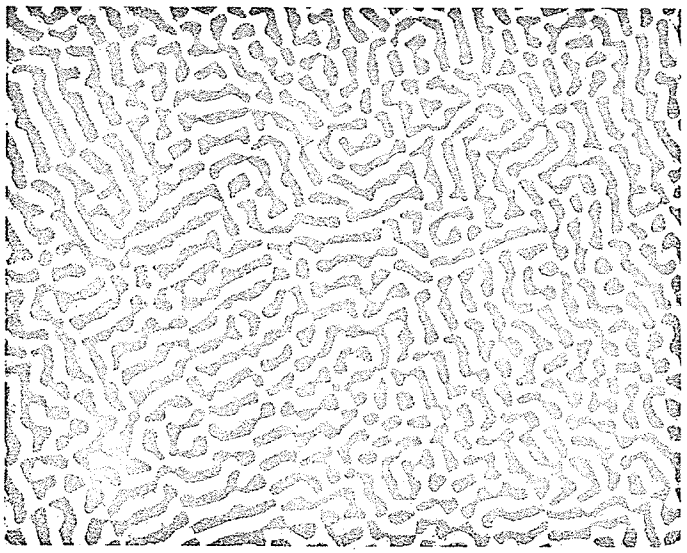

Fig. 31 Degenerate Al-Cu eutectic[39]

by the greater diffusion distances possible at low values of R. The greater diffusion distances result in a coarse structure with a relatively small interfacial area and hence lower interfacial energy. Because of the decreased total energy it is assumed that a preferred crystallographic relationship between the phases is not as important as it is during lamellar growth.

Formation of a Rod-like Structure:

There is considerable controversy about the causes of formation of a rod-like morphology. One school of thought maintains that it is a direct result of impurity content being a transformation of the lamellar structure. Another maintains that it can be explained by interfacial energy considerations. In the light of experimental evidence it must be concluded that neither explanation is all-inclusive and the rod structure must be dependent on both impurity content and interfacial energy considerations. The effect of impurity content will

be discussed first.

In discussing colony formation above it was assumed that $k_x^\alpha = k_x^\beta$. However, if the distribution coefficients are different in the two phases and if the ratio G/R is low enough, a transformation from lamellar to rod-like structure is likely. Consider the ternary phase diagram of A, B and impurity X shown partially in Fig. 32.

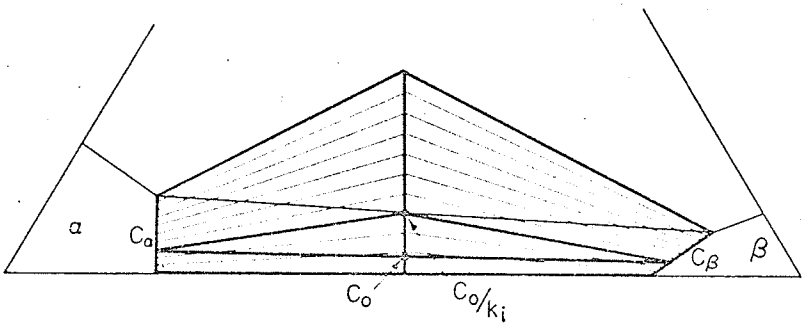

Fig. 32[38] Idealized three-phase field of ternary eutectic having $k_x^\alpha > k_x^\beta$

Note that $k_x^\beta < k_x^\alpha < 1$ so that upon solidification a lamella of β rejects more X than a lamella of α. The concentration distributions of X ahead of the α and β lamellae are shown in Fig. 33(A) and are described by the equations:

$$C_x^\alpha = C_o + C_o \frac{(1 - k_x^\alpha)}{k_x^\alpha} \exp\left(-\frac{Rx}{D}\right)$$

$$C_x^\beta = C_o + C_o \frac{(1 - k_x^\beta)}{k_x^\beta} \exp\left(-\frac{Rx}{D}\right)$$

The concentration of X ahead of the β lamellae is greater than that ahead of the α lamellae resulting in a lower equilibrium (freezing) temperature of the liquid in contact with β and the β lamellae will grow behind the α lamellae. The equilibrium temperatures preceding the α and β lamellae and the average equilibrium temperature are shown in Fig. 33(B) in which

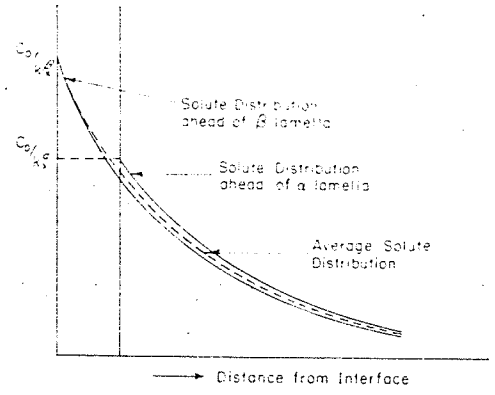

(A)

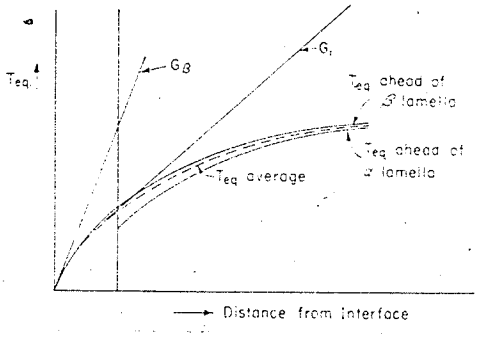

(B)

Fig. 33[38] (A) Liquid composition ahead of solid-liquid interface
(B) Equilibrium temperatures ($T_{eq.}$) ahead of the interface

G_β is the minimum value of applied temperature gradient possible without causing constitutional supercooling ahead of the β lamellae while G_i is the minimum temperature gradient possible without constitutionally supercooling the liquid across the entire interface. If $G_i < G < G_\beta$, then the liquid ahead of the β lamellae will be constitutionally supercooled and the β-liquid interface will be unstable. Any protrusion of β from the interface will grow to an equilibrium distance and reject A atoms. The A-enriched region will promote the overlapping of the β

lamellae by the α lamellae so that the protrusion will be in the form of a rod surrounded by α. Under the influence of a gradient $G_i<G<G_\beta$, β-protrusions will be periodic along the β lamellae and a rod morphology will result as shown in Fig. 34. Since $G>G_i$, the overall shape of the interface will be planar.

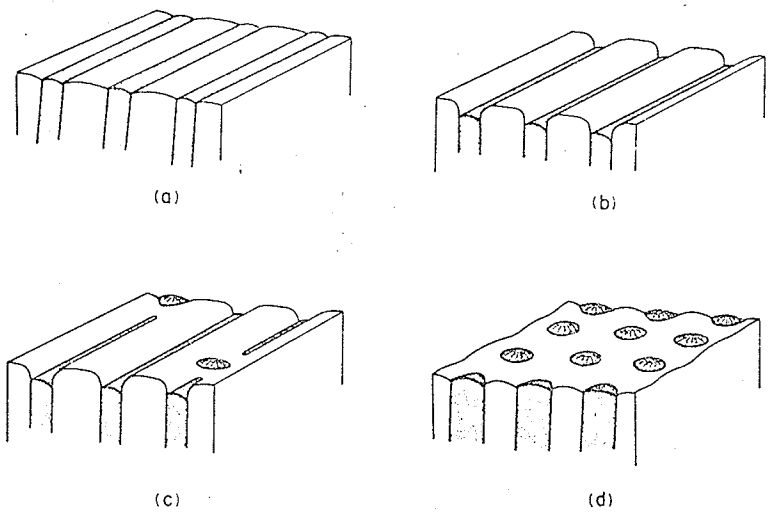

Fig. 34[34] Stages in development of a rod-like structure.

If, however, $G<G_i$, a constitutionally supercooled zone will be formed ahead of the whole solid-liquid interface resulting in a cellular interface. Since G is also less than G_β, the β lamellae will break down to a rod-like structure as described above.

Althouth the solid-solid interfacial energies of two phase alloys are not known thus negating a quantitative energy analysis, Cooksey et al.[40] have shown that for a eutectic with equal interphase boundary energies in lamellar and rod-like forms, the rod-like structure is more stable at volume fractions less than 28%. Cooksey et al. concede that preferred interphase crystallographic relationships probably result in a lower interfacial energy for a lamellar morphology even at low volume

fractions of second phase since there is no such possible relationship for a cylindrical fiber. This explanation would account for the existence of lamellar structures at a volume fraction of reinforcement of 7.7% for the Sn-Zn system. It is probable that there is a tendency during solidification for an alloy to produce a rod-like morphology at low volume fractions of reinforcement in order to minimize overall interfacial energy but the actual preference of a particular alloy for a lamellar or rod-like morphology is subject to the variation of interfacial energies between the two structures i.e. unit interfacial energy of a lamellar structure may be so much less than that of a rod-like structure that at low second phase volume fractions the lamellar structure will have a lower overall interfacial energy in spite of its much larger interfacial area compared to a rod-like structure. Rod-like structures, however, are not dependent only on interfacial energy minimization but may be formed due to impurity effects as described above at very high volume fractions of reinforcement such as exists in the Al-Cu eutectic.

A transition from lamellar to rod-like morphology is also caused by a cellular interface. Chadwick[38] postulates that the transition to a rod type of morphology is due to an inconstant ratio of k_x^α/k_x^β across the cell cap. A rod-like structure can be justified on the basis of impurity concentration gradients across cell caps knowing that the transition from a lamellar to rod-like structure occurs first at the cell boundaries. If at the centre of the cell, at low impurity concentration $k_x^\alpha \simeq k_x^\beta$, but at the edge of the cell where impurity concentration is higher $k_x^\beta < k_x^\alpha$, then solidification at the cell boundaries would result in a rod-like morphology as described above for the

appropriate temperature gradient. The type of ternary phase diagram which would permit such a relationship between k_x^α and k_x^β is shown in Fig. 35. However, this does not explain why rods may be formed only at cell boundaries which are parallel to the lamellae[38] while lamellae may grow undisturbed at cell walls perpendicular to them.

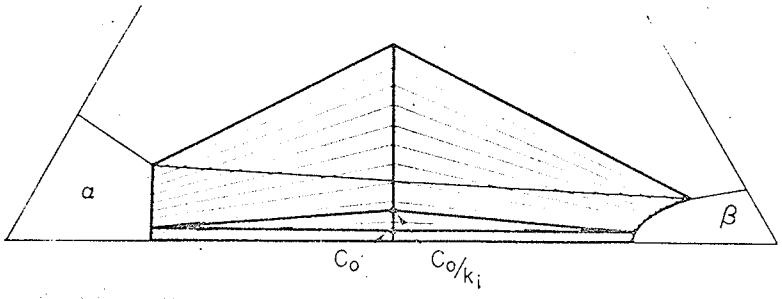

Fig. 35[38] Ternary phase diagram for which $k_x^\alpha \simeq k_x^\beta$ at C_x small with k_x^α/k_x^β varying with C_x.
(C_x = concentration of impurity, X)

An explanation of the latter phenomenon is given by Hunt and Chilton[47] who unidirectionally solidified various pure alloys of differing volume fractions of reinforcing phase around an obstacle thereby varying the curvature of the solid-liquid interface. Their apparatus along with positions of the advancing interface is shown in Fig. 36. As was mentioned previously, solidification occurs in a direction normal to the solid-liquid interface. As solidification occurs around the inset of Fig. 36 the conditions of cellular growth are simulated but without the impurity effect. Hunt and Chilton found that eutectics with lamellae perpendicular to the tip of the inset grew undisturbed around the inset. Only lamellae parallel to the inset edge broke down as shown in Fig. 37. Eutectics with volume fractions of reinforcement as high as 30% exhibited a rod-like structure in the

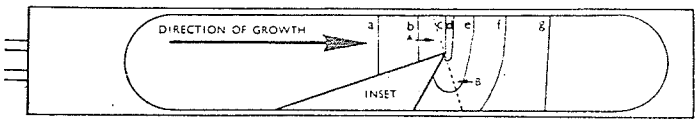

Fig. 36[47] Boat used by Hunt & Chilton to vary curvature of solid-liquid interface. Line AB indicates where ingots were sectioned for microscopical examination.

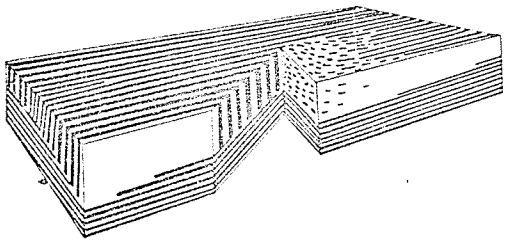

Fig. 37[47] Transition to rod type of morphology. Lower grain remains lamellar.

region of large solid-liquid interfacial curvature. As the interface became planar, lamellar growth was restored. The Sn-Pb eutectic with 37% Pb reverted to a wavy lamellar structure rather than rods. Since growth occurs normal to the solid-liquid interface, a curved interface forces growth in a non-preferred direction and probably causes departure from the preferred interphase crystallographic relationship. When these conditions occur, a transition to a rod type of structure is energetically feasible and in some cases desirable. Lamellae growing parallel to a cell boundary must curve to accommodate the surface curvature of the cell cap and in so doing must deviate from the preferred growth direction. Lamellae normal to a cell boundary can accommodate cellular curvature within the preferred growth direction. Thus it is

seen that the transformation from lamellae to rods in cellular growth may be only indirectly attributable to impurity content being caused by curvature of the solid-liquid interface.

Discontinuous Eutectics:

As stated previously a discontinuous eutectic contains a dispersed phase. As solidification proceeds repeated nucleation of the discontinuous phase occurs. Although discontinuous eutectic solidification is not well understood, it has been observed that the discontinuous phase is always present in small quantities although volume fraction of second phase is not itself a criterion of discontinuous growth. A necessary condition for discontinuity is a large degree of growth anisotropy of the discontinuous phase.[39] The Al-Si eutectic is a prime example. During solidification silicon nucleates, probably heterogeneously, ahead of the solid-liquid interface and grows anisotropically in the form of small platelets bound by parallel {111} planes.[38] Growth is approximately normal to the solid-liquid interface although there is no preferred epitaxial relationship between the aluminum matrix and silicon platelets. As platelets converge or diverge, existing platelets cease to grow and are overtaken by the matrix and new platelets are nucleated in order to keep diffusion distances in line with solidification rate. An example of this type of growth is shown in Fig. 38.

Another explanation for the occurrence of a discontinuous morphology is that the discontinuous phase might have a slower growth rate than the matrix phase at a given undercooling.[48] If this were the case, the second phase would grow by a process of repeated nucleation and envelopement by the matrix.

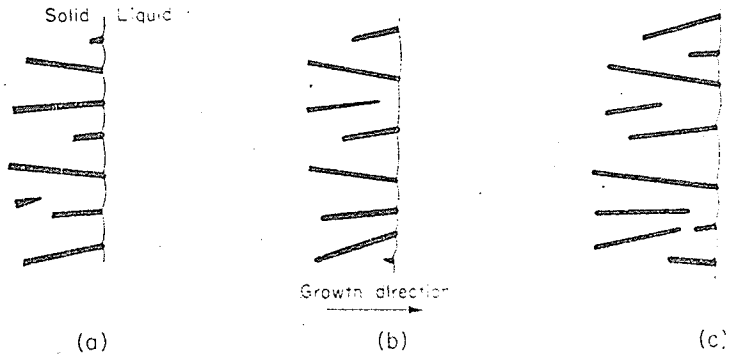

Fig. 38 Growth of discontinuous eutectic.(A), (B), (C) in successively later stages of growth[38]

Rapid cooling of the discontinuous Al-Si eutectic not only results in refinement of the structure but also causes the formation of primary aluminum dendrites. The formation of primary aluminum has been explained by the presence of a "coupled region" in the Al-Si phase diagram.[38,48] Only in this region can co-operative growth of the two phases occur when the temperature of eutectic arrest is depressed because of rapid growth rates (See Fig. 39). The occurrence of aluminum dendrites is due to the suppression of the growth of silicon crystals with undercooling which has been estimated in the order of $10^{o}C$ for a growth rate of 6 cm/min.[48] The eutectic composition would then be to the left of the coupled region when the melt is undercooled thereby behaving as a hypoeutectic alloy.

Elevated Temperature Stability:

The large interfacial areas of fiber composites may provide a degree of instability at elevated temperatures. Some manufactured fiber composites have shown serious deterioration at elevated temperatures because of chemical interaction between matrix and reinforcement.[49]

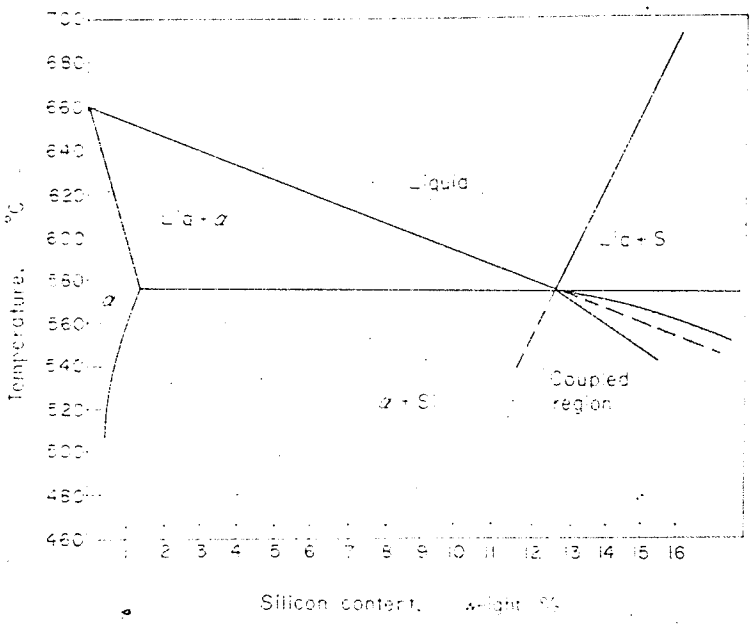

Fig. 39 Portion of Al-Si phase diagram illustrating the coupled region.[38]

Since eutectic phases are chemically compatible, this problem is not present with eutectics although large changes in solid solubility with temperature or phase changes may adversely affect eutectic properties. Since most eutectics exhibit preferred interphase crystallographic relationships, interfacial energy is relatively low and the driving force (minimization of interfacial energy) for spheroidization or coarsening is usually small. Some coarsening of structures has been observed, however, at faults and discontinuities and in cases where the microstructure is very fine (fast solidification rates).[49] Spheroidization has been reported 65°C below the eutectic temperature for Al-Pd[50] which does have a strongly preferred orientation relationship between phases. Generally speaking, though, eutectic structures are very stable at elevated temperatures because of their preferred interphase relationships with stability reported within 10°C of the

eutectic temperature for the Al-Cu eutectic.[49]

Unidirectional Dendritic Solidification:

Dendritic growth can yield fiber composite structures when an alloy of non-eutectic composition is unidirectionally solidified. For the best type of rod-like morphology the growth characteristics of the primary phase should be highly anisotropic and the dendrites should align themselves before the matrix phase solidifies around them.[51] During unidirectional solidification dendritic growth may be columnar with the primary dendrite arm aligned in the direction of solidification. A low value of G/R and high solute content favour columnar growth over fibrous dendritic growth.[36] At high solidification rates solute cannot redistribute itself to form fibrous dendrites so branching of the primary arms occurs. The spacing of secondary dendrite arms is sensitive to solidification rate decreasing as R increases since diffusion distances in the liquid decrease with increasing R.

Provided that G/R is large enough plane front solidification will occur in a non-eutectic alloy. Mollard and Flemings[52] quantitatively analyze in detail the plane front eutectic-like growth of non-eutectic alloys at high values of G/R and have calculated critical values of G/R at various compositions of Sn(rich)-Pb alloys above which plane front growth should occur. They have also shown[53] that Sn(rich)-Pb alloys do indeed follow the quantitative predictions and that a true eutectic-like fibrous morphology is obtained when plane front solidification occurs.

This development opens up new possibilities for fiber composite materials since it allows flexibility in alloy compositions (eutectics are at fixed compositions) thus permitting manipulation of the volume fraction of reinforcement which implies the tailoring of composite properties to suit the application.

EXPERIMENTAL

Specimen Preparation and Testing:

Heretofore most unidirectionally solidified alloys produced in the laboratory have commanded the use of rather elaborate apparatus to effect controlled solidification. It is the purpose of the present investigation to determine the adequacy of a comparatively simple and fast technique to produce aligned structures in three binary alloy systems, namely Al-Ni, Al-Cu and Al-Si and to study some mechanical and microstructural properties previously not dealt with. The method of unidirectional solidification is similar to that used by Cahoon and Paxton.[54] Aluminum was melted in a graphite crucible to which the alloying element was added. Purity of the materials used is as follows: For Al-Ni and Al-Cu systems Al-99.9%, Ni-99.9%, Cu-99.96%; for the Al-Si system Al-99.999% and Si-99.999%. The melt was stirred until the alloying element was dissolved followed by pouring back and forth between two crucibles to insure adequate mixing. It was then bubbled with argon for 15 minutes in order to degas. The melt was then poured into a preheated alumina mold situated on a steel base plate inside a radiation furnace (Fig. 40). Impingement of a water jet on the base plate caused unidirectional solidification. This yielded cylindrical ingots 7 cm. long and 5 cm. in diameter. The solidification rate, which was not controlled, was approximately 80 cm/hr. After solidification was completed, the ingot and mold were removed from the casting

furnace as a unit and were allowed to cool at ambient conditions. Casting temperatures were as follows:

Alloy(wt.%)	Melt Temp.(^{o}C)	Casting Furnace Temp.(^{o}C)
Al-4.6%Ni	750	750
Al-6.1%Ni	700	750
Al-7%Ni	700	700
Al-20%Ni	850	850
Al-33%Cu	700	750
All Al-Si Alloys	700	750

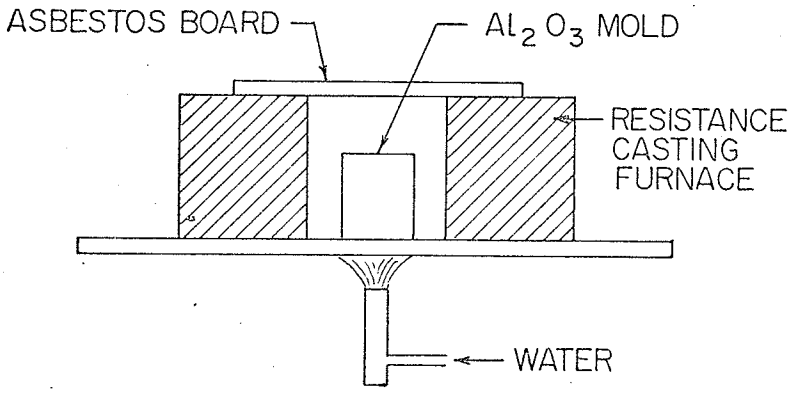

Fig. 40 Casting Apparatus

Eutectic compositions were (wt.% given): Al-6.1%Ni,[55] Al-33.2%Cu[55] and Al-12.5%Si.[48]

Typical macrostructures of the ingots are shown in Fig. 41. The chill crystals at the bottom of the ingots were formed either due to quenching by the base plate when the melt was poured into the mold or because of rapid heat transfer caused by vapourization of quench water when the jet was turned on.

Test specimens were machined on a lathe from blanks cut from the central portions of the ingots. Specimen dimensions were 0.16" diameter by 0.75" gauge length for tensile tests and 0.16" diameter by 0.50" long for compression. All tests were conducted on an Instron

testing machine at a strain rate of 1.76×10^{-4} sec^{-1} in tension and 2.64×10^{-4} sec^{-1} in compression.

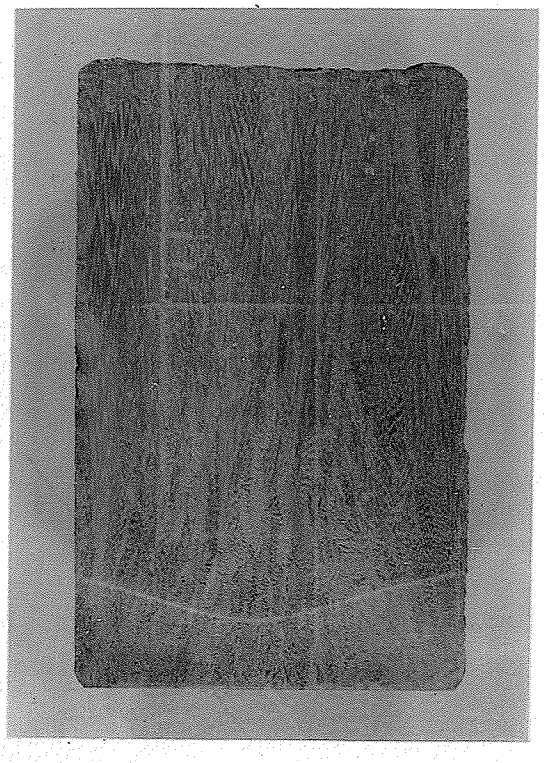

(A)

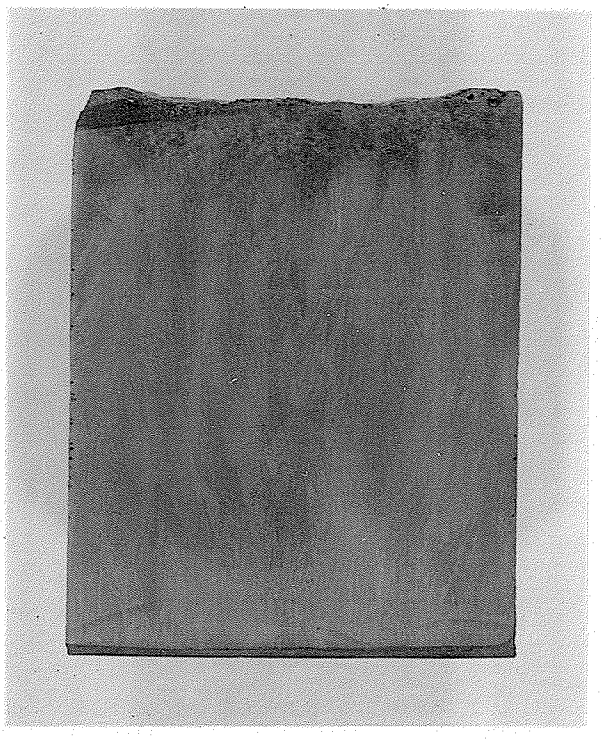

(B)

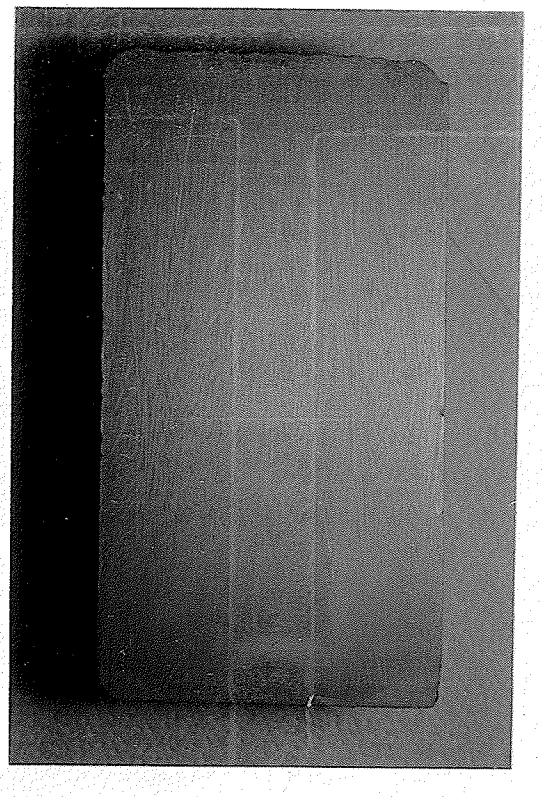

(C)

Fig. 41 Typical macrostructures of ingots A) Al-6.1%Ni
B) Al-33%Cu C) Al-11.6%Si

RESULTS AND DISCUSSION

Al-Ni System:

A typical microstructure of the Al-Ni eutectic is shown in Fig. 42.

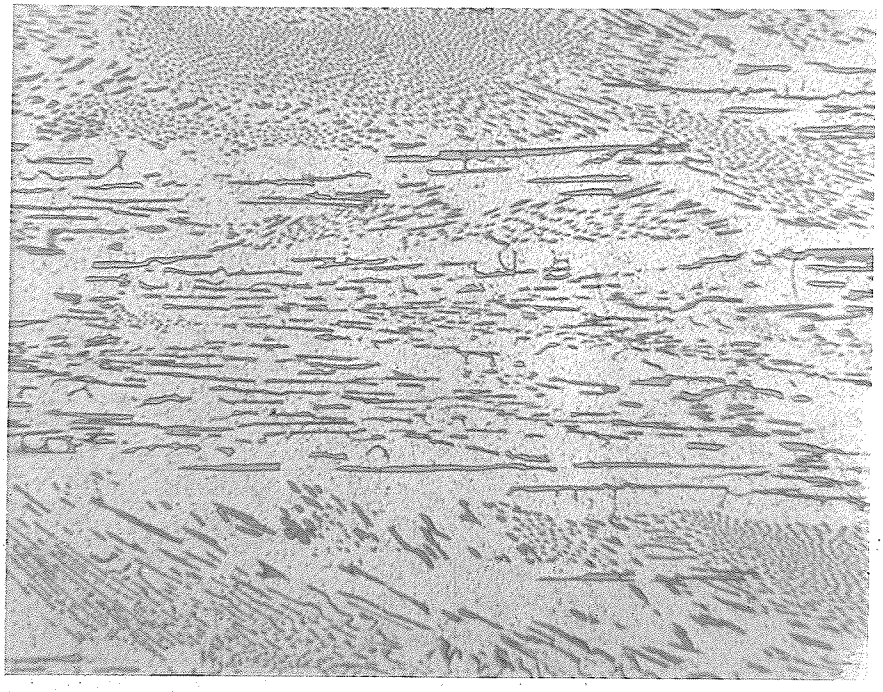

(A) x 550

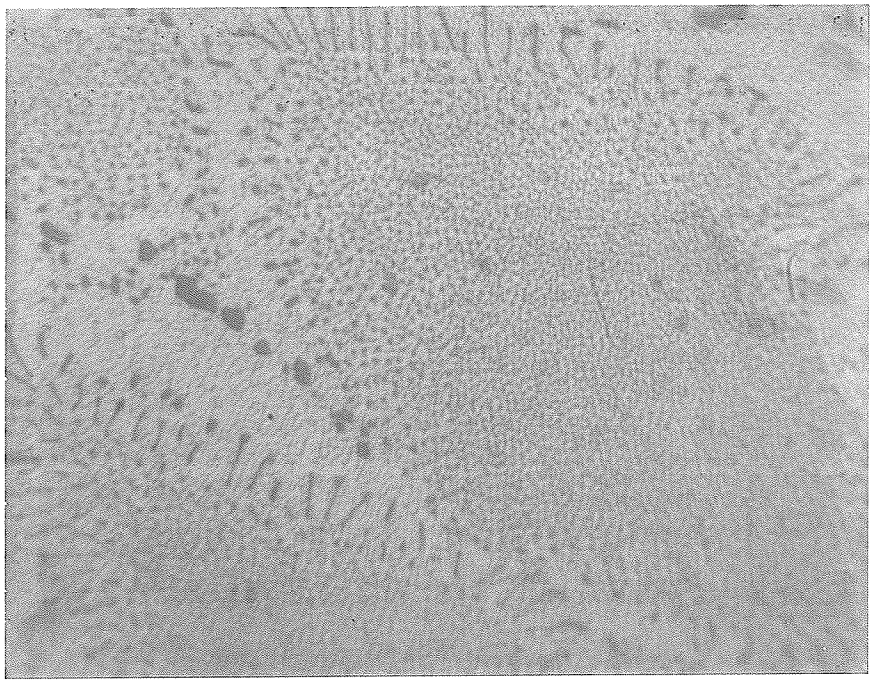

(B) x 1430

Fig. 42 Al-6.1% Ni A) Longitudinal section showing fibers both aligned and misaligned. B) Transverse section showing fiber colonies surrounded by fiber-depleted regions. The dark phase is Al_3Ni while the light matrix phase is aluminum.

The Al_3Ni intermetallic forms 10 vol.% of the eutectic and can be seen to grow in fibrous form. A fibrous morphology is to be expected at the solidification rate used. Lemkey et al[56] report a transition from a platelet to fibrous morphology at R ≃ 2.6 cm/hr in a temperature gradient of about 30°C/cm (as R is decreased the platelet structure becomes more prevalent). The presence of fiber colonies indicates that growth occurred with a cellular interface and that at the impurity level of the melt the temperature gradient was not steep enough to pre-

vent the formation of a constitutionally supercooled region. It is obvious from Fig. 42(A) that the structure is very imperfect with fiber alignment occurring in only a fraction of the colonies and that the colonies are surrounded by fiber depleted regions. Regions of fiber depletion were noticed by Hertzberg et al.[57] in some specimens which exhibited tensile strengths lower than specimens with a more perfect morphology. The preferred growth direction of the Al-Ni eutectic has been found to be <010> $_{Al_3Ni}$ which is parallel to <110> $_{Al}$ and the preferred (low energy) fiber-matrix interface is {331} $_{Al}$.[56] Deviation from the preferred growth direction and interfacial relationship is evident in Fig. 42(A) which shows individual Al_3Ni fibers changing direction during growth. Non-preferred interfacial relationships result from changes in the growth direction of individual fibers assuming crystal continuity along the fibers and from the different degrees of alignment of different fibers in the same cell (assuming that the matrix phase in each cell is a single crystal). The fibers themselves can also be seen in Fig. 42(A) to be of irregular shape and cross-section. Imperfections in the fibers are attributed to the very high growth rate at which slight inhomogeneities in the melt can cause deflection of the fibers from the preferred growth direction. Lemkey et al.[56], in the limited range of solidification rates observed (as high as 19 cm/hr), noticed that the number of fiber faults such as branching and the nucleation of new fibers increased as solidification rate was increased. The large degree of misalignment of some colonies and the lack of a continuous microstructure are probably due to a combination of cellular growth, rapid solidification rate and vibrations created by the water jet on the base plate. The degree of refinement of the microstructure

within the colonies is greater than expected. Lemkey et al[56] have extrapolated their findings of interfiber spacing, λ, vs R and at R = 80 cm/hr. their extrapolated value of λ is 0.7μ. It was found on the optical microscope at a magnification of 1430X that $\lambda \approx 0.5\mu$ or smaller corresponding to R > 100 cm/hr in the results of Lemkey et al.

Results of mechanical tests on Al-Ni specimens are given in Table 1.

Table 1

No.	UTS(psi)	0.2%offset Y.S.(psi)	ELONG(%)	R.A.(%)*	Treatment
Al-6.1%Ni					
1	27,550	15,300	5	6	As Solidified
2	27,400	12,350	5	6	
3	28,200	11,350	5	6	
4	30,400	19,700	3	3	
5	26,600	12,500	10	17	3½hr.@585°C
6	25,100	12,400	14	16	3½hr.@585°C
7	23,600	11,000	15	16	22hr.@585°C
8	23,600	11,200	15	15	22hr.@585°C
9(Transverse)	17,300	9,700	14	Elliptical fracture surface	
10(Transverse)	18,400	11,100	12	Elliptical fracture surface	
Al-4.6%Ni					
11	19,000	10,200	6	7	As Solidified
12	18,700	10,200	7	8	
13	18,800	10,200	7	7	
14	18,000	10,900	7	7	
Al-5.7%Ni					
15	26,700	12,700	5	5	
Al-7%Ni					
16	23,900	15,900	3	1	
17	22,800	19,300	3	1	
18	24,600	21,600	4	2	
Al-20%Ni					
19	19,000	16,000	3	3	
20	19,100	15,800	3	2	11days@580°C
21	17,300	15,800	7	3	

Table 1 (Cont'd)

Compression Al-6.1%Ni

	ULT. STRENGTH (psi)	Y.S.(psi) (Actual)	
22	33,500	20,600	As Solidified
23	36,400	19,900	
24	36,000	19,400	
25	34,800	20,200	
26(Transverse)	NO ULTIMATE	11,100	0.2% offset
27(Transverse)	NO ULTIMATE	11,400	

Compression Al-20%Ni

28	44,200	15,600	
29	42,800	14,600	
30	44,700	14,900	
31	41,000	15,600	

*R.A.-Reduction of Area

The rule of mixtures predicts an ultimate tensile strength for the eutectic of approximately 48,000 psi[57] based on a UTS of 420,000 psi for the Al_3Ni fibers at a composite fracture elongation of 2.1%. The strength of the eutectic was found to be of the order of 28,000 psi at 5% elongation with some scatter in results depending on the degree of perfection of the microstructure. Although this value is much less than the rule of mixtures strength, it does not seem too low considering that the rule of mixtures strength is for a perfectly aligned composite. The composites tested not only exhibited large deviations from alignment but possessed fiber depleted regions surrounding fibrous colonies. Gross imperfections in whisker geometry can be expected to significantly decrease fiber strengths resulting in a reduction in composite strength. In spite of these imperfections eutectic strengths compare favourably with the strengths obtained by Hertzberg et al.[57] for eutectic specimens with fiber depleted regions (a low of 25,300 psi at 4% elongation and a high of 34,600 psi at 2.7% elongation).

Table 1 indicates a low of 27,400 psi at 5% elongation and a high of 30,400 psi at 3% elongation. That fiber strengthening occurs is apparent from the broken fibers and void formation showin in Fig. 43.

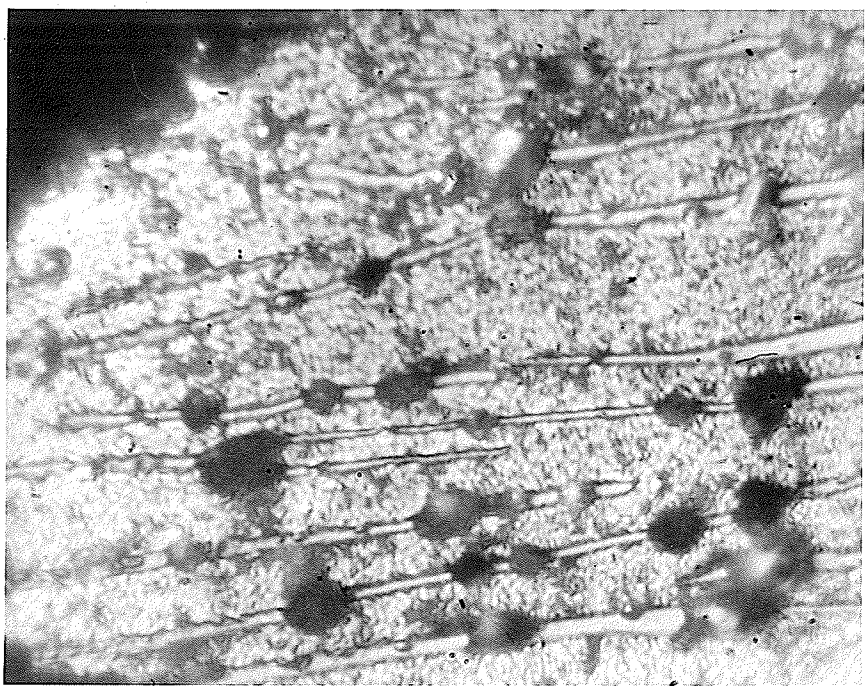

Fig. 43 Broken fibers and voids at fiber fractures near the fracture surface.

Composite failure occurred by the growth and coalescence of voids nucleated at fiber fractures. The strength obtained, although falling short of the 49,700 psi reported by George et al.[16], still represents greater than a two-fold increase over that of the random as-cast structure (13,600 psi at 15-20% elongation[56]).

The transverse strength of the eutectic (Specimens 9 and 10) is approximately 18,000 psi at 13% elongation compared to 9,800 psi at 16% elongation found by George et al.[16] The improved strength and smaller elongation are due to greater transverse fiber reinforcement made possible by large fiber misalignments.

The hypoeutectic alloys are expected to possess a lower U.T.S. and Y.S. than the eutectic alloys because of lower volume fractions of reinforcing phase. This they do and Table 1 indicates that for the two hypoeutectic alloys tested (4.6% and 5.7%Ni) U.T.S. and Y.S. decrease with nickel concentration. Although it is not evident in Specimen 15 (5.7%Ni), the expected increase in fracture elongation with decreasing nickel content shows up in the 4.6%Ni alloy being 7% compared to 5% for the eutectic. A typical hypoeutectic microstructure is shown in Fig. 44 which clearly shows the primary aluminum dendrites and the interdendritic eutectic.

Fig. 44 Al-4.6%Ni X 90

A view of the fracture surface indicating that strengthening is provided by aligned fibers in the interdendritic eutectic is shown in Fig. 45.

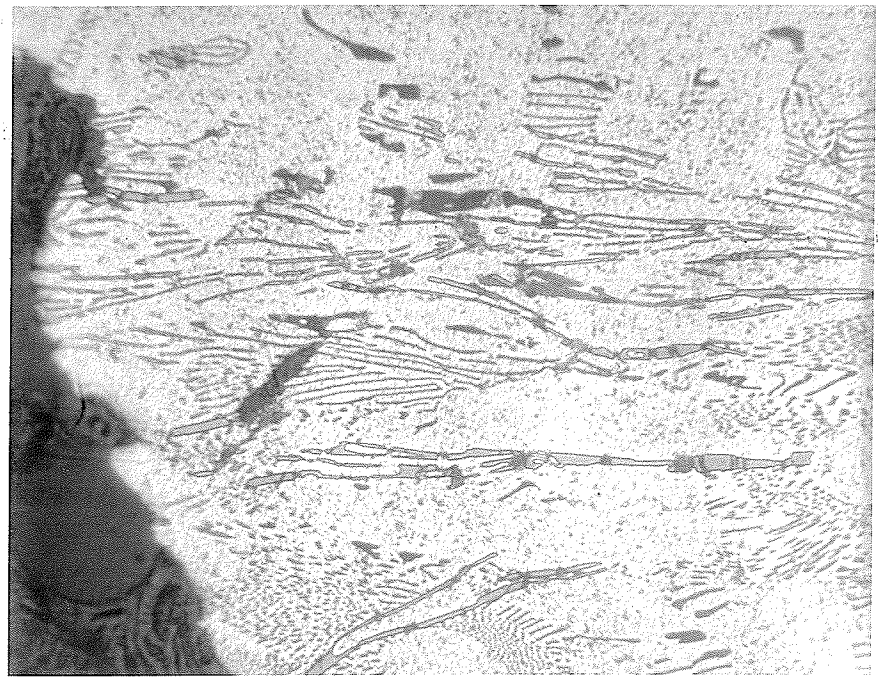

Fig. 45 Al-4.6%Ni showing fracture through a fibrous region indicating that fiber strengthening occurs X455.

The hypereutectic alloys tested exhibited two different types of microstructure. Al-7%Ni had a colony eutectic morphology with large Al_3Ni particles sparsely dispersed throughout. The colonies were fairly continuous along the specimens tested and were separated by regions denuded of Al_3Ni. Most fibers appeared to be very short although it could not be definitely determined if they were short or if they were severely misaligned so that the longitudinal section viewed showed their cross-sections. Al-20%Ni exhibited a dendritic structure with a fibrous interdendritic eutectic. The very large size of the Al_3Ni dendrites as compared to fibrous Al_3Ni is depicted in Fig. 46.

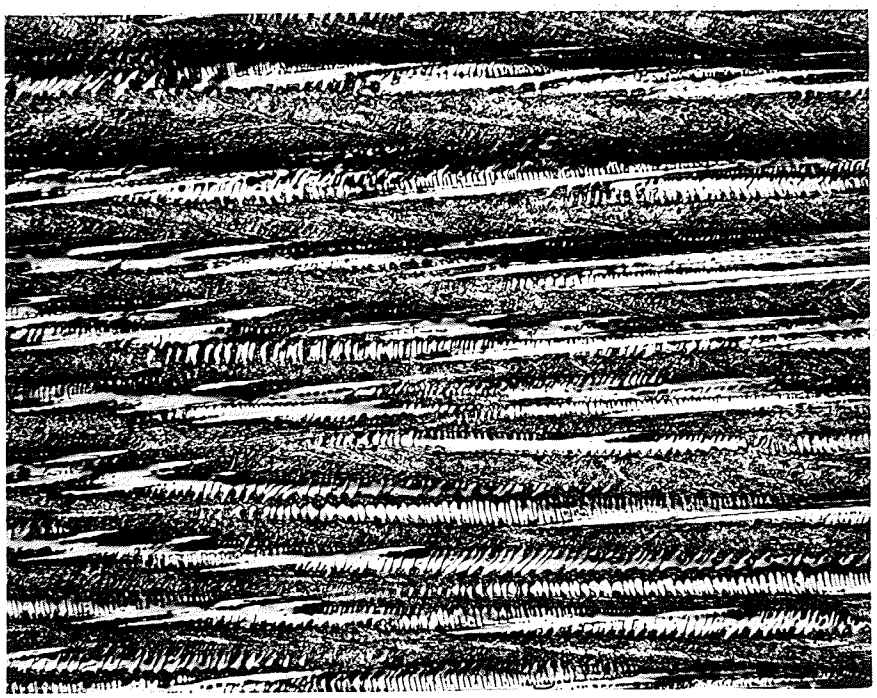

Fig. 46 Longitudal section of Al-20%Ni x 70

Table 1 (Specimens 16, 17, 18) indicates that the U.T.S. of the Al-7%Ni alloy is less than that of the eutectic while the yield strength is greater. One would expect that in a fibrous hypereutectic alloy both U.T.S. and Y.S. would be higher than in the eutectic by virtue of a large volume fraction of reinforcement. However, as stated above, the primary Al_3Ni solidified in the form of dispersed particles--not as fibers and it was these particles which decreased the U.T.S. while raising the Y.S. Fig. 47 shows a portion of an Al-7%Ni fracture surface. Fracture in Al-7%Ni tended to occur along a brittle path through primary Al_3Ni. However, the volume fraction of primary Al_3Ni was not large enough to traverse any one section of the specimens and failure occurred through

Fig. 47 Al-7%Ni fracture surface X 400

the fibrous colonies thereby enabling them to provide reinforcement. The area fraction of reinforcement at the fracture surface is decreased by the large, weak Al_3Ni particles and this effect is reflected in a decreased U.T.S. Since Al_3Ni is strong and brittle, the Y.S. was raised while ductility was decreased.

Looking at Fig. 46 it would be expected that Al-20%Ni would be much stronger than the eutectic because of the well aligned dendrites. But specimens 19 and 20 in Table 1 have a U.T.S. lower than the eutectic by about 10,000 psi. The lower U.T.S. is due to two factors. First, the relatively large size of the dendrites and their concomitant imperfections given them a much lower U.T.S. than the rod-line fibers in the eutectic.

Second, when the weak dendrites fail, the fairly brittle eutectic matrix is unable to redistribute the locallized overburden because of an incapability of large plastic flow and fracture occurs at the weakened cross-section. Fig. 48 shows the fracture surface of an Al-20%Ni specimen.

Fig. 48 Al-20%Ni fracture surface X 85

That the Al_3Ni dendrites carry most of the load is obvious from Fig. 48 (multiple fractures near the fracture surface while most eutectic fibers remain unbroken). Incapacity of the matrix for large plastic deformation is evident in that no voids were formed at dendrite fractures. The effect of the brittle dendrites is to raise the yield strength above the eutectic value (Table 1) and to decrease elongation at fracture.

Table 1 indicates an ultimate compressive strength of about 36,000 psi for the Al-Ni eutectic. The "ultimate" strength is not actually the highest stress sustained by the specimens but it is the highest value

obtained before a decrease in stress occurred. After a decrease in stress, the stress again rose as the specimen was flattened. Transverse specimens exhibited no drop in stress as the strain was increased but the stress-strain curve exhibited a positive slope as the specimens were flattened. Al-20%Ni can be seen (Table 1) to be much stronger in compression than the eutectic. This is because of added reinforcement by the Al_3Ni dendrites. In compression, the imperfections of the dendrites are not as critical as in tension so that composite compressive strength is not adversely affected by the dendrites. The stress-strain behaviour of the Al-20%Ni alloy was the same as the eutectic behaviour. The specimens did not break but flattened as the fibers (dendrites) were broken.

It was stated previously that unidirectionally solidified eutectics normally exhibit excellent high temperature stability. However, in the present series of tests it was found that high temperature exposure caused coarsening and if the exposure was long enough, fiber shortening and agglomeration of Al_3Ni occurred. Fig. 49 shows such deterioration of the structure of specimen 8 after only 22 hr. at 585°C (the eutectic temperature is 640°C). Although the degree of coarsening is not great, the rounding of sharp edges indicates that coarsening has begun. The broken fibers reveal that they still reinforce the matrix. Table 1 indicates that room temperature strength decreases and elongation to failure increases with increasing time of high temperature exposure both for the Al-Ni eutectic (specimens 5-8) and for Al-20%Ni (specimen 21). This behaviour is caused by microstructional deterioration. Such deterioration is in contrast to the results of Bayles et al.[58] who have found that exposure of the Al-Ni eutectic to temperatures as high as 608°C for 100 hr did not impair room temperature strength. However, they did find that

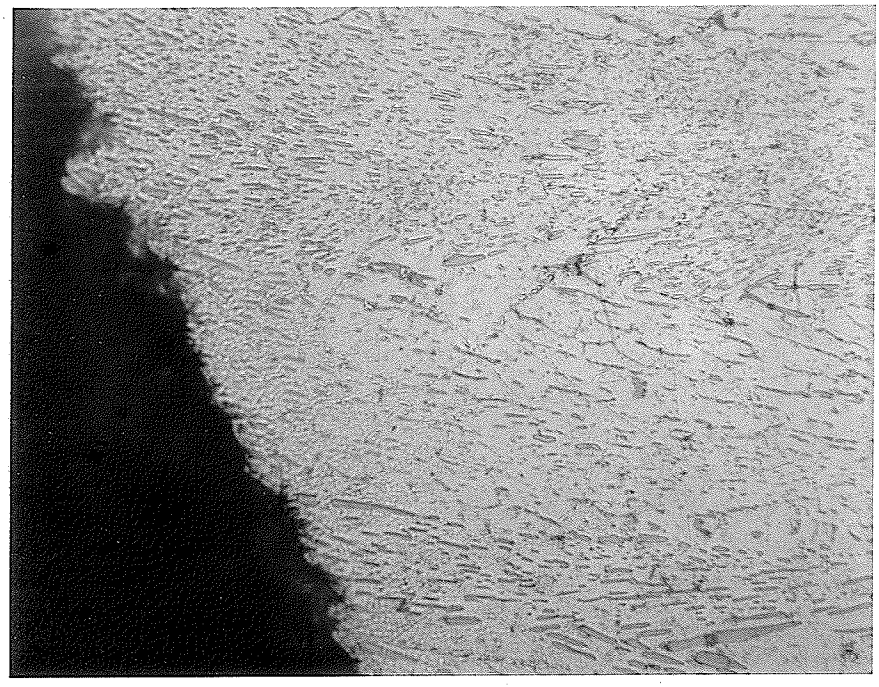

Fig. 49 Al-Ni eutectic after 22 hr at 585°C X 400

at 608°C the rate of coarsening of the microstructure (number of fibers/ cm^2 in a transverse section) increased as solidification rate increased and that specimens solidified at 10.6 cm/hr exhibited a lower final density of fibers than specimens solidified at 4.9 cm/hr and 2.2 cm/hr. Thus, the degree of coarsening is dependent on initial fiber density. Since the specimens tested were solidified at about 80 cm/hr, the degree of coarsening is expected to be much greater than the results of Bayles et al. indicate. Also in contrast to the results of Bayles et al., high temperature exposure was found to destroy the fibrous structure by spheroidization and agglomeration. These phenomena are due partially to the increased degree of coarsening of a very fine microstructure and partially to the original lack of alignment of the fibers. Since the

driving force for agglomeration and spheroidization is the minimization of interfacial energy, deviation from the preferred interfacial crystallographic relationship provided the impetus for these phenoma. It was observed, however, that some aligned regions of the test specimens exhibited little or no deterioration at elevated temperature and this stability is due to the presence of a preferred interfacial relationship.

Table 2 shows the results of elevated temperature tests on the Al-Ni eutectic.

Table 2

All specimens aged for 50 hr. at test temperature.
0.2% offset yield strength given.

Test Temp.	U.T.S.(psi)	Y.S.(psi)	Elongation(%)	R.A.(%)
200°C	18,700	11,000	10	15
300°C	12,900	9,500	15	43
400°C	6,650	5,680	20	47
500°C	2,920	2,640	25	85

As Table 2 clearly shows, U.T.S. and Y.S. steadily decrease with increasing temperature while elongation and R.A. increase. Fig. 50 more clearly illustrates this behaviour. Since all specimens were aged 50 hours at the test temperature prior to testing, microstructural deterioration was observed, being more severe with increasing temperature.

Attempts at cold rolling the Al-Ni eutectic revealed that the yield strength could be raised to the vicinity of 20,000 psi and the U.T.S. to over 31,000 psi. Tables 3 and 4 contain the results of tests on the cold worked specimens. The percentages given are reduction in thickness of a bar type specimen after passing through a pair of flat rolls. Beginning with specimen blanks approximately $^{3}/_{32}$" thick, the thickness was decreased several thousandths each pass.

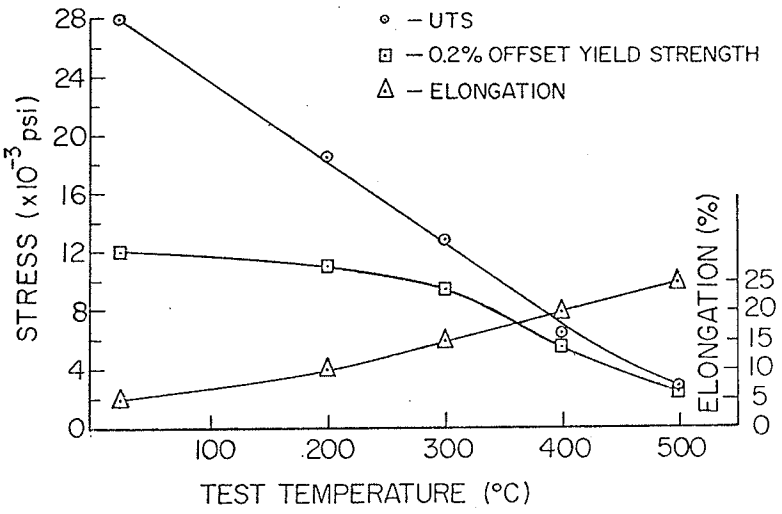

Fig. 50 Variation of U.T.S., Y.S. and elongation with temperature of the Al-Ni eutectic.

Table 3

Percent Cold Work	U.T.S.(psi)	0.2% Offset Y.S.(psi)
2.3	26,500	17,700
4.7	28,400	18,600
21	29,000	18,900
22	31,100	20,400
26	27,800	18,500

Table 4

All specimens aged 2 hr. at 600°C before testing at room temperature.

Percent Cold Work	U.T.S.(psi)	0.2% Offset Y.S.(psi)
2.0	23,000	8,200
6.5	22,700	6,900
15	21,000	10,200
22	21,000	9,000
30	20,200	7,700
40	19,200	7,600
60	17,900	9,400

Referring to Table 3 it is seen that, although the yield strengths have been raised several thousand psi compared to the eutectic (specimens 1-4 in Table 1), generally speaking, fiber breakages led to a decrease in the U.T.S. At small values of plastic deformation (cold rolling) fiber breakage adversely affects the U.T.S. since the amount of cold work is inadequate to strengthen the matrix sufficiently to compensate for the loss of reinforcement. At a large amount of deformation (26% reduction in thickness) the loss in strength due to fiber breakage is too great to be made up by work hardening the matrix. The optimum amount of cold work was found to be in the order of 22% reduction in thickness where the loss of strength due to fiber breakage is made up by work hardening the matrix with a resultant increase in composite strength.

The results of Table 4 are depicted in Fig. 51.

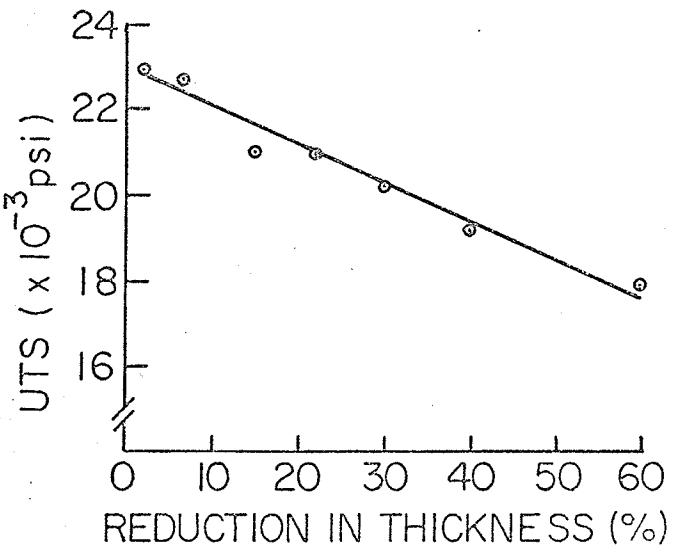

Fig. 51 U.T.S. of Al-Ni eutectic after cold rolling and ageing at 600°C for 2 hr.

Although the yield strengths do not appear to follow any pattern, it is seen from Fig. 51 that the U.T.S. after high temperature exposure decreases steadily, with cold work. All specimens exhibited gross spheroidization of the broken fibers after high temperature exposure with the spheroidization becoming more severe as the amount of cold work was increased. Fig. 52 shows how the structure of the eutectic appeared after 15% cold work and 2 hr. at 600^{o}C. It was noticed that fracture elongation increased with cold work. This is to be expected since the smaller broken fibers permit larger plastic strains in the matrix.

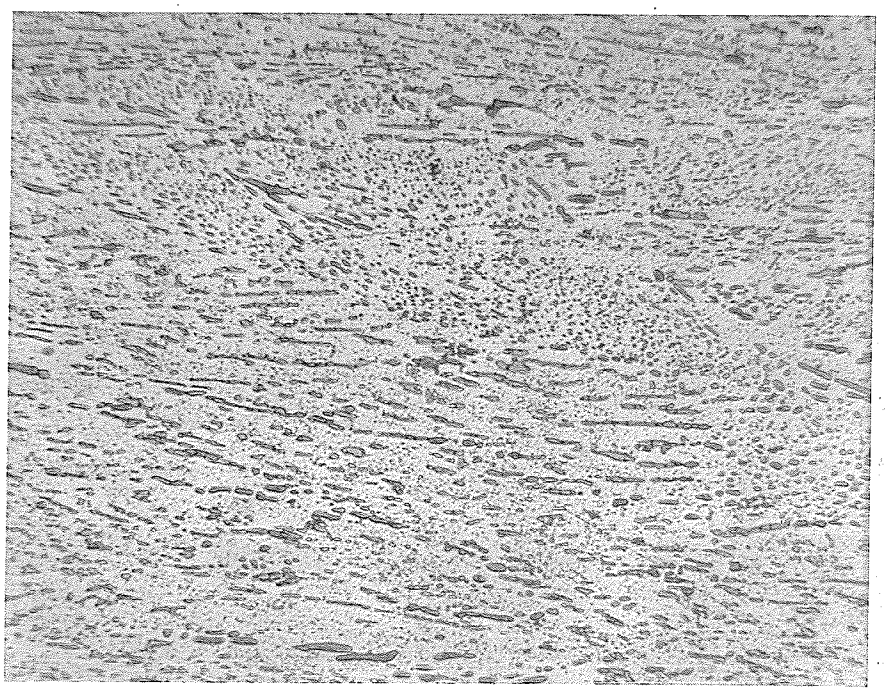

Fig. 52 Al-Ni eutectic after 15% cold work and 2 hr. at 600^{o}C (after tensile testing) X 400.

Al-Cu Eutectic:

The Al-Cu eutectic, when unidirectionally solidified, exhibits a lamellar structure of alternating $CuAl_2$ and Al (rich)-Cu solid solution platelets with $CuAl_2$ forming 47.5 vol.% of the alloy. Typical microstructures of the eutectic are shown in Fig. 53 which indicates that the continuous lamellar structure obtained by other researchers[46, 57, 59] was not obtained. Rather, the alloy consists of short colonies of lamellar structure separated by regions of degeneracy. Previous studies have shown that the lamellar structure is formed in order to minimize the Al solid solution-$CuAl_2$ interfacial energy which results in the crystallographic relationship between phases being $\{111\}_{Al}$ // $\{211\}_{CuAl_2}$ // lamellar interfaces and $\langle 10\bar{1}\rangle_{Al}$ // $\langle 120\rangle_{CuAl_2}$ with the growth direction being $\langle 11\bar{2}\rangle_{Al}$.[60] The regions of degeneracy running transversely are similar to severe banding described by Kraft and Albright[61] and are considered to be inherent in the solidification process although vibrations in the casting apparatus probably contribute to the frequency of banding. The very fast solidification rate would render any perturbation in the solidification process significant since the short diffusion time would not allow lamellar solidification to continue unless conditions were ideal.

The interlamellar spacing, λ, was found to be approximately 1μ, much smaller than that obtained in other investigations in which solidification rates were less than 10 cm/hr. However, Chadwick[46] has solidified the Al-Cu eutectic at rates as high as 60 cm/hr with a resulting continuous lamellar structure and $\lambda<1\mu$ Chadwick's temperature gradient was 70^{o}C/cm giving a value of G/R of 1.167^{o}C/hr. Since it is the value of G/R, not R alone which determines the type of microstructure and since the temperature gradient in the present tests is unknown, a com-

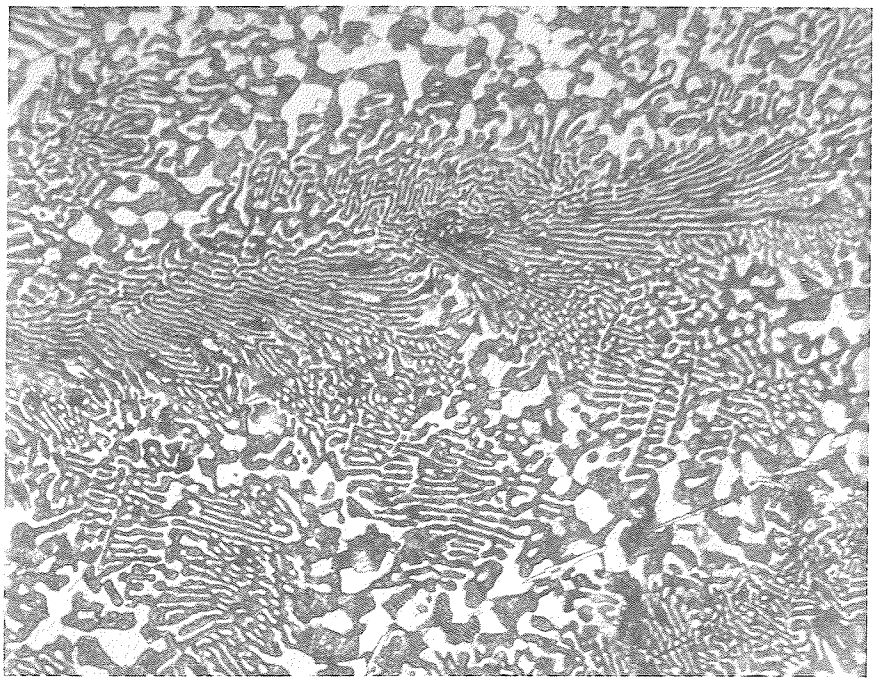

A) Longitudinal X 660

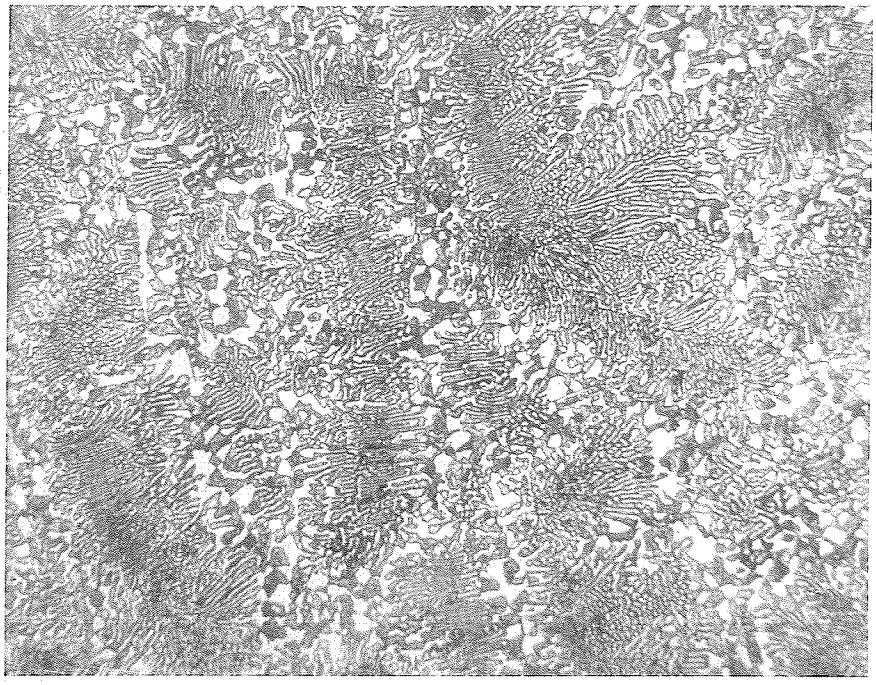

B) Transverse X 400

Fig. 53 Al-33%Cu unidirectionally solidified.

parison of the effect of G/R is impossible. It is also significant that the solidification apparatus employed by Chadwick provided a constant solidification rate (the 80 cm/hr previously stated is only an average value) and temperature gradient with no vibrations.

Fig. 53(A) illustrates the gross imperfections of the lamellar structure in the present investigation. Not only are the lamellae wavy but many are discontinuous with lamellar terminations contributing to the deviation from an ideal structure. Ingots quenched with an air jet exhibited the same general type of morphology but the interlamellar spacing was slightly larger since the solidification rate (about 60 cm/hr) was less than that for the water quenched ingots.

The tensile properties are shown in Table 5 which indicates a U.T.S. of approximately 29,000 psi for the water quenched specimens and about 27,000 psi for the air quenched specimens. All specimens tested at room temperature exhibited brittle fracture (ductility immeasurable on a Hounsfield elongation gauge).

Table 5 Al-33%Cu Tensile Tests

In all cases the yield strength is the same as the U.T.S. because of brittle behaviour and elongation and reduction of area are zero.

Specimen Number	U.T.S.(psi)	Treatment
1	28,000	
2	30,500	
3	28,000	
4	29,800	
5	29,500	
6	26,400	
7	28,000	
8	26,800	
9	27,900	Air quenched
10	26,000	Air quenched

Table 5 (Cont'd)

Specimen Number	U.T.S.(psi)	Treatment
11	35,200	1 hr @ 490°C and 8 hr @ 175°C
12	36,600	1 hr @ 490°C and 8 hr @ 175°C
13 Transverse	20,400	
14 Transverse	30,000	
15 Transverse	23,100	
16	27,700	5 hr @ 500°C
17	25,000	17 hr @ 500°C
18	18,500	23 hr @ 500°C

The rule of mixtures predicts a U.T.S. of 45,000 psi for a continuous microstructure based on a $CuAl_2$ platelet strength of 80,000 psi.[62] Since the microstructures obtained are discontinuous, this strength was not attained nor was it expected. The U.T.S. of specimens 1-8 (Table 5) was considerably less than ideally because of discontinuities, intercolony degeneracy and imperfections in the lamellar colonies but the strength obtained represents almost a 50% improvement over the as-cast (random) structure strength of about 20,000 psi. The strengths are higher than those obtained by Crossman et al.[62] whose highest solidification rate was 4.7 cm/hr yielding a U.T.S. of 26,000 psi with $\lambda = 2.7\mu$. Crossman et al. found that the U.T.S. was increased by increasing the solidification rate while decreasing λ. The improved strength in the present investigation is due to the added reinforcement of the finer structure in spite of the large degree of imperfection when compared to the structures obtained by Crossman et al. Fig. 54 shows the fracture surface of a typical specimen. The fact that fracture exhibits no preferential path but passes through lamellar colonies and intercolony degenerate structure alike attests to the strength of the degenerate regions. If they were much weaker than the colonies, failure would be expected to bypass the colonies. Their fine

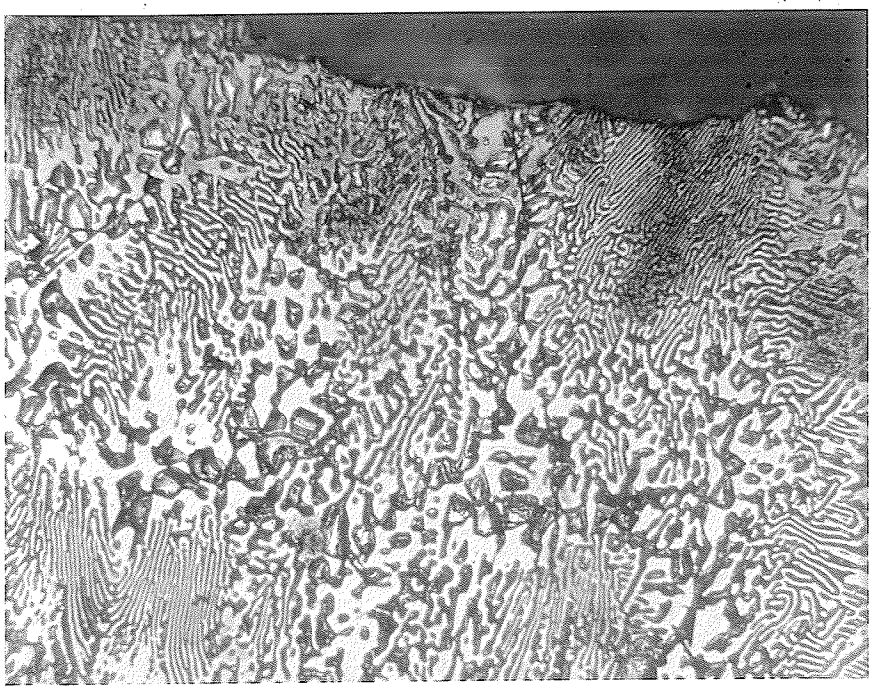

Fig. 54 Al-33%Cu at fracture surface X 400

structure is doubtlessly responsible for their strength. Thus, although composite strength is much less than that predicted by the rule of mixtures, the fineness of both lamellar and degenerate structures provides a strength higher than more perfect but coarser structures. Similarly, the slightly lower strength of the air quenched specimens (9 and 10 in Table 5) compared to the water quenched specimens is a result of a coarser structure. It should be noted in Fig. 54 that very few platelet failures occurred prior to composite fracture in contrast to the many failures observed by Crossman et al.[62] near the fracture surface. This behaviour is indicative of the inability of the thin aluminum platelets to redistribute the stress of a broken lamella. Once a crack is initiated in either the degenerate or lamellar structure,

it proceeds rapidly across the specimen and results in extreme brittleness of the composite.

Also of importance is that eutectic strengths varied slightly above and below the representative value of 29,000 psi depending on the degree of perfection of any given specimen. The more perfect a specimen, the higher its strength.

By solution heat treating the eutectic for 1 hr. at 490°C and ageing for 8 hr. at 175°C the strength of the water quenched specimens was boosted to a maximum of over 36,000 psi (specimen 12, Table 5) compared to 32,800 psi obtained by Crossman et al.[62] for R=4.7 cm/hr.

Table 5 (specimens 13-15) indicates that transverse ultimate tensile strengths ranged from 20,400 psi to 30,000 psi. A typical fracture surface of a transverse section is shown in Fig. 55 which indicates that the random transverse orientation of the lamellar colonies is responsible for considerable reinforcement. The variation in transverse strength is dependent upon the degree of transverse alignment, composite strength increasing as more colonies are aligned parallel to the stress axis. Crossman et al.[62] obtained a transverse U.T.S. of about 16,000 psi for a transverse specimen axis parallel to the lamellae (R=1 cm/hr) and only 13,000 psi when the specimen axis was normal to the lamellae (R-4.7 cm/hr) in single grained specimens. It is apparent that high solidification rate and random transverse lamellar orientation serve to markedly increase transverse composite strength.

Some specimens were aged at elevated temperature prior to testing at room temperature. The results in Table 5 (specimens 16, 17, 18) indicate that strength is adversely affected by high temperature exposure with the U.T.S. decreasing as ageing time is increased. The degree of

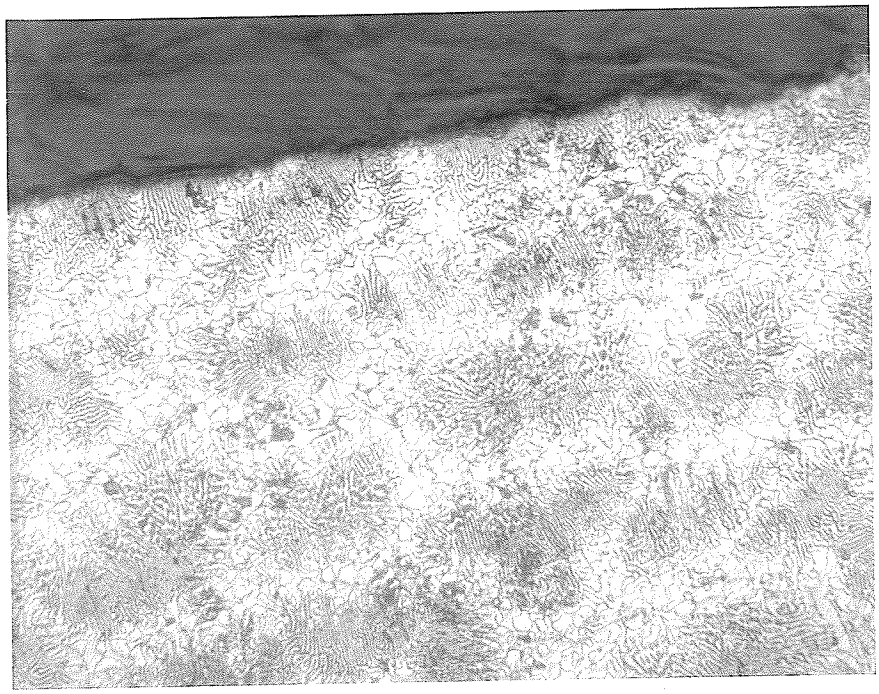

Fig. 55 Al-33%Cu transverse fracture surface indicating reinforcement by lamellar colonies X 400.

brittleness was not measurably affected. It was observed that minor coarsening of the microstructure occurred beginning in the intercolony degenerate regions and extending to the lamellar colonies as ageing time was increased. This effect was small in specimens 16, 17, and 18 but could be readily discerned in the specimens tested at elevated temperatures since they were aged for a longer period of time. Although, as previously stated, eutectic structures and the Al-Cu eutectic in particular, are normally stable at elevated temperatures, stability is decreased by deviation from preferred lamellar crystallographic orientations. Deviation is evident in Fig. 53(A) in that the lamellae are wavy and different colonies are misaligned by several degrees. The

fact that coarsening occurs first in the degenerate regions where the preferred interfacial relationship is absent is indication that departure from the preferred relationship is the cause of high temperature instability. The most extreme case of coarsening and general transition to degeneracy after high temperature exposure occurred after 50 hrs. at 500°C. This specimen is shown in Fig. 56. Although the lamellar colonies exhibit alignment between the Al-solid solution and $CuAl_2$ platelets, their wavy, faulted structure and small interlamellar spacing provide sufficient driving force for coarsening to produce the structure in Fig. 56. These results are in agreement with those of Kraft et al.[63] who, after ageing three types of Al-Cu eutectic structures, namely: lamellae distorted and twisted, lamellae faulted (terminations, mismatch surfaces) and lamellae regular, found that only the latter type of structure remained stable after high temperature exposure while the others spheroidized.

Results of compression tests are shown in Table 6.

Table 6 Al-33%Cu in Compression

Specimen Number	U.T.S.(psi)	0.2% Offset Y.S. (psi)	Treatment
19	96,400	96,400	
20	94,700	94,700	
21	103,900	103,900	1 hr@490°C & 8 hr@175°C
22	92,300	92,300	1 hr@490°C & 8 hr@175°C
23 Transverse	73,800	22,400	
24 Transverse	78,500	24,700	
25 Transverse	72,400	26,000	

Again the very fine microstructure is responsible for compressive strengths superior to those obtained by Yue et al.[59] who found ultimate strengths of 37,300 psi for the unidirectionally solidified eutectic and

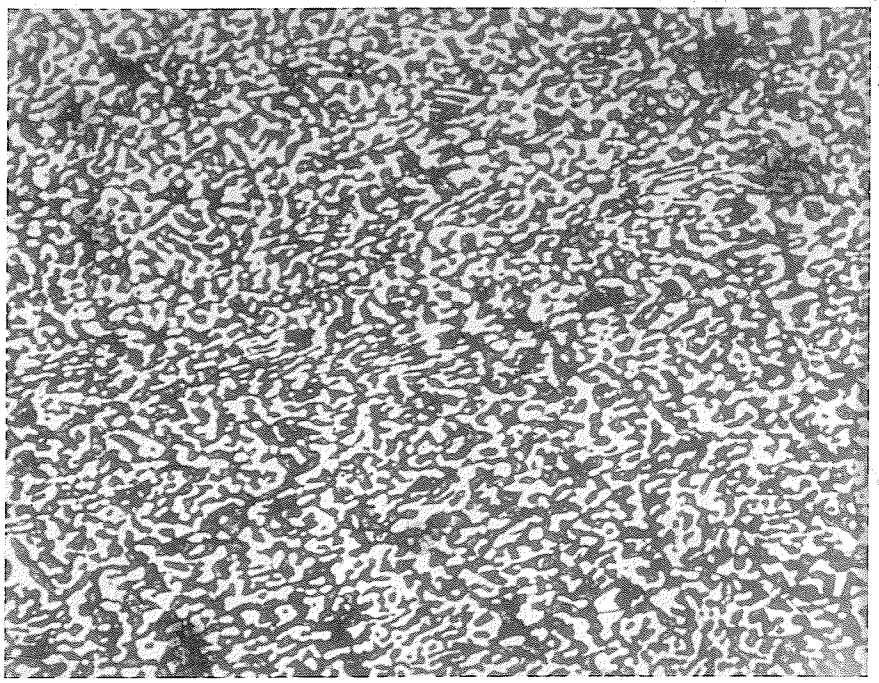

Fig. 56 Al-33%Cu after 50 hr at 500°C indicating degenerate structure X 455.

about 93,000 psi for the heat treated and aged condition. These strengths are much below the comparable values of 96,400 psi and 103,900 psi respectively obtained in the present investigation although it should be considered that some precipitation may have occurred in specimens 19 and 20 (Table 6) during cooling of the ingot which would be responsible for the large ultimate strength attained by these specimens. Because of extreme brittleness, the yield strength in compression in the longitudinal direction is the same as the U.T.S. The transverse compressive strength is relatively high because of the random transverse orientation of the lamellar colonies but greater ductility in the transverse direction is responsible for a large drop in 0.2% offset Y.S. com-

pared to the longitudinal orientation. The increase in compressive strength is approximately two-fold compared to the as-cast (random) structure strengths of 47,200 psi for the untreated condition and 58,300 psi when heat treated and aged.[59]

Table 7 contains the results of tests at elevated temperatures.

Table 7 Al-33%Cu High Temperature Results

All specimens were aged 50 hr. at the test temperature prior to testing.

Test Temperature(^{o}C)	U.T.S.(psi)	0.2% Offset Y.S. (psi)
200	36,600	36,600
300	24,200	22,300
380	12,200	12,200
500	4,040	3,980

The results indicate that with the exception of the test at 200^{o}C, the U.T.S. and Y.S. decrease with increasing temperature. This behaviour is due to weakening of the matrix and $CuAl_2$ platelets with increasing temperature as well as spheroidization as explained above. The lamellar colonies were evident after 50 hr. at 400^{o}C but after 50 hr. at 500^{o}C the structure shown in Fig. 56 resulted. Lamellar strengthening was manifest in substantial reinforcement at temperatures as high as 400^{o}C. Elongation and reduction of area increased steadily from 0% at 200^{o}C to over 100% at 500^{o}C. The high strength of the eutectic at 200^{o}C is attributed to precipitation strengthening of the matrix. After 50 hr. at 200^{o}C composite strength is the same as after a precipitation heat treat (cf. specimen 12 in Table 5) but would be expected to decrease somewhat after prolonged exposure. A comparison of the strengths obtained with the results of Crossman et al.[62] (for R=1 cm/hr) is given in Fig. 57.

Fig. 57 indicates that both the U.T.S. and Y.S. are substantially higher than the values of the more perfect but coarser structure obtained by Crossman et al. Also, the region of inflection (region of rapid decrease in strength with increasing temperature) is moved to a higher temperature range by refining the microstructure.

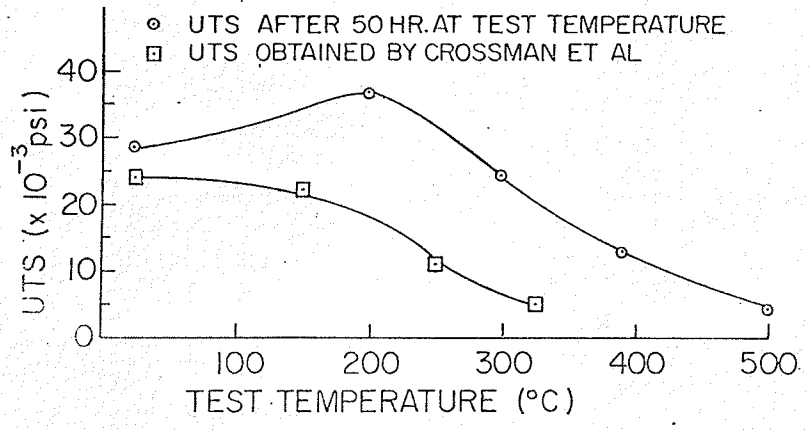

(A)

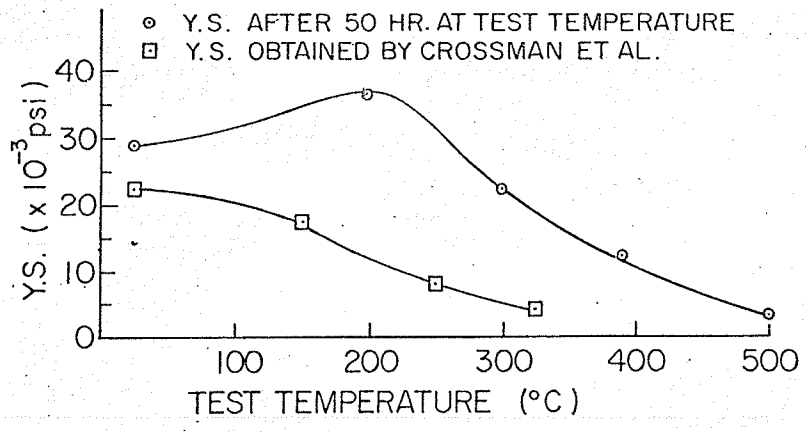

(B)

Fig. 57 A comparison of the U.T.S$_{62}$ and Y.S. with the values obtained by Crossman et al. for R=1 cm/hr.

Al-Si System:

As mentioned previously directionally solidified Al-Si eutectic (12.5 wt.%Si) has a discontinuous morphology with 14.2 vol.% of Si platelets[48] in an Al matrix. There has been considerable doubt concerning the location of the eutectic point and before the 12.5%Si was settled upon, a eutectic composition of Al-11.6%Si was predicted.[64] This alloy was also tested to see if the slight change in composition would affect mechanical properties. Fig. 58 shows the microstructure of Al-12.5%Si. (Hansen states that Al-11.6%Si is the eutectic composition although Hellawell[48] suggests 12.5% or 12.7%Si as the eutectic composition.)

It is readily seen that the Al-12.5% alloy possesses primary Al dendrites surrounded by a eutectic matrix. This morphology is due to the presence of a coupled growth region alluded to previously. Because of undercooling during solidification the eutectic composition is lower than that of the coupled region and the eutectic solidifies as a hypo-eutectic alloy. Most of the microstructure, however, is of the expected eutectic form comprising silicon platelets in an Al matrix. Al-11.6% Si exhibited a similar structure with a slightly greater volume fraction of Al dendrites. In trying to more closely approximate the eutectic structure Al-15%Si was solidified in the hope that this composition would fall in the coupled region. The microstructure obtained is shown in Fig. 59.

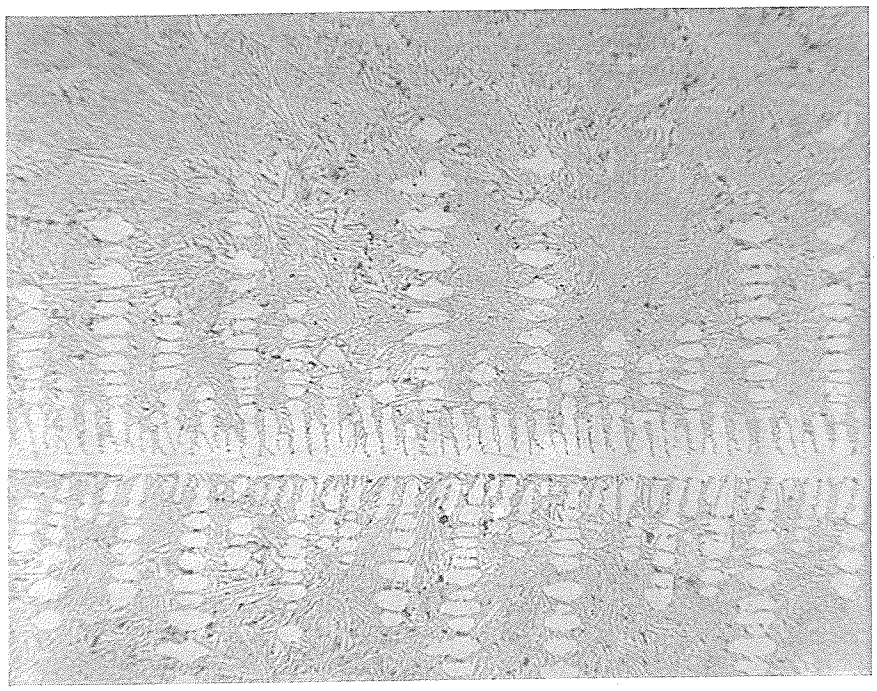

A) Longitudinal X 130.

B) Transverse X 130.

Fig. 58 Al-12.5%Si microstructure.

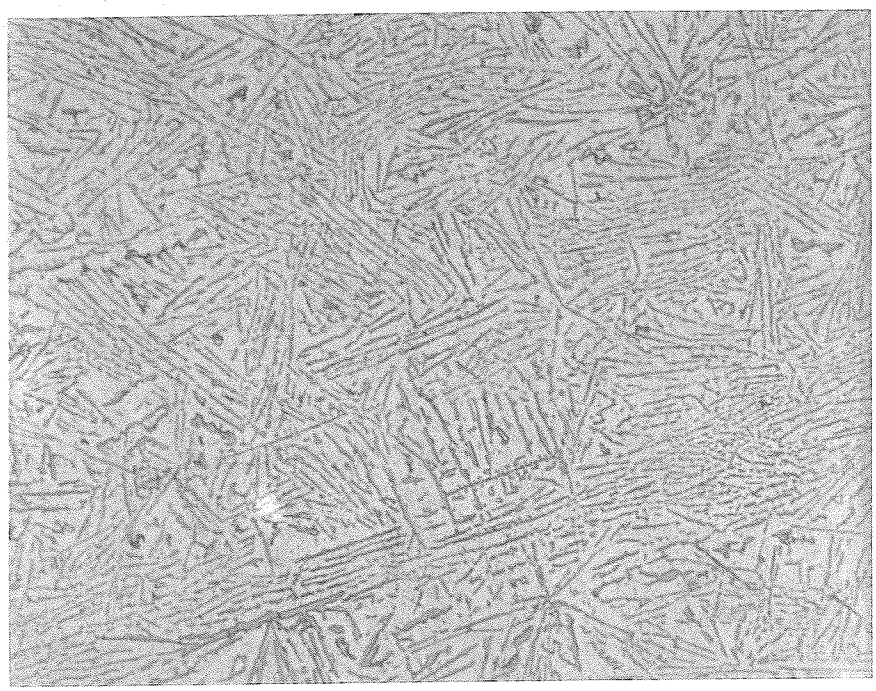

A) Longitudinal X 290.

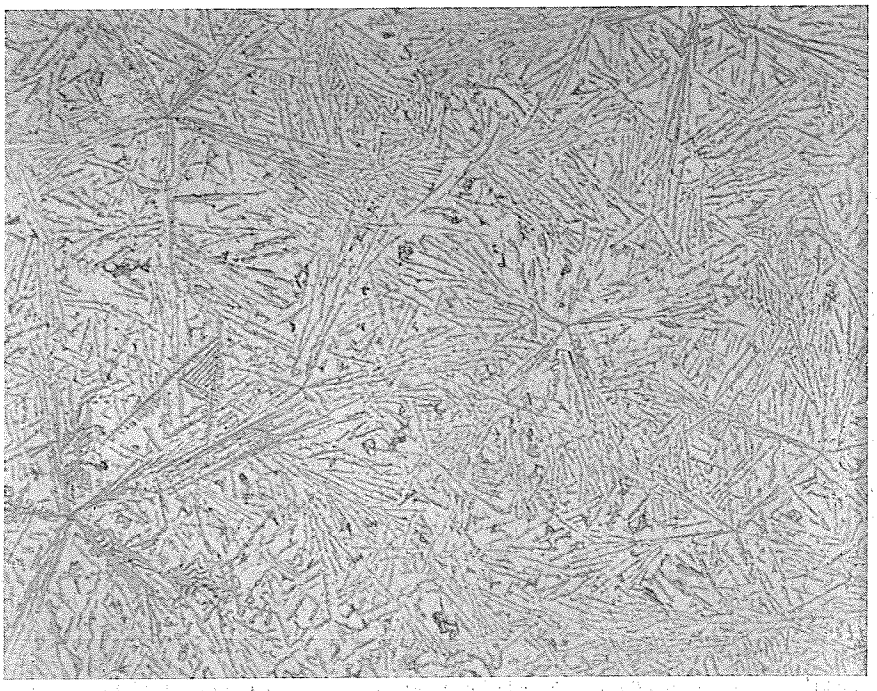

B) Transverse X 220.

Fig. 59 Al-15%Si microstructure.

It is clear from Fig. 59 that Al-15%Si is at a slightly higher composition than the coupled region. Although Si dendrites are present, the 15%Si alloy more closely approximates the eutectic structure than the 12.5%Si alloy and in view of the minimal differences in mechanical properties with varying composition of the three alloys tested, the 15%Si alloy may be assumed to approximate eutectic behaviour. Fig. 58 (A) and 59 (A) indicate that only a fraction of the Si platelets are aligned thus verifying the difficulty of attaining unidirectionality of the Si platelets. The lack of alignment is due to two factors. First, silicon does not exhibit a preferred epitaxial relationship to aluminum. Secondly, the Al-Si eutectic inherently possesses a discontinuous structure when solidified at "ordinary" rates. The process of Si platelet growth is controlled by liquid diffusion, and though there is a strongly preferred growth direction, the very high solidification rates of the present tests result in a short diffusion time causing repeated growth arrest and nucleation of the silicon. Because of a lack of a preferred epitaxial relationship freshly nucleated platelets have a random orientation and hence random growth directions. Aligned structures of Al-12.5%Si[48] and Al-11.7%Si[65] alloys containing rod-like Si crystals with no primary phase have been obtained at solidification rates in the order of 2 cm/day (approx. 0.083 cm/hr) thus attesting to the fact that liquid diffusion time is a critical solidification parameter. Miura and Hamanaka[66] have obtained excellent directionality in Al-11.7% Si at solidification rates less than 0.15 cm/hr with a temperature gradient of 10^{o}C/cm although imperfections existed in the elongated Si crystals. As the growth rate was increased from 0.1 cm/hr to 3 cm/hr progressively greater deviation from perfect alignment occurred.

Tensile test results for the eutectic and hypoeutectic concentrations are recorded in Table 8.

Table 8 Al-Si Hypoeutectic and Eutectic Tensile Results

R signifies a random structure obtained by solidification in a room temperature mold.
0.2% offset yield strengths are given.

Specimen Number	U.T.S.(psi)	Y.S.(psi)	Elong (%)	R.A.(%)	Treatment
Al-11.6%Si					
1R	20,900	10,900	7	5	
2R	20,900	10,900	7	5	
3	24,500	13,500	16	28	
4	24,800	13,400	16	31	
5	24,800	13,100	22	50	3 hr@550^{o}C
6	24,400	13,400	20	47	7 hr@550^{o}C
Al-12.5%Si					
7	24,200	12,900	15	28	
8	24,200	13,800	15	26	

The U.T.S. of unidirectionally solidified Al-11.6%Si is about 24,600 psi at 16% elongation compared to 20,900 psi at 7% for the as-cast (random) structure while the yield strength is about 2500 psi higher in the unidirectionally solidified specimens.

Short heat treatments (specimens 5 and 6) did not affect the U.T.S. or Y.S. but caused increased ductility as indicated in larger fracture elongation and reduction of area. This behaviour is likely due to annealing of the matrix thus enabling a greater ductility. The length of heat treat was not enough to cause microstructural deterioration so the degree of platelet strengthening was unchanged. Softening of the matrix would not be expected to seriously affect composite strength because of the relatively small matrix contribution.

Al-12.5%Si (specimens 7 and 8, Table 8) exhibited essentially the same strength as Al-11.6%Si with slightly less ductility. Both alloys fractured in the same manner and Fig. 60 indicates the type of fracture surface observed.

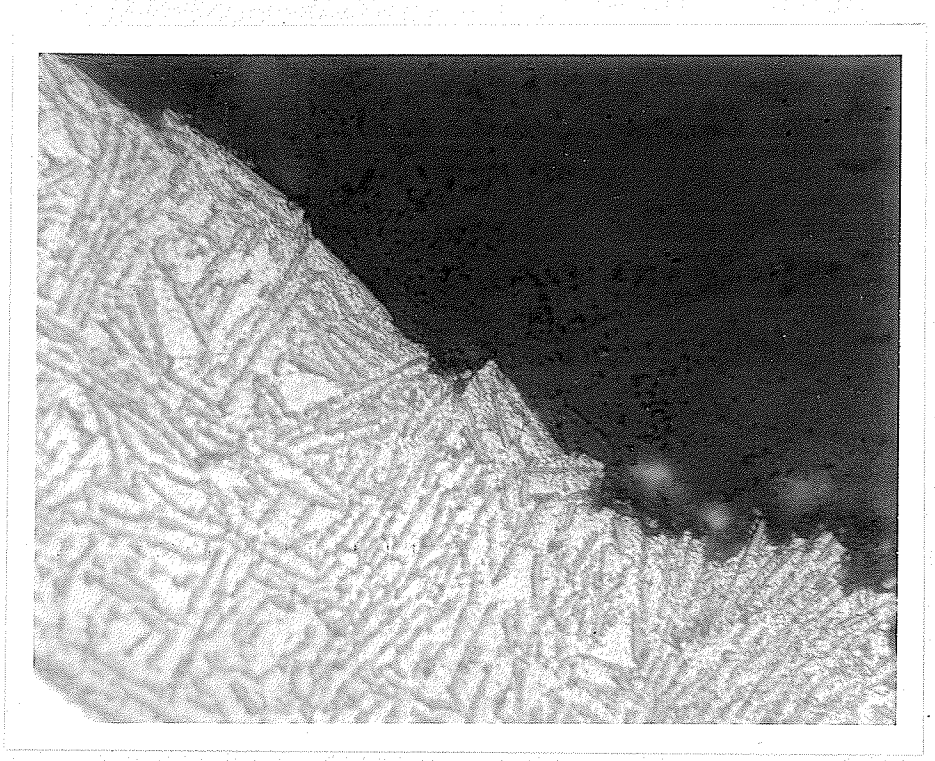

Fig. 60 Al-15%Si fracture surface (typical of hypo-eutectic alloy fractures also) X 560.

It is obvious from Fig. 60 that interfacial failure is a prevalent mode of fracture although the fracture surface passes through regions of aligned Si platelets. It is the aligned platelets which are responsible for most of the reinforcement. There is also a tendency to follow a brittle fracture path since fracture passes beside transverse Si platelets whenever possible.

Results of tests on Al-15%Si given in Table 9 show that this alloy possesses approximately the same U.T.S. as the 11.6 and 12.5%Si alloys

but that the 0.2% offset yield strength is increased to over 14,000 psi while fracture elongation is decreased to about 5%.

Table 9 Al-15%Si Tensile Results

R signifies a random structure

Specimen No.				
9R	18,200	12,600	3	2
10R	18,400	13,800	3	2
11	24,100	15,200	5	4
12	25,200	14,200	5	10
13	24,900	13,300	5	7
14	24,700	14,800	6	6
15 Transverse	22,200	13,900	4	4
16 Transverse	21,600	13,400	5	2
17 Transverse	22,500	13,600	5	2

The increased Y.S. and decreased fracture elongation are due to the presence of a larger volume fraction of silicon, partly in the form of dendrites, compared to primary aluminum dendrites in alloys of the hypoeutectic and eutectic compositions. The fact that the U.T.S. is approximately constant in the composition range 11.6 to 15%Si suggests that the failure modes of the different alloys are the same. Failure of Al-15%Si typifies this mode which is exemplified in Fig. 60 and 61. The tendency is for fracture to follow a brittle path (which is easier in the 15%Si alloy because of a larger volume fraction of silicon) with silicon particle failure initiating voids within the specimen. With increasing strain, void growth and coalescence occurs as Fig. 61 shows. It should be noted that, although a brittle fracture path was preferred, it did not exist across any test section and fracture had to pass through both aligned and misaligned regions. Fig. 61 reveals that both primary silicon and platelets strengthen the alloy since multiple fractures occur in both forms of silicon.

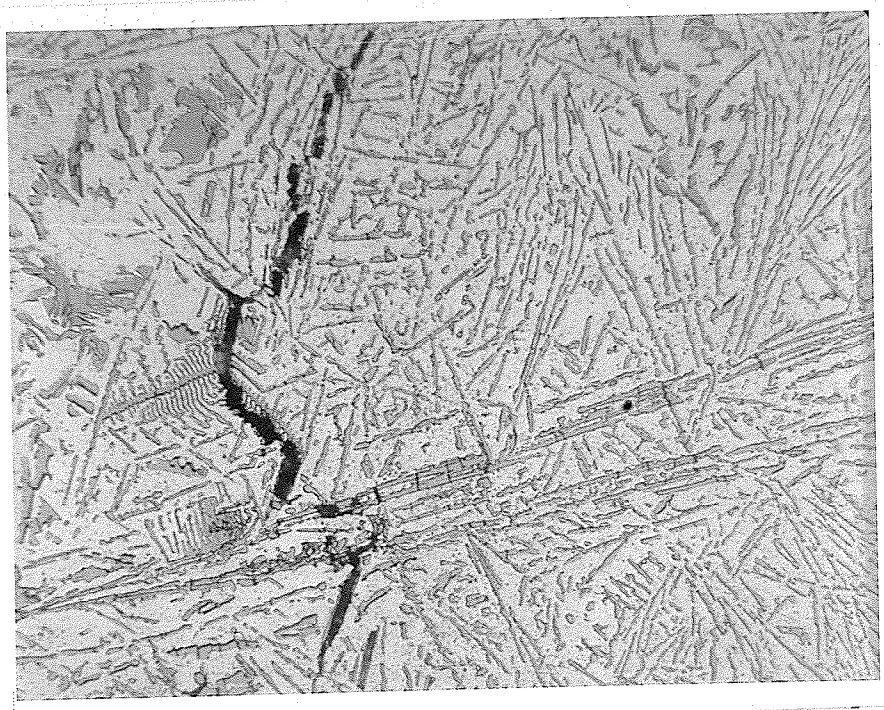

Fig. 61 Al-15%Si typifying failure mode X 365.

Using the rule of mixtures equation for continuous fibers (equation 4), it is possible to find an idealized composite U.T.S. For silicon whiskers with a characteristic transverse dimension less than 50μ Pearson et al.[68] have found that $\sigma_f \simeq 2.2 \times 10^{10}$ dynes per cm^2 (319,000 psi) at 1% elongation. At a strain of 1% $\sigma_m' \simeq 1000$ psi for pure Al unidirectionally solidified by a water quench. Substituting these values into equation 4 ($V_f = 0.142$) yields a σ_c of 46,160 psi. This is the maximum U.T.S. possible for the Al-Si eutectic since it assumes that the silicon is in the form of continuous whiskers. Since the rule of mixtures analysis bears no relationship to the Al-Si alloys tested because of the remoteness of their structures from an aligned fibrous or platelet structure, the comparison between rule of

mixtures strength and the strengths obtained is misleading. An indication of the improvement in mechanical properties of unidirectionally solidified specimens can be found in a comparison with as cast specimens. The U.T.S. of the as cast specimens (9R and 10R, Table 9) is about 7,000 psi less than the U.T.S. of the unidirectionally solidified specimens while the Y.S. is about 1500 psi less. An increase of 2% in ductility is also evident in the unidirectionally solidified specimens. This behaviour is explained by the greater probability of a weak, brittle failure path existing in the as cast structure and an absence of alignment. With platelets having a transverse orientation, a crack formed at a platelet will be larger than if the platelets had a longitudinal orientation and the crack size will more likely exceed the critical size. The short distance between platelets in the transverse direction allows crack propagation to proceed more easily than if platelets were aligned longitudinally. Since the as cast structure has more transverse platelets than the directionally solidified structures, more of the fracture will occur through brittle silicon. The same type of behaviour occurs in the 11.6 and 12.5%Si alloys as Table 8 shows.

The ultimate strengths obtained for the "aligned" structure are much higher than the 17,800 psi reported by Miura and Hamanaka[67] for Al-11.7%Si solidified at 0.1 cm/hr. They found that the aligned structure possessed a lower U.T.S. than the as cast structure. The low strength obtained by them must be due to the coarseness of their structures. Silicon crystals grew with cross-sections in the form of a swastika (卍) with the platelets (arms of the swastika) about 2μ thick, interplatelet dimensions in the order of 100μ and intercrystal spacings of about 30μ. This structure is much coarser than the as cast structure

which has a refinement comparable to that of the unidirectionally solidified specimens of the present investigation. Silicon platelet thicknesses are less than 1μ and interplatelet spacings are about 3μ and less. Constriction of the matrix is greater in the fine structure and silicon crystal strength is expected to be much higher. Both of these characteristics of the fine structure typified in Fig. 59 are responsible for the strength improvement of the alloys tested over the strengths observed by Miura and Hamanaka. The 0.2% offset yield strength obtained by Miura and Hamanaka is 16,300 psi, slightly higher than found in the present series of tests. Just as partial silicon platelet alignment is responsible for increasing the yield strength over the as cast yield strength in Tables 8 and 9, so too is the excellent alignment of the microstructures of Miura and Hamanaka responsible for the higher yield strength found by them.

Results of transverse tests in Table 9 indicate that both the U.T.S. and Y.S. of transverse specimens are only slightly lower than in longitudinal specimens. Good strength retention at large misalignments of the specimen axis from the solidification direction is due to the random array of the silicon platelets. The random platelets provide reinforcement in the transverse direction. The fracture surface and mode of failure were similar in transverse and longitudinal specimens.

Exposure of all three alloys tested to elevated temperatures indicated that they were not stable except for very short times (e.g. specimens 5 and 6 of Table 8). After 50 hr at 300°C only minor changes such as the rounding of pointed edges had occurred. After 50 hr at 400°C it was evident that spheroidization had begun (the eutectic temperature is 577°C). After 50 hr at 500°C the microstructures appeared similar to that shown in Fig. 62 for Al-15%Si. The same rate of microstructural

deterioration was evident in all three silicon alloys. It would not be expected for Al-Si alloys to be stable at elevated temperatures (except perhaps for a coarse aligned structure) since there is no preferred low energy interfacial relationship between aluminum and silicon.

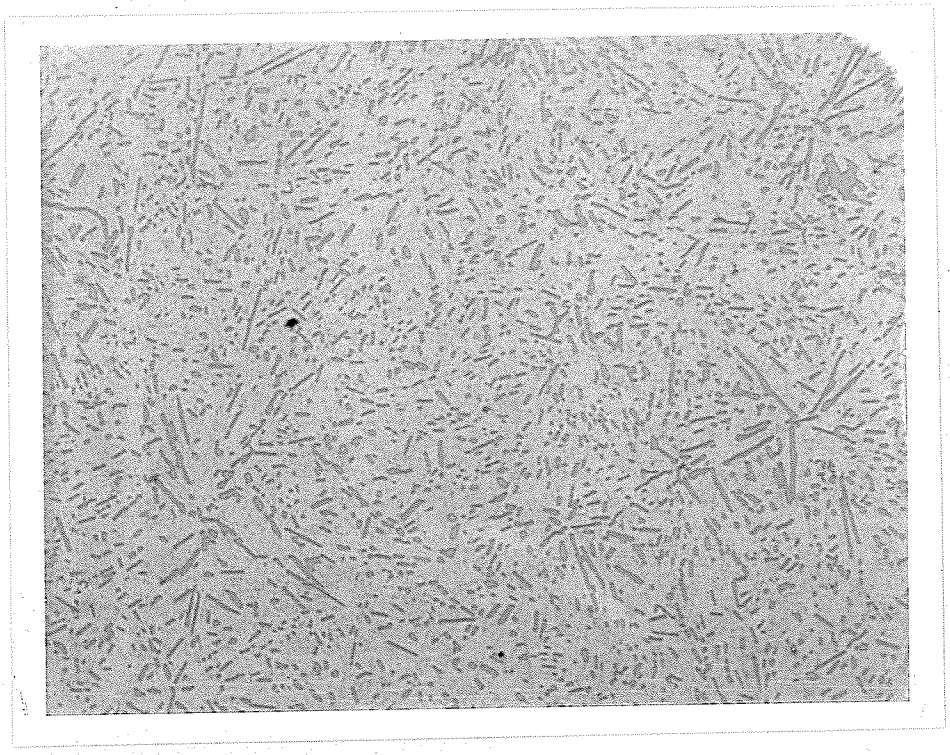

Fig. 62 Transverse section of Al-15%Si after 50 hr at 500°C. Notice the remnants of silicon dendrites X 260.

The results of elevated temperature tensile tests are given in Table 10.

Table 10 Al-Si High Temperature Results

0.2% offset Y.S. given.
All specimens aged for 50 hr. at test temperature prior to testing.

Test Temp (°C)	U.T.S.(psi)	Y.S.(psi)	Elong.(%)	R.A.(%)
Al-11.6%Si				
200	10,700	8,000	15	26

Test Temp (^{o}C)	U.T.S.(psi)	Y.S.(psi)	Elong.(%)	R.A.(%)
Al-11.6%Si				
300	6,000	4,500	15	32
400	2,200	1,800	76	58
500	605	570	142	90
Al-15%Si				
200	13,180	9,220	10	13
300	7,130	5,680	15	20
400	2,580	2,060	51	50
500	770	570	100	74

It is apparent from Table 10 that Al-15%Si is stronger and less ductile than Al-11.6%Si at elevated temperatures, the result of a larger volume fraction of silicon. Strengths given in Table 10 are superior to those obtained by Miura and Hamanaka[67] except above about 400^{o}C where spheroidization causes a large drop in strength and increase in elongations (highest elongation recorded by Miura and Hamanaka is 6½% at 300^{o}C). A comparison of high temperature strengths is given in Fig. 63.

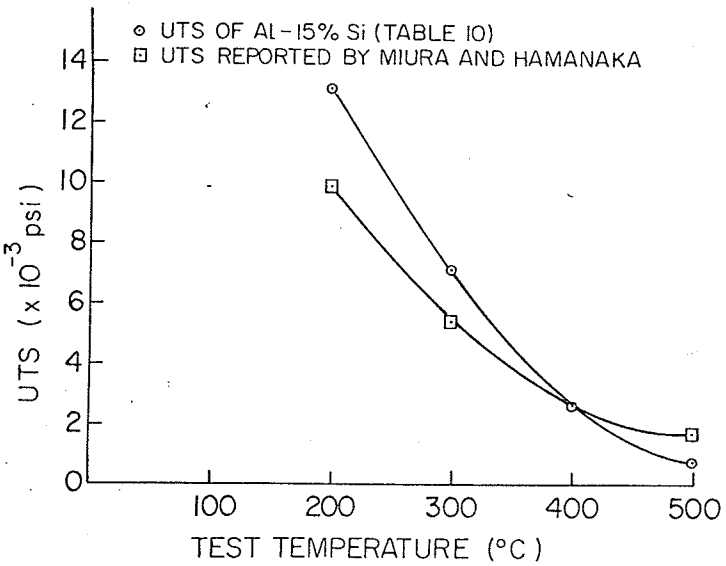

Fig. 63 Comparison of elevated temperature U.T.S. to results of Miura and Hamanaka.[67]

CONCLUSIONS

1. It is unnecessary to carefully control solidification variables in order to obtain mechanical properties superior to those of random structures. An uncontrolled water quench produced partially aligned fibrous and lamellar structures with a high degree of refinement. Although the Al-Ni eutectic strength is not as high as that of more perfect structures, it is more than twice as great as that of the random as cast structure. Al-Cu and Al-Si eutectic strengths are superior to the strengths of specimens produced under carefully controlled laboratory conditions because of their refinement. Large misalignments of the reinforcing phase are responsible for excellent transverse strength.

2. Unidirectionally solidified off-eutectic Al-Ni alloys exhibited lower tensile strengths than the eutectic alloys although the Y.S. of hypereutectic alloys was increased. An aligned hypereutectic alloy had improved compressive strength compared to the eutectic.

3. The imperfect structures, in contrast to better aligned structures produced at slow solidification rates, were unstable at elevated temperatures and exhibited severe deterioration with prolonged high temperature exposure. Room temperature strength is decreased after microstructural deterioration occurs. In spite of this deterioration, reinforcement by the second phase is provided at elevated temperatures with Al-Cu and Al-Si elevated temperature strengths being superior to previously published values for slowly solidified structures.

4. There is an optimum amount of cold work for which the U.T.S. and Y.S. of the Al-Ni eutectic are increased several thousand psi over the as cast (aligned) structure. However, any amount of cold work leads to fiber breakage which tends to decrease the strength. However, at small amounts of cold work (up to 22%) this decrease is offset by the increased strength of the matrix. Cold worked specimens are not suitable for use at elevated temperatures because of strength loss caused by both spheroidization of the broken fibers and annealing of the cold worked matrix.

5. Longitudinal and transverse compressive strengths of the Al-Cu eutectic obtained by uncontrolled rapid unidirectional solidification are superior to previously published values for slowly solidified structures.

6. Al-Si strengths are essentially constant in the region around the eutectic composition (11-15%Si).

7. For the eutectic systems investigated, unidirectionally solidified castings provide essentially equivalent or better properties than slowly solidified structures. This method provides a more practical means of producing composite materials than slow solidification. Further work should be done on systems of more practical interest such as alloys having good elevated temperature properties (e.g. Ta-Ta_2C which has a eutectic temperature of 2800^{o}C).

BIBLIOGRAPHY

1. Leslie Holliday, ed., Composite Materials, Elsevier Publishing Company: Amsterdam, 1966.

2. W. W. Webb and W. D. Forgeng, Mechanical Behaviour of Microcrystals, Acta Met., 6, 1958, P. 462.

3. American Society for Metals, Fiber Composite Materials, American Society for Metals: Metals Park, Ohio, 1965.

4. Derek Hull, Introduction to Dislocations, Pergamon Press: London, 1965.

5. G. J. Davies, On the Strength and Fracture Characteristics of Intermetallic Fibers, Phil. Mag., 9, 1964, P. 953.

6. H. W. Rauch, W. H. Sutton and L. R. McCreight, Ceramic Fibers and Fibrous Composite Materials, Academic Press: New York, 1968.

7. R. L. McCullough, Fundamental Concepts of Composite Materials, Boeing Scientific Research Laboratories, Paper No. D1-82-0970, 1970.

8. D. R. McDanels, R. W. Jech and J. W. Weeton, Metals Reinforced with Fibers, Met. Prog., 78, Dec. 1960, P. 118.

9. A. Kelly, Strong Solids, Clarendon Press: Oxford, 1966.

10. G. A. Cooper and A. Kelly, The Deformation of Composite Materials, Paper from Déformation Plastique des Métaux et Alliages, G. Champier and G. Saada, editors, Paris Masson et cie, 1968, P. 281.

11. A. Kelly and W. R. Tyson, Fiber-Strengthened Materials, Paper from High Strength Materials, V. F. Zackay, ed., John Wiley and Sons: New York, 1965, P. 578.

12. A. Kelly, the Strengthening of Metals by Dispersed Particles, Proc. Roy. Soc. A, 282, 1964, P. 63.

13. J. E. Gordon, Some Considerations in the Design of Engineering Materials Based on Brittle Solids, Proc. Roy. Soc. A, 282, 1964, P. 16.

14. A. Kelly and G. J. Davies, The Principles of the Fiber Reinforcement of Metals, Met. Rev., 10(37), 1965, P. 1.

15. P. W. Jackson and D. Cratchley, the Effect of Fiber Orientation on the Tensile Strength of Fiber-Reinforced Metals, J. Mech. Phys. Solids, 14 (1), 1966, P. 49.

16. F. D. George, J. A. Ford and M. J. Falkind, The Effect of Fiber Orientation and Morphology on the Tensile Behaviour of Al_3Ni Whisker Reinforced Aluminum, Paper from Metal Matrix Composites, P. 59.

17. B. W. Rosen, Mechanics of Composite Strengthening, ibid. Ref. 3.

18. S. K. Mitra and J. E. Dorn, On the Nature of Strain Hardening in Polycrystalline Aluminum and Al-Mg Alloys, TMS-AIME, 227, 1963, P. 1015.

19. R. W. Hertzberg and R. W. Kraft, Fracture Mechanisms in Controlled Cu-Cr Eutectic Alloy, TMS-AIME, 227, 1963, P. 580.

20. H. C. Rogers, The Tensile Fracture of Ductile Metals, TMS-AIME, 218, 1960, P. 498.

21. G. Y. Chin, W. F. Hosford, Jr. and W. A. Backofen, Ductile Fracture of Aluminum, TMS-AIME, 230, 1964, P. 437.

22. J. W. Weeton and R. A. Signorelli, Fiber-Metal Composites, Paper from Strengthening Mechanisms - Metals and Ceramics, J. J. Burke, N. L. Reed and V. Weiss, editors, Syracuse University Press: Syracuse, New York, 1966, Chapter 19.

23. T. J. Koppenaal and N. M. Parikh, Microstraining in Fiber-Reinforced Silver, TMS-AIME, 224, 1962, P. 1173.

24. G. A. Cooper and A. Kelly, Role of the Interface in the Fracture of Fiber-Composite Materials, Paper from Interfaces in Composites, ASTM STP 452, Philadelphia, Pa., 1969, P. 90.

25. M. J. Salkind, The Role of Interfaces in Fiber Composites, Paper from Surfaces and Interfaces II, Physical and Mechanical Properties, J. J. Burke, N. L. Reed and V. Weiss, editors, Syracuse University Press: Syracuse, New York, 1968, P. 417.

26. H. E. Cline and D. F. Stein, Strengthening by Interfaces in the Ag-Cu Directionally Solidified Eutectic, TMS-AIME, 245, 1969, P. 841.

27. D. L. McDanels, R. W. Jech and J. W. Weeton, Analysis of Stress-Strain Behaviour of Tungsten - Fiber - Reinforced Copper Composites, TMS-AIME, 233, 1965, P. 636.

28. L. B. Greszczuk, Theoretical Studies of the Mechanisms of the Fiber-Matrix Interface in Composites, ibid. Ref. 24, P. 42.

29. W. H. Sutton and J. Chorné, Factors Affecting the Tensile Strength of Metals Reinforced with Strong Fibers, ibid. Ref. 22, Chapter 21.

30. R. Hill, Theory of Mechanical Properties of Fiber-Strengthened Materials: I. Elastic Behaviour, J. Mech Phys. Solids, 12, 1964, P. 199.

31. A. Kelly and H. Lilholt, Stress-Strain Curve of a Fiber Reinforced Composite, Phil. Mag., 20, Aug. 1969, P. 311.

32. R. Hill, Theory of Mechanical Properties of Fiber-Strengthened Materials: II. Inelastic Behaviour, J. Mech. Phys. Solids, 12, 1964, P. 213.

33. S. W. Tsai, J. C. Halpin and N. J. Pagano, editors, Composite Materials Workshop, Technomic, Stamford, Conn., 1968.

34. A. H. Cottrell, Strong Solids, Proc. Roy. Soc. A, 282, 1964, P. 2.

35. R. W. Kraft, Controlled Eutectics, J. Metals, Feb. 1966, P. 192.

36. M. C. Flemings, Directional Solidification and Composite Structures, ibid. Ref. 25, P. 313.

37. R. W. Hertzberg, Potential of Unidirectionally Solidified Eutectic Alloys as Reinforced Composites, ibid. Ref. 3, P. 77.

38. G. A. Chadwick, Eutectic Alloy Solidification, Prog. Mat. Science, 12, 1963, P. 97.

39. B. Chalmers, Principles of Solidification, John Wiley and Sons: New York, 1964.

40. D. J. Cooksey, D. Munson, M. P. Wilkinson and A. Hellawell, The Freezing of Some Continuous Binary Eutectic Mixtures, Phil. Mag. 10, 1964, P. 745.

41. R. W. Hertzberg, Composite Materials Formed by the Directional Solidification of Eutectic Alloys, Paper from Modern Composite Materials, L. J. Broutman and R. H. Krock, editors, Addison-Wesley: Reading, Mass., 1967, Chapter 15.

42. H. E. Bates, F. Wald and M. Weinstein, Controlled Solidification of Metal Matrix Composites Utilizing Monovariant Eutectic Reactions, J. Mat. Science, 4, 1969, P. 25.

43. A. H. Cottrell, Theoretical Structural Metallurgy, Edward Arnold: London, 1948.

44. J. J. Kramer, G. F. Bolling and W. A. Tiller, Solute Segregation During Cellular Solidification, TMS-AIME, 227, 1963, P. 374.

45. G. A. Chadwick, Modification of Lamellar Eutectic Structures, J. Inst. Metals, 91, 1962-63, P. 298.

46. G. A. Chadwick, Solidification of $CuAl_2$ - Al Eutectic Alloys, J. Inst. Metals, 91, 1962-63, P. 169.

47. J. D. Hunt and J. P. Chilton, An Investigation of the Lamella → Rod Transition in Binary Eutectics, J. Inst. Metals, 91, 1962-63, P. 338.

48. A. Hellawell, The Growth and Structure of Eutectics with Silicon and Germanium, Prog. Mat. Science, 15, 1970, P. 1.

49. M. J. Salkind, Interfacial Stability of Eutectic Composites, ibid. Ref. 24, P. 149.

50. R. Kossowsky and W. Johnston, Deformation and Stability of a Directionally Solidified Al-Pd Eutectic Alloy, TMS-AIME, 245, 1969, P. 1826.

51. G. J. Davies, The Growth of Fiber Structures from the Melt, ibid. Ref. 11, P. 603.

52. F. R. Mollard and M. C. Flemings, Growth of Composites from the Melt - Part 1, TMS-AIME, 239, 1967, P. 1526.

53. F. R. Mollard and M. C. Flemings, Growth of Composites from the Melt - Part 11, TMS-AIME, 239, 1967, P. 1534.

54. J. R. Cahoon and H. W. Paxton, The Mechanical Properties of Some Unidirectionally Solidified Aluminum Alloys Part 1: Room Temperature Properties, TMS-AIME, 245, 1969, P. 1401.

55. K. Van Horn, ed., Aluminum Vol. 1, American Society for Metals, Metals Park, Ohio, 1967.

56. F. D. Lemkey, R. W. Hertzberg and J. A. Ford, Microstructure, Crystallography and Mechanical Behaviour of Unidirectionally Solidified Al-Al_3Ni Eutectic, TMS-AIME, 233, 1965, P. 334.

57. R. W. Hertzberg, F. D. Lemkey and J. A. Ford, Mechanical Behaviour of Lamellar (Al-$CuAl_2$) and Whisker Type (Al-Al_3Ni) Unidirectionally Solidified Eutectic Alloys, TMS-AIME, 233, 1965, P. 342.

58. B. J. Bayles, J. A. Ford and M. J. Salkind, The Effect of Elevated - Temperature Exposure on the Microstructure and Tensile Strength of Al_3Ni Whisker - Reinforced Aluminum, TMS-AIME, 239, 1967, P. 844.

59. A. Yue, F. W. Crossman, A. E. Vedoz and M. Jacobson, Controlled Microstructures of Al-$CuAl_2$ Eutectic Composites and Their Compressive Properties, TMS-AIME, 242, 1968, P. 2441.

60. G. C. Weatherly, An Electron Microscope Investigation of the Lamellar Al-$CuAl_2$ Eutectic, Metal Science Journal, 2, 1968, P. 25.

61. R. W. Kraft and D. L. Albright, Microstructure of Unidirectionally Solidified Al-$CuAl_2$ Eutectic, TMS-AIME, 221, 1961, P. 95.

62. F. Crossman, A. Yue and A. Vedoz, Tensile Properties of Unidirectionally Solidified Al-$CuAl_2$ Eutectic Composites, TMS-AIME, 245, 1969, P. 397.

63. R. W. Kraft, D. L. Albright and J. A. Ford, Anomalous Thermal Stability of Al-$CuAl_2$ Eutectic Specimens, TMS-AIME, 227, 1963, P. 540.

64. M. Hansen, The Constitution of Binary Alloys, (McGraw Hill: New York, 1958).

65. J. A. Bell and W. C. Winegard, Structure of Pure Aluminum - Silicon Eutectics, J. Inst. Metals, 93, P. 318.

66. Ishi Miura and Hitoshi Hamanaka, Microstructures of Al-Si Eutectic Fibrous Composites Produced by Unidirectional Solidification, Nippon Kinzoku Gakkai - Si, 32 (8), 1968, P. 784 (In Japanese).

67. Ishi Miura and Hitoshi Hamanaka, Mechanical Properties of Al-Si Eutectic Fibrous Composites Prepared by Unidirectional Solidification, Nippon Kinzoku Gakkai - Si, 32 (9), 1968, P. 898, (In Japanese).

68. G. L. Pearson, W. T. Read and W. L. Feldmann, Deformation and Fracture of Small Silicon Crystals, Acta Met., 5, 1957, P. 181.